Università Degli Studi Di Padova
Facoltà di Scienze Matematiche Fisiche e Naturali
Dipartimento di Fisica "GALILEO GALILEI"

Scuola di Dottorato di Ricerca in Fisica.
Ciclo XXI

PARTICLE DARK MATTER AND ASTROPHYSICAL CONSTRAINTS

DOTTORANDO:
Marco Taoso

RELATORI : Prof. Antonio Masiero, U. Padova.

: Dr. Gianfranco Bertone, U. Pierre et Marie Curie.

COORDINATORE DEL DOTTORATO : Prof. Attilio Stella, U.Padova

Anni Accademici: 2006-2008

Abstract

Numerous astrophysical and cosmological observations support the existence of non-baryonic Dark Matter in the Universe. Its presence is well established at different scales, from galaxies to large scale structures and cosmological scales. However, despite the numerous and independent evidences, the nature of Dark Matter in not yet understood. Among the large number of Dark Matter candidates proposed in literature, Weakly Interacting Massive Particles (WIMPs) are the most popular. The reasons are manifold: they can naturally match the correct relic abundance from thermodynamics arguments in the expanding Universe (the so-called WIMP miracle), they arise in many motivated theories beyond the Standard Model (SM) and their phenomenology is particulary exiting. These particles can in fact be searched for with underground detectors, with the Large Hadron Collider or indirectly through the detection of their annihilation products.

Intermediate Mass Black Holes (IMBHs) are promising targets for indirect DM searches since large DM over-densities, called mini-spikes, could be formed around them due to gravitational effects. We study the prospect for detecting WIMP annihilations in mini-spikes with gamma-ray experiments. We focus in a population of IMBHs in the Andromeda galaxy. We show that FERMI should be able to detect a significant number of sources, the exact number depending on the values of WIMP parameters, while for current Air Cherenkov Telescopes the prospects are less promising.

WIMP annihilation in cosmological mini-spikes could be searched in the diffuse cosmic gamma-ray background (CGB), in particular from the analysis the CGB angular anisotropy. We show that angular correlations of the CGB provide a tool to disentangle the signal induced by DM annihilation in mini-spikes from a conventional astrophysical component. Treating blazars as a known background, we study the prospects for detecting DM annihilations with Fermi for different choices of WIMP mass and annihilation channel.

WIMP annihilations have been proposed at the origin of the cosmic-ray positron excess recently reported by PAMELA and ATIC experiments. We challenge this interpretation comparing the regions favored by $e^{\pm}$ data in the plane annihilation cross section and DM mass, with the constraints from photon observations of the galactic center and dwarf spher-

oidal galaxies. We investigate both models with DM annihilations into new light states and models with WIMPs annihilating into SM particles. We show that the positron excess can not be explained in terms of Dark Matter annihilations unless to consider DM profiles significantly less steep than Einasto or to invoke large local boost factors for positrons with at the same time negligible enhancement of the photon signals.

Finally, we show that WIMP annihilations could dramatically alter the evolution of the first stars. For sufficiently high DM densities the nuclear reactions are shut down and the stars are supported only by DM annihilations. These anomalous stars would appear colder and bigger with respect to what expected from a standard evolution. These characteristics could allow to distinguish them from normal stars.

Sintesi

L'esistenza di Materia Oscura non-barionica è provata da numerose osservazioni astrofisiche e cosmologiche. Tracce della sua presenza si trovano a scale molto diverse, dai sistemi galattici e sub-galattici alle strutture a larga scale e alle scale cosmologiche. Nonostante queste molteplici osservazioni, la natura della Materia Oscura è ancora ignota. Una delle possibilità più discusse è che la Materia Oscura sia composta da particelle massive debolmente interagenti, chiamate WIMPs (da Weakly Interacting Massive Particles). Queste particelle emergono infatti in numerose estensioni del Modello Standard (SM), la loro abbondanza nell'Universo può essere naturalmente spiegata da considerazioni termodinamiche e possono essere rivelate per mezzo di differenti strategie: attraverso rivelatori in laboratori sotterranei, grazie a ricerche agli acceleratori, LHC in particolare ed infine attraverso la rivelazione dei loro prodotti di annichilazione.

Buchi neri di massa intermedia (IMBHs, da Intermediate Mass Black Holes) rappresentano degli oggetti di grande interesse per le ricerche indirette di Materia Oscura perchè nelle loro vicinanze si possono formare grandi concentrazioni di Materia Oscura, dette mini-spikes. In questa tesi, abbiamo studiato le prospettive per la rivelazione di raggi gamma prodotti dalle annichilazioni di WIMPs nei mini-spikes. In particolare, abbiamo considerato una popolazione di IMBHs nella galassia di Andromeda. La rivelazione di molteplici sorgenti fornirebbe una prova diretta di questo scenario, probabilmente più convincente rispetto alla rivelazione di IMBHs galattici, che potrebbero invece essere erroneamente confusi con sorgenti astrofisiche extra-galattiche standard. Abbiamo dimostrato che l'esperimento FERMI ha le potenzialità per rivelare un numero significativo di sorgenti mentre le prospettive sono meno incoraggianti per gli Air Cherenkov Telescopes.

Tracce di annichilazioni di WIMPs in mini-spikes possono essere cercate anche nel fondo gamma extragalattico (CGB da Cosmic Gamma-ray Background), in particolare attraverso lo studio delle sue anisotropie angolari. Abbiamo infatti dimostrato che lo spettro angolare del fondo diffuso gamma permette di distinguere il segnale prodotto dalle annichilazioni di WIMPs in mini-spikes dall'emissione associata a sorgenti astrofisiche tradizionali. Considerando l'emissione dei blazar come un fondo noto, abbiamo studiato le prospettive per

la rivelazione di annichilazioni di WIMPs per diverse masse delle WIMPs e diversi canali di annichilazione.

Le annichilazioni di Materia Oscura rappresentano una possibile spiegazione all'eccesso di positroni nei flussi di raggi cosmici rivelati dagli esperimenti PAMELA ed ATIC. Oltre a particelle cariche, le annichilazioni di Materia Oscura generano inevitabilmente dei flussi di fotoni, la cui la cui non osservazione da parte di esperimenti esistenti esclude delle regioni dello spazio dei parametri della Materia Oscura. Abbiamo confrontato le combinazioni di massa e sezione d'urto di annichilazione compatibili con i risultati di PAMELA e ATIC, con i limiti di esclusione a questi parametri derivanti da osservazioni gamma e radio del centro galattico e delle galassie nane. Abbiamo ripetuto l'analisi assumendo che le particelle di Materia Oscura annichilino in particelle del Modello Standard o eventualmente in nuovi stati leggeri. Abbiamo dimostrato che le annichilazioni di Materia Oscura non possono spiegare l'eccesso di positroni, a meno che il profilo di densità di Materia Oscura nella nostra galassia sia meno ripido del profilo Einasto o il segnale di antimateria prodotto dalle annichilazioni locali sia innalzato da effetti astrofisici che non modificano invece i flussi gamma.

Infine abbiamo studiato le conseguenze delle annichilazioni delle WIMPs nella prima generazione di stelle. Se la densità di Materia Oscura attorno a queste stelle è sufficientemente alta, l'evoluzione stellare è notevolmente alterata rispetto agli scenari tradizionali. In particolare, le reazioni nucleari all'interno della stella non sono attive e la stella è invece sostenuta dalle annichilazioni di Materia oscura. Stelle di questo tipo apparirebbero più fredde e grandi rispetto a quanto atteso in assenza di annichilazioni di Materi Oscura, caratteristiche che permetterebbero di distinguerle dalle stelle usuali.

Résumé

L'existence de Matière Noire non-baryonique dans l'univers est aujourd'hui bien établie par de nombreuses observations astrophysiques et cosmologiques. Notamment, sa présence est confirmée à différentes échelles, des systèmes galactiques et sub-galactiques jusqu'aux structures à grandes échelles et aux échelles cosmologiques. Toutefois, malgré ces nombreuses et preuves indépendantes, la nature de la matière sombre est encore inconnue. Différentes hypothèses ont été émises et explorées quant à la composition de la Matière Noire, parmi lequelles l'une des plus débattues disant que la Matière Noire soit formée de WIMPs, acronyme de l'anglais Weakly Interacting Massive Particles. Ces particules se posent dans de nombreuses théories au-delà du Modèle Standard (SM) et leur abondance cosmologique est bien expliquée, dans le cadre du modèle cosmologique standard, par des considérations purement thermodynamiques. D'ailleurs, les WIMPs peuvent être recherchés avec des détecteurs souterrains, produits dans les accélérateurs, par exemple le Large Hadron Collider ou révéles indirectement grâce à la détection de leurs produits d'annihilation.

Les trous noirs de masse intermédiaire (IMBHs, de l'anglais Intermediate Mass Black Holes) sont des objets de grand intérêt pour la recherche indirecte de Matière Noire car, autour d'eux, en raison des effets gravitationnels, il peut avoir de grandes concentrations de Matière Noire, qu'on appelle mini-spikes. Dans cette thèse, nous étudions les perspectives de détection des rayons gamma produits par l'annihilation de WIMPs en mini-spikes. En particulier, nous examinons la population de IMBHs dans la galaxie d'Andromède. Nous montrons que FERMI est en mesure de détecter un nombre important de sources, tel de verifier ce model, tandis que pour les actuels Télescopes Air Cherenkov les perspectives sont moins prometteuses.

Les traces d'annihilation de WIMPs en mini-spikes cosmologiques peuvent également être cherchées dans le fond diffus gamma (CGB, de l'anglais Cosmic Gamma-ray Background), notamment à travers l'étude de ses anisotropies angulaires. Nous montrons qu' à partir du spectre de puissance angulaire de fond diffus gamma, il est possibile de distinguer le signal produit par l'annihilation de WIMP en mini-spikes de composantes astrophysiques conventionnelles. Grâce à cette technique et considérant l'émission de blazars comme un

fond connu, nous étudions les perspectives pour la détection de l'annihilation de WIMPs pour différentes masses de WIMPs et différents spectres d'annihilation.

Ce qui semble être un excès de positrons dans les rayons cosmiques, détecté par les éxperiences Pamela et ATIC, pourrait être expliqué par l'annihilation de particules de Matière Noire. Les annihilations de WIMPs et la propagation des positrons et des electrons dans le champ magnétique galactique produisent également des flux de photons, qui peuvent s'étendre des ondes radio jusqu'aux rayons gamma. Les observations à différentes longueurs d'ondes peuvent donc mettre des contraintes sur les paramètres des WIMPs, en particulier sur leur masse et leur section efficace d'annihilation. Dans cet espace de paramètres, nous comparons les régions favorisées par les résultats des expériences de rayons cosmiques avec celles exclues par les observations du centre galactique et des galaxies naines. Nous étudions des modèles dont les produits d'annihilation de la Matière Noire sont particules dans le Modèle Standard, ou également de nouvelles particules légers. Nous montrons que les annihilations de Matiére Noire ne peuvent pas expliquer l'excès de positrons dans les rayons cosmiques, à l exception de profils de densité de Matière Noire dans notre galaxie qui seraient plus faibles que le profil Einasto. De façon alternative, il doit exister des processus astrophysiques qui augmentent le signal d'antimatière sans en même temps augmenter le flux de photons.

Enfin, nous montrons que les annihilations de WIMPs pourraient modifier radicalement l'évolution des premières étoiles. Pour des densités suffisamment fortes de Matière Noire, les réactions nucléaires sont bloquées et les étoiles sont soutenues uniquement par l'énergie produite par les annihilations de WIMPs. Ces étoiles seraient plus grandes et froides de ce qu' on attend d'une évolution standard. Ces caractéristiques peuvent ainsi permettre de les distinguer des étoiles usuelles.

Contents

Chapter 1

Dark Matter: Cosmology and Particle Physics

After more than 70 years from the first hints, there are nowadays compelling cosmological and astrophysical evidences for the existence of non-baryonic Dark Matter. This arguments strongly supports the existence of new physics Beyond the Standard Model of particle physics.

1.1 The Standard Cosmological Model

The Standard Cosmological Model describes the expansion and evolution of the Universe starting from a perturbed Robertson-Walker space-time (see e.g. [1, 2] for textbooks):

$$ds^2 = dt^2 - a(t)^2 \left[\frac{dr^2}{1-kr^2} + r^2 d\Omega^2 \right].$$

$a(t)$ is the cosmological scale factor and the spatial curvature k takes the values $+1,0,-1$ respectively for open, flat or closed universes. The dynamics is governed by the Einstein's equations, which relate the energy content of the Universe with its geometry, described by the metric. In particular, the time evolution of the scale factor $a(t)$ is given by the following Friedman equation:

$$\sum \Omega_i - 1 = \frac{k}{H^2 a^2}$$

where the normalized abundance Ω_i is $\Omega_i = \rho_i/\rho_c$, with ρ_c the critical density. The Hubble parameter $H(t)$ is defined as $H(t) = \dot{a}(t)/a(t)$ and its present value is $H_0 \equiv 100h$ km s^{-1} Mpc^{-1}, with $h = 0.72 \pm 0.03$ (statistical) ± 0.07 (systematic) [3]. The sum runs over all the different species contributing to the total energy density of the Universe, therefore at least radiation, matter (M) and dark energy (Λ).

The Standard Cosmological Model has been successfully tested by a large number of cosmological observations, which have lead to the establishment of the so-called ΛCDM model,

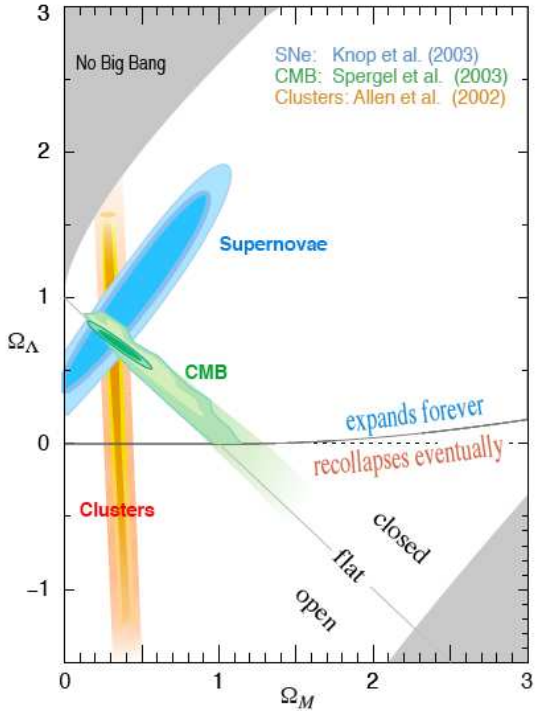

Figure 1.1: Best fit confidence regions in the $\Omega_M - \Omega_\Lambda$ plane. From Supernovae Cosmology Project.

which describes a flat ($k = 0$) Universe whose present energy density is dominated by Dark Energy and Matter: $\Omega_\Lambda \sim 0.7$ and $\Omega_M \sim 0.3$. The exact values of the parameters depend on the cosmological data-sets considered. The matter component is mainly composed by non-baryonic Cold Dark Matter (CDM), a non-luminous, slowly moving and poorly interacting massive specie (see Sec.2.3 for a discussion about the coldness of Dark Matter), with a subdominant contribution from baryons: $\Omega_{CDM} \sim 0.25$ and $\Omega_b \sim 0.05$. Therefore, among the ingredients of the cosmological model there are two unknown components, Dark Matter and Dark Energy.

Without any attempt of completeness, we now briefly mention some of the key observations which are at the basis of the ΛCDM model.

- *Cosmic Microwave Background (CMB).* The angular power spectrum of the CMB is excellently fitted by the ΛCDM model, assuming a gaussian, adiabatic and nearly scale invariant power spectrum of primordial fluctuations. The structure of the acoustic peaks requires the presence of CDM and the best fit of WMAP V data gives:

$$\Omega_b h^2 = 0.02273 \pm 0.00062 \qquad \Omega_M h^2 = 0.1326 \pm 0.0063.$$

- *Large Scale Structures.* The matter distribution is probed by observing the spatial distribution of galaxies, properly taking in account the biasing. Galaxy clustering constraint the combination $\Omega_M h$ and probes the nature of the Dark Matter since the power spectrum of density perturbations depends on the properties of Dark Matter particles, like their velocities at the time of structures formation.

- *Lyman α forest.* The matter power spectrum is reconstructed from the absorption lines in quasars spectra.

- *Gravitational lensing.* The mass fluctuations is probed measuring the distortion of galaxy images produced by the matter distribution along the line of sight. The measurements are sensitive to the combination of Ω_M and the amplitude of density perturbations.

- *Peculiar velocities.* The mass fluctuations in the Universe are obtained from measurements of the peculiar velocities of galaxies.

- *Supernovae.* Type Ia Supernovae are used as standard candles to measure the luminosity distance as a function of the redshift. SN alone can constraint a combination of Ω_M and Ω_Λ. When combined with CMB data the degeneracy is broken and the global fit points to the existence of Dark Energy.

- *Galaxy Clusters* The clusters number density as a function of redshift is sensitive to density perturbations. In addition, these systems can be used to measure the baryon fraction, $f_b = \Omega_b/\Omega_M$, as a function of the redshift. An estimate of Ω_M can be inferred taking Ω_b from other observations, e.g. Big Bang Nucleosynthesis.

- *Big Bang Nucleosynthesis (BBN).* BBN predicts the abundances of light elements produced by primordial nuclesynthesis, occurred at a temperature $T \sim 1$ MeV. The predictions are in nice agreement with observations for $0.017 < \Omega_b h^2 < 0.024$ (95 % CL). This estimate of the baryonic density is consistent with that from CMB.

Fig. 1.1 show the preferred regions in the $\Omega_M - \Omega_\Lambda$ plane for different observations. A good agreement between independent data-sets is obtained for Ω_M much larger than the baryon density inferred from BBN and CMB, evidencing the need for Dark Matter. In addition, we stress that the existence of a "cold" and almost non-interacting matter component, i.e. *non-baryonic* Dark Matter (or simply Dark Matter), is at the basis of the satisfactory explanation of the formation and growth of cosmological structures in the context of ΛCDM model.

		$SU(3)_C \otimes SU(2)_L \otimes U(1)_Y$
Left-handed quarks	$\begin{pmatrix} u \\ d \end{pmatrix}_L, \begin{pmatrix} c \\ s \end{pmatrix}_L, \begin{pmatrix} t \\ b \end{pmatrix}_L$	$(\mathbf{3}, \mathbf{2}, 1/6)$
Right-handed quarks	$u_R \quad c_R, \quad t_R$ $d_R \quad s_R \quad b_R$	$(\mathbf{3}, \mathbf{1}, 2/3)$ $(\mathbf{3}, \mathbf{1}, -1/3)$
Left-handed leptons	$\begin{pmatrix} \nu_e \\ e \end{pmatrix}_L, \begin{pmatrix} \nu_\mu \\ \mu \end{pmatrix}_L, \begin{pmatrix} \nu_\tau \\ \tau \end{pmatrix}_L$	$(\mathbf{1}, \mathbf{2}, -1/2)$
Right-handed leptons	$e_R, \ \mu_R, \ \tau_R$	$(\mathbf{1}, \mathbf{1}, -1)$
$SU(3)_C$ gauge bosons	$g_\mu^a \ (a = 1, ..., 8)$	$(\mathbf{8}, \mathbf{1}, 0)$
$SU(2)_L$ gauge bosons	$W_\mu^a \ (a = 1, 2, 3)$	$(\mathbf{1}, \mathbf{3}, 0)$
$U(1)_Y$ gauge boson	B_μ	$(\mathbf{1}, \mathbf{1}, 0)$
Higgs	$\Phi = \begin{pmatrix} \phi^+ \\ \phi^0 \end{pmatrix}$	$(\mathbf{1}, \mathbf{2}, 1/2)$

Table 1.1: Particle content of the Standard Model.

1.2 Evidences for Dark Matter

In the previous sections we have shown that Dark Matter is a fundamental element of the ΛCDM model, which is widely considered the best description of present cosmological observations (see e.g. [4, 5, 6, 7] for reviews on Dark Matter).

Evidences of Dark Matter come also from observations of individual astrophysical objects. For example, one of the first hints of Dark Matter was obtained by F.Zwicky from observations of the mass-to-light ratio of the Coma cluster [8]. The galaxy cluster 1E0657-56, also known as Bullet cluster, provide the most direct and spectacular evidence for Dark Matter [9]. In this system, the collision between two clusters of galaxies produces the separation of baryons and Dark Matter in the smaller cluster. This conclusion is obtained from the combination of optical and X-ray images with the weak lensing map. The centroid of the mass distribution is coincident with that of galaxies, while the gas distribution, which is the dominant baryonic component, is left ahead.

At galactic scales, compelling evidences for Dark Matter are found from the analysis of the stars and gas rotation curves. From Newton's laws, the expected circular velocity is $v(r) = \sqrt{GM(r)/r}$ where $M(r)$ is the mass inside the radius r. Therefore, beyond the galactic disk the circular velocity should fall as $v(r) \simeq 1/\sqrt{r}$ while the observed velocity profiles usually flatten even far beyond the disk. These observations support the existence of large Dark Matter halos.

1.3 The Standard Model of Particle Physics

The Standard Model (SM) of particle physics describes the dynamics of fundamental interactions. It is a gauge theory based on the group $SU(3)_C \otimes SU(2)_L \otimes U(1)_Y$, with $SU(3)_C$ and $SU(2)_L \otimes U(1)_Y$ respectively referring to strong and electroweak interactions. The particle content with the associated gauge group transformations is listed in Table 1.1. The electroweak symmetry group undergoes the spontaneous symmetry breaking

$$SU(3)_C \otimes SU(2)_L \otimes U(1)_Y \rightarrow SU(3)_C \otimes U(1)_Q,$$

where Q and Y denotes the electric and weak hypercharge generators. This mechanism produces massive $W_\mu^\pm$ and Z_μ bosons while the photon A_μ remains massless, with

$$W_\mu^\pm = (W_\mu^1 \mp i W_\mu^2)/\sqrt{2} \quad Z_\mu = -B_\mu \sin(\theta_W) + W_\mu^3 \cos(\theta_W) \quad A_\mu = B_\mu \cos(\theta_W) + W_\mu^3 \sin(\theta_W).$$

The weak angle θ_W is defined as $\tan(\theta_W) = g'/g$, with g' and g respectively the $U(1)_Y$ and $SU(2)_L$ gauge couplings. The massive and neutral Higgs scalar field is the only remaining part of the scalar doublet Φ after electroweak symmetry breaking. Fermions acquire mass, in virtue of their Yukawa couplings with Φ, with the exception of neutrinos.

We refers to reviews and textbooks for more complete discussions on the SM structure (see. e.g. the reviews in [10]). We just remind here that despite the impressive success of the SM in describing a large number of experimental data, there exist serious motivations for physics beyond the Standard Model, that we briefly mention in the next section.

1.4 Dark Matter and Beyond the Standard Model

The Standard Model does not provide any explanation for Dark Matter. Neutrino oscillations strongly support the existence of neutrino masses however neutrinos would behave as Hot Dark Matter and this argument rules out this specie as dominant Dark Matter component (see discussion in Sec.2.3). Consequently, Dark Matter is a motivation to search for new physics beyond the SM (or even it might be thought as an evidence).

In addition, there are further observational and theoretical reasons for considering the Standard Model an incomplete description of particle physics and fundamental interactions. The strongest one is the experimental evidence for neutrino oscillations, which oblige us to extend the SM in order to include neutrino masses.

A list of problems of the SM includes:

Observation

- Neutrino masses
- Dark Matter

- Baryon asymmetry
- Inflation
- Dark Energy

  Theory

- Hierarchical problem
- Strong CP problem
- Gauge coupling unification
- Quark and lepton masses and mixing
- Gravity has to be included

Standard Model is nowadays thought as the low-energy limit of a more fundamental theory. The challenge of theoretical particle physics is to find an explanation for the issues mentioned above. In particular, the Dark Matter problem has stimulated the formulation of a large number of new models which propose viable Dark Matter candidates. On the other hand, cosmological and astrophysical observations constraint the properties of Dark Matter and therefore the parameter space of these theories.

In this thesis, we study the prospects for Dark Matter detection through astrophysical observations. In the first chapter, we present some of the best motivated Dark Matter candidates and we discuss the Dark Matter properties. We then consider a specific class of Dark Matter candidates, the so-called Weakly Interacting Massive Particles (WIMPs). These particles could be searched for *indirectly* through the detection of their annihilation products. In Chapter 3 we focus on gamma-rays searches and in Chapter 4 we study the implications of multi-wavelength observations for the Dark Matter interpretation of existing antimatter cosmic-rays data. 4. We then consider the effects of WIMPs annihilations in the first stars.

Chapter 2

Dark Matter particles: candidates and properties

In this chapter we review the basic properties of Dark Matter proposing a ten-point test that every "good" Dark Matter candidate has to satisfy.

This chapter is based on [11].

2.1 Introduction

In the previous chapter we have reviewed the most relevant astrophysical and cosmological evidences for non-baryonic Dark Matter. We have also stressed that particle Dark Matter models, calling for the existence of a "dark" massive specie in the Universe roughly 6 times more abundant than baryons, has necessary to invoke new physics Beyond the Standard Model of Particle Physics.

This exiting connection between the Dark Matter problem and particle physics has prompted the proliferation of Dark Matter candidates that are currently being searched for in an impressive array of accelerator, direct and indirect detection experiments. Remarkably, some of them are predicted in theories originally proposed for different intents (e.g. Supersymmetry or the Peccei-Quinn model) and which could also have important implications in other cosmological contexts, strengthening therefore the link between particle physics and cosmology.

As our understanding of particle physics and astrophysics improves, we accumulate information about the properties of Dark Matter which progressively reduces the allowed regions in the parameter space of these theories. In this chapter, we present a 10-point test that new particles have to pass in order to be considered good DM candidates. We will therefore present the fundamental properties of particle DM and review some of the best motivated Dark Matter candidates which have been proposed in the literature.

We will work under the assumption that a single DM species dominates the DM relic density, while contribution from other species is subdominant; it is straightforward to generalize the discussion to the case of multi-component DM. Furthermore, we will consider a standard ΛCDM cosmological model, although we discuss the consequences of more general models, allowing for instance a non-standard expansion history at the epoch of DM freeze-out.

Each of the following ten points, that represent *necessary* conditions for a particle to be considered a good DM candidate, will be discussed in a dedicated section, where we will review the literature on the subject and present the most recent results. In each section we will discuss how robust the constraints are, especially for those that heavily rely on astrophysical quantities such as the local DM density and velocity distribution, or the extrapolation of DM profiles at the center of galactic halos, often affected by large uncertainties.

A particle can be considered a good DM candidate only if a positive answer can be give to *all* the following points:

1. *Does it match the appropriate relic density?*
2. *Is it cold?*
3. *Is it neutral?*
4. *Is it consistent with BBN?*
5. *Does it leave stellar evolution unchanged?*
6. *Is it compatible with constraints on self-interactions?*
7. *Is it consistent with direct DM searches?*
8. *Is it compatible with gamma-ray constraints?*
9. *Is it compatible with other astrophysical bounds?*
10. *Can it be probed experimentally?*

The distinction between *gamma-ray constraints* and *other astrophysical bounds*, in points 8) and 9), is rather artificial, and it simply reflects the privileged role of photons in astrophysics, since they propagate along straight lines (unlike charged particles), and they can be detected with better sensitivity than, say, neutrinos. The fact of considering gamma-ray photons is then due to the fact that the decay or annihilation of some of the most common candidates falls in this energy range.

We also note that, strictly speaking, the last point is not really a *necessary* condition, as DM particles could well be beyond the reach of current and upcoming technology. However, measurable evidence is an essential step of the modern scientific method, and a candidate

that cannot be probed, at least indirectly, would never be accepted as the solution to the DM puzzle.

2.2 Does it match the appropriate relic density?

The analysis of the Cosmic Microwave Background (CMB) anisotropies is a powerful tool to test cosmological models, and to extract the corresponding cosmological parameters. For instance, the angular position of the peaks in the power spectrum of temperature anisotropies is a sensitive probe of the curvature of the Universe (see e.g. [12, 2] for a review and a more extended discussion). The power spectrum of CMB anisotropies is fitted within the Standard Cosmological Model with a number or free parameters that depends onto the priors.
The best fit of the five years WMAP data, with a 6 parameters flat ΛCDM model and a power-law spectrum of primordial fluctuations, gives [13]

$$\Omega_b h^2 = 0.02273 \pm 0.00062 \qquad \Omega_M h^2 = 0.1326 \pm 0.0063$$

for the abundance of baryons and matter, respectively. The WMAP analysis is consistent with the results from other cosmological observations, like small scale CMB experiments, Large-Scale Structures and SuperNova (See [14] for joint-likelihood analysis on larger data-sets).

In addition, note that the inferred baryonic density is consistent with the determination from big bang nucleosynthesis [15]

$$0.017 < \Omega_b h^2 < 0.024 \text{ (95 \% CL)}.$$

For a new particle to be considered a good DM candidate, a production mechanism that reproduce the appropriate value of the relic density must exist. Moreover, to guarantee its stability, its lifetime must exceed the present age of the Universe. Taking in account the estimates of the Hubble Space Telescope Key Project [3] and in agreement with the result derived by WMAP, $H_0 = 72 \pm 3$ (statistical) ± 7 (systematic) km s^{-1}Mpc^{-1}, we require a lifetime $\tau \gtrsim 4.3 \times 10^{17}$ s.

In many proposed extensions of the Standard Model of particle physics, the stability of the DM particle is ensured by imposing a symmetry that forbids the decay of DM into Standard Model particles. For example, R-parity in Supersymmetry models (SUSY) [16, 17], K-parity in Universal Extra Dimensions Models (UED) [18], and T-parity in Little Higgs Models [19], prevent the lightest *new* particle in the respective theories from decay (see for example Ref.[4] for a detailed discussion on SUSY DM and Ref.[7] for a review on UED DM).

Thermal relics

Among the best DM candidates, there is a class of particles called WIMPs (for weakly interacting massive particles), that are thermal relics and naturally achieve the appropriate relic density.

The scenario goes as follows: the WIMP is in thermodynamic equilibrium with the plasma in the early Universe, and it decouples when its interaction rate drops below the expansion rate of the Universe. For a non-relativistic particle at decoupling, the number density over the entropy density remains frozen, i.e. the thermal relic *freezes-out*. The evolution of the number density of a generic species χ in the Universe, is described by the following Boltzmann equation:

$$\dot{n}_{eq} + 3Hn = -\langle\sigma_{ann}v\rangle \left[n^2 - n_{eq}^2\right].$$

The second term in the l.h.s of the equation takes into account the dilution of the number density due to the expansion of the Universe. $\langle\sigma_{ann}v\rangle$ is the thermal average of the annihilation cross section times velocity and it is parametrized with a non-relativistic expansion in powers of v^2, as: $\langle\sigma_{ann}v\rangle = a + b\langle v^2\rangle + \mathcal{O}(\langle v^4\rangle) \simeq a + 6b/x$, with $x \equiv m/T$.

n_{eq} is the equilibrium density of WIMPs in the plasma at temperature T and for a non-relativistic specie is given by $n_{eq} = g(\frac{mT}{2\pi})^{3/2}e^{-\frac{m_\chi}{T}}$, where g denotes the number of degrees of freedom of χ and m_χ is the WIMP mass.

The Boltzmann equation can be solved integrating it in two extreme regions, long before and long after the WIMP freeze-out (e.g. WIMP decoupling), and matching then the solutions. Skipping the calculation details, that can be reviewed e.g. in [1], the relic density today for a generic WIMP χ is [6]:

$$\begin{aligned}\Omega_\chi h^2 &\approx \frac{1.07\times10^9\ \text{GeV}^{-1}}{M_{Pl}}\frac{x_f}{\sqrt{g_{*f}}}\frac{1}{(a+3b/x_f)} \\ &\approx \frac{3\times10^{-27}\ \text{cm}^3\text{s}^{-1}}{\langle\sigma_{ann}v\rangle}.\end{aligned} \tag{2.1}$$

where g_{*f} counts the relativistic degrees of freedom at the decoupling, M_{Pl} is the Planck mass and $x_f \equiv m_\chi/T_f$ with T_f the freeze-out temperature. The last line is an order of magnitude estimate and it shows that the relic abundance of a non relativistic decoupled specie strictly depends on the annihilation cross section at freeze-out [4]. Furthermore, it has to be noticed that the annihilation cross section, for a particle of given mass, has a maximum, imposed by the partial wave unitarity of the S matrix, $\langle\sigma_{ann}v\rangle_{max} \sim 1/m_\chi^2$ [39, 40]. Thus, with the use of Eq. 2.1, the requirement $\Omega_M h^2 \lesssim 1$ implies the following constraint on the mass of the DM particle, also called "unitarity bound" [39]

$$m_{DM} \lesssim 340\ \text{TeV}.$$

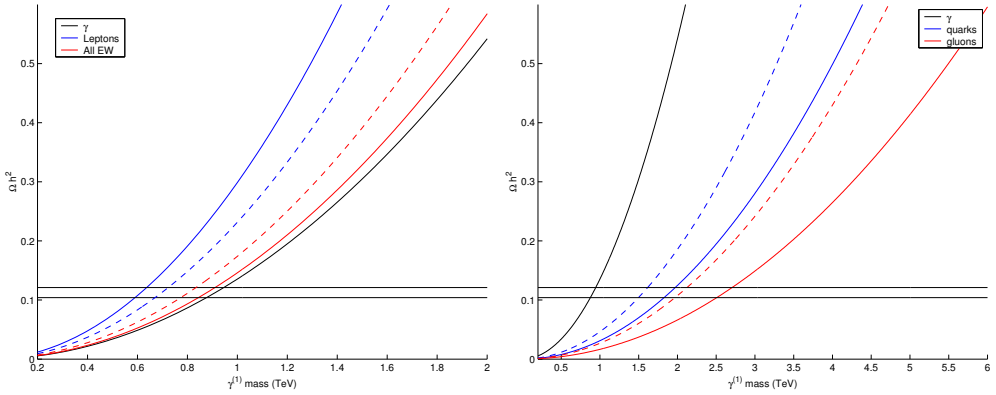

Figure 2.1: Left: Relic Abundance of $B^{(1)}$ in the UED model as a function of its mass after including no coannihilation (black line), coannihilation with all leptons (blue) and all electroweak particles (red). For the cases with coannihilation, the solid and dashed lines are computed with a mass splitting $\delta = 0.01$ and 0.05 respectively. Right: The same as in the left panel but accounting for coannihilation of $B^{(1)}$ with all electroweak particles and quarks (blue line), and all level-one KK particles, including KK gluons (red line). Solid and dashed lines are for a mass splitting $\delta = 0.01$ and 0.05 respectively. From Ref.[26].

Applying the more stringent constraint, obtained by WMAP, the upper bound on m_{DM} becomes:

$$m_{DM} \lesssim 120 \text{ TeV}.$$

However, this constraint was derived under the assumption that particles were in thermal equilibrium in the early universe, thus it applies only to thermal relics, and can be evaded by species which are non-thermally produced.

The standard computation of the thermal relic abundance discussed above presents three important exceptions, as it has been shown, following previous ideas [20], by Griest and Seckel [21]. They take place for WIMPs lying near a mass threshold, for annihilations near to a pole in the cross section, or in presence of coannihilations. The last effect occur when a particle that shares a quantum number with the WIMP, is nearly degenerate in mass with it. If the mass gap is low enough (roughly $\lesssim 10\%$) the coannihilation reactions, involving WIMP particles, can control the WIMP abundance and lower or enhance it.
Full relic density calculations, including all coannihilations, have been performed e.g. for the supersymmetric neutralino, for which numerical codes such as DarkSUSY [22] and micrOMEGAs [23] are publicly available. Coannihilations have a dramatic effect on the relic density, and they can lower it by a factor of up to several hundreds (see e.g. [24]).

Coannihilations are also important in UED models, where the relic density of the first excited state of the B, which may be the lightest Kaluza-Klein particle (LKP) and a viable

DM candidate, may be enhanced or lowered depending on the coannihilation channel [25, 26, 27]. See Fig.2.1.

Deviations from Standard Cosmology can substantially change the picture. For example, due to the presence of scalar fields, the universe may undergo a period of much higher expansion rate and the relic abundance of a WIMP may result increased by several orders of magnitude [28, 29]. Furthermore, the production of entropy in the Universe after the WIMP decoupling may dilute its abundance, e.g. due to out-of-equilibrium decays of non-relativistic particles or to first-order phase transitions [30, 31, 32, 33].

It is also possible that DM particles did not experience the thermal history depicted above, and that they have inherited the appropriate relic density through the decay of a more massive species, that has earlier decoupled from the thermal bath. This is e.g. the case for SuperWeakly Interacting Massive Particles (SWIMP), such as the LSP gravitino in SUSY and the first excitation of the graviton in UED, which are produced by late decays of the next-to lightest particles (NLSP/NLKP) in the respective theories [34, 35, 36, 37] and whose relic abundances are simply the rescaled thermal relic densities of the NLPs:

$$\Omega_{\rm SWIMP} = \frac{m_{\rm SWIMP}}{m_{\rm NLP}}\Omega_{\rm NLP}.$$

Other production mechanisms may actually be concomitant for such candidates, such as the production at reheating after the end of the inflationary era (see e.g. [36, 38]. See also below for a brief discussion of gravitino production).

Other production mechanisms

Very heavy DM candidates, such as the so-called wimpzillas, have been proposed, with masses as large as 10^{15} GeV, i.e. well above the unitarity limit (see e.g. [41] for a review). For mechanisms that produce these super-massive particles with $\Omega_{DM} \sim 1$, departure from thermal equilibrium is automatic [41], and the challenge is not to overproduce them. Several mechanisms have been proposed: for instance they could be created during reheating after inflation, with masses a factor 10^3 larger than the reheating temperature [42], or during a pre-heating stage, with masses up to the Grand Unification scale (10^{15} GeV) [43] or even to the Planck Scale [44], or again from bubble collisions if the inflation exit is realized by a first-order transition [45]. Another very interesting mechanism is of gravitational nature: wimpzillas may be created by amplification of quantum fluctuations in the transition between the inflationary regime and the matter (radiation) dominated one, due to the nonadiabatic expansion of the spacetime [46, 47]. This scenario can produce particles

with mass of the order of the inflaton mass and do not require couplings of wimpzillas with inflaton or other particles.

These particles can be accommodated in existing theoretical frameworks. For instance, stable or metastable bound states called cryptons arise in M-theory, and other possibilities are contemplated in string theories [48]. Furthermore, messenger bosons in soft supersymmetry breaking models may be very massive and in presence of accidental symmetries in the messengers sectors, might be stable [49].

Although wimpzillas have been invoked in top-down scenarios that seek to explain the origin of Ultra High Energy Cosmic Rays [47, 50, 51], this interpretation is today problematic because it predicts a large photon component in the UEHCRs spectrum, in disagreement with the recent results of the Auger experiment [52].

Several production mechanisms can act together to produce a given species, and its relic abundance receives contributions from each of them. The calculation depends on the details of the particle physics and cosmological models adopted. In the case of axions, i.e. light pseudoscalar particles introduced to solve the Strong CP Problem, the production mechanisms in the early Universe are scattering in the hot thermal plasma and possibly radiation by topological defects like axion-strings. Another relevant production mechanism is the so-called *misalignment*: the axion field rolls towards its minimum, near the QCD epoch, and it ends with coherent oscillations that produce a Cold Dark Matter condensate. A lower bound on the axion mass can be inferred requiring that they do not overclose the Universe, but the uncertainties in the calculation of their production make the constraint rather weak (for recent reviews of axions see [54, 55]).

As mentioned before, gravitinos can be copiously emitted by the decay of the NLP in SUSY but they can also be produced, during reheating, by inelastic $2 \rightarrow 2$ scattering processes off particles in the thermal bath and in some scenarios they can act as Cold Dark Matter candidates (e.g. [56, 57, 58, 59, 60, 61], see e.g. [62, 63] for more details and references on gravitino DM models). The efficiency of the production depends on the reheating temperature T_R so the bound on Ω_{DM} translates into an upper limit on T_R [38, 59, 64]. In addition to thermal production and late decays of the NLSP, other non thermal and inflation model dependent contributions can arise and change considerably the predictions [65, 66].

Sterile neutrinos, which arise naturally in theoretical frameworks [67, 68, 69, 70] or in the phenomenological νMSM [71], have been proposed as a solution of the LSND anomaly [72], as explanation of the high pulsar velocities [73] and as Dark Matter candidates. Recently, the MiniBoone collaboration has reported its first results, excluding at 98% C.L. the two-neutrino appearance oscillation scheme obtained from LSND data [74]. The (3+1) scheme, involving one sterile neutrino specie, is excluded and also models with two or three sterile

species are not viable because of the tension between appearance and disappearance data [75].

Sterile neutrinos may be produced in the early Universe from collision oscillation conversions of active thermal neutrinos. Their momentum distribution is significantly distorted with respect to a thermal spectrum due to the effects of quark-hadron transition, the modification of the neutrino thermal potential caused by the presence of thermal leptons and the heating of the coupled species (see e.g. [76] for precise computation of relic abundance). Moreover it has been proposed an enhanced resonant production, in presence of a lepton asymmetry in the early universe significantly higher than the baryonic one [78, 77].

2.3 Is it cold?

The evolution of perturbations in the Universe depends on the microscopic properties of DM particles. The standard picture, widely accepted, is that after equality, when the Universe becomes Matter Dominated, the DM density perturbations begin to grow, and drive the oscillations of the photon-baryonic fluid around the DM gravitational potential wells. Soon after recombination, baryons kinematically decouple from photons and remain trapped in DM potential wells. Their density perturbations then grow to form the structures that we observe today in the Universe (see for more details [1, 2]).

Hot Dark Matter

The imperfect coupling between baryons and photons at recombination leads to a damping of small scale anisotropies, also known as Silk damping [79]. A collisionless species, moving in the universe from higher to lower density regions, also tends to damp the fluctuations above its free-streaming scale. This a key property of Hot Dark Matter, which consists of species which are relativistic at the time of structures formation and therefore lead to large damping scales [80].

The prototype of HDM are Standard Model neutrinos: they were thermally produced in the early Universe and they thermodynamically decoupled again relativistic at $T \sim 1$ MeV, leading to a relic abundance today that depends on the sum of the flavor masses, $m_\nu = \sum_{i=1}^{3} m_{\nu_i}$:

$$\Omega_\nu h^2 = \frac{m_\nu}{90 \text{ eV}}. \tag{2.2}$$

Their free-streeming length is [1]:

$$\lambda_{FS} \sim 20 \left(\frac{30 \text{ eV}}{m_\nu} \right) \text{ Mpc}.$$

Hot DM models are today disfavored (see e.g. [81] for a more complete discussion). For instance, the power spectrum of density perturbations should be suppressed beyond the free-streaming length of HDM particles, that for neutrino masses in the eV range corresponds roughly to the size of superclusters. Furthermore, HDM models predict a top-down hierarchy in the formation of structures, with small structures forming by fragmentation of larger ones, while observations show that galaxies are older than superclusters.

Small amounts of HDM can still be tolerated, provided that it is compatible with large scale structure and CMB data. Assuming an adiabatic, scale-invariant and Gaussian power spectrum of primordial fluctuations, WMAP data set an upper limit on the sum of light neutrino masses [13] (or equivalently, through Eq. 2.2, on Ω_ν)

$$\sum m_\nu < 2.11 \text{ eV (95 \% CL)}.$$

The combination of data from WMAP, large scale structure and small-scale CMB experiments, further strengthens the constraint, but it also introduces potentially large systematic effects [82, 83, 84, 85]. A significantly improved constraint can been obtained combining Ly-α forest, CMB, SuperNovae and Galaxy Clusters data [86, 87]:

$$\sum m_\nu < 0.17 \text{ eV (95 \% CL)}.$$

These limits can be applied to a generic hot Dark Matter candidate, e.g. to thermal axions [55, 88, 89] or to hot sterile neutrinos [90].

Cold Dark Matter

The standard theory of structure formation thus requires that Dark Matter is *cold*, i.e. it is made of particles that have become non-relativistic well before the matter domination era, and that can therefore clump on small scales. The prototype of cold DM candidates is the supersymmetric neutralino, whose free-streaming length is such that only fluctuations roughly below the Earth mass scale are suppressed [91, 92]. CDM candidates can be heavy thermal relics, such as the aforementioned neutralino, but also light species, non-thermally produced, like axions (see Sec. 2.2 for further comments and references).

N-body simulations of ΛCDM Universe are in agreement with a wide range of observations, such as the abundance of clusters at $z \leq 1$ and the galaxy-galaxy correlation functions (see e.g. [93] for a review of CDM), making it a successful and widely accepted cosmological model.

However, the emergence of some discrepancies has lead some authors to question the CDM model and to propose alternative scenarios. For example, the number of satellite halos in Milky Way-sized galaxies, as predicted by simulations, exceeds the number of observed Dwarf galaxies [94, 95]. Furthermore, the rotation curves of low surface brightness

(LSB) galaxies point to DM distributions with constant density cores rather than the cuspy profiles preferred by N-body simulations [96, 97, 98, 99]. An additional problem arises when considering the angular momentum of dark matter halos: in simulations gas cools at early time into small mass halos, leading to massive low-angular momentum cores in conflict with the observed exponential disks [100].

Several astrophysical processes have been invoked in order to solve these problems, such as major mergers and astrophysical feedback[101]. The low efficiency of gas cooling and star formation may decrease the number of satellites in Milky Way-sized galaxies [102, 103, 104] and tidal stripping may have dramatically reduced the size of these substructures or disrupted a fraction of them [106, 107]. Furthermore, new ultra-faint dwarf galaxies have been recently detected, alleviating the discrepancy between CDM predictions and observations [105]. It has also been pointed out that the measurements of the LSB galaxies rotation curves may suffer of observational biases, for example due to the fact that DM halos are triaxials rather than spherically symmetric [108]. Moreover, small deviations of the primordial power spectrum from scale invariance, the presence of neutrinos [109] or astrophysical processes [110, 111] can sensibly affect the halo profiles. Anyway, the lack of convincing explanations of the problems discussed above leaves the door open to alternatives to the CDM scenario.

Warm Dark Matter

To alleviate these problems, Dark Matter candidates with a strong elastic scattering cross section (SIDM) [112], or large annihilation cross sections [113] have been proposed. It has also been suggested that Dark Matter is *warm*, i.e. made of particles with velocity dispersion between that of HDM and CDM particles. The larger free-streaming length of WDM, with respect to CDM, reduces the power at small scales, suppressing the formation of small structures [114, 115]. For instance, a WDM particle with a mass of 1 keV and an abundance that matches the correct Dark Matter density, has a free-streaming length of order of galaxy scales $\lambda_{FS} \sim 0.3$ Mpc [116]. Measurements of the growth of structures in galaxy clusters and Ly-α forest can then be used to set a lower bound on the mass of the WDM particle. Gravitinos in gauge-mediated supersymmetry breaking models might be warm DM candidates, if they decouple when the number of degrees of freedom was much larger than at the neutrino decoupling [117]. However, explicit computations show that such a light thermal gravitino cannot account for all the DM [116].

Another WDM candidate is the sterile neutrino, produced in the early Universe by oscillation conversion of thermal active neutrinos, with a momentum distribution significantly suppressed and distorted from a thermal spectrum [118, 71, 78]. Its free-streaming scale is

given by (see e.g. [31])

$$\lambda_{FS} \approx 840 \text{ Kpc h}^{-1} \left(\frac{1 \text{ KeV}}{m_s}\right) \left(\frac{< p/T >}{3.15}\right),$$

where m_s is the mass state associated to the sterile flavor eigenstate. $< p/T >$ is the mean momentum over temperature of the neutrino distribution and the ratio $< p/T > /3.15$ ranges from ≈ 1 for a thermal WDM particle to ≈ 0.9, for a non-thermal sterile neutrinos distribution.

The suppression of the power spectrum by a thermal WDM of a given mass m_{WDM}, is identical to that produced by sterile neutrinos of mass m_s derived by [119, 116]:

$$m_s = 4.43 \text{ KeV} \left(\frac{m_{WDM}}{1 \text{ KeV}}\right)^{4/3} \left(\frac{0.25(0.7)^2}{\Omega_{WDM}}\right)^{1/3}.$$

This one-to-one correspondence allows to translate the bounds on sterile neutrinos to a generic thermal relic and viceversa.

A detailed analysis of the production of sterile neutrinos and of the evolution of their perturbations, as well as a comparison with the measured matter power spectrum, have been performed in Refs. [116, 120, 121, 122, 123]). The resulting lower limits on the mass of the WDM particles strongly depend on the dataset used in the analysis. For example, in [120], a combination of the SDSS 3D power-spectrum and SDSS Ly-α forest allowed to constrain the sterile neutrino mass to

$$m_s \geq 1.7 \text{ KeV (95 \%CL)},$$

that translates in terms of a thermal WDM particle to

$$m_{WDM} \geq 0.50 \text{ KeV}.$$

The inclusion of high resolution Ly-α data makes the constraint even stronger, even if it has been pointed out that they may suffer of large systematic uncertainties [120, 116].

More recently, very stringent bounds on the mass of WDM particles have been obtained by different groups: [122]

$$m_s \geq 14 \text{ KeV (95 \% CL)} \ (m_{WDM} \geq 2.5 \text{ KeV})$$

and [123]:

$$m_s \geq 28 \text{ KeV } (2\sigma) \ (m_{WDM} \geq 4 \text{ KeV}).$$

The Lyman-α bounds have been revisited recently in [124] and new limits have been derived for the case of a mixed Cold plus Warm Dark Matter model.

The delay of the reionization of the Universe also sets a constraint on the WDM mass [125, 126, 127]. In the case of sterile neutrinos, the X-rays produced by their decays can modify the picture, enhancing the production of molecular hydrogen and releasing heat in gas clouds [128, 129, 130].

2.4 Is it neutral?

Some extensions of the Standard Model of particle physics predict the existence of new, stable, electrically charged particles, such as the lightest messenger state in gauge-mediated supersymmetry breaking models [131] or even the LSP in the R-parity conserving Minimal Supersymmetric Standard Model (MSSM).

Massive charged particles, independently on the context they emerge, have been proposed as Dark Matter candidates by De Rújula *et* al and dubbed CHAMPs [132]. Evaluating their thermal relic abundance, with simple assumptions on the annihilation cross sections, the authors found a viable mass range of $\sim 1 - 1000$ TeV. They also pointed out that a positively charged particle X^+ can capture an electron to form a bound state chemically similar to an heavy hydrogen atom. An X^- can instead bind to an α^{++} particle and an electron, resulting again in a heavy hydrogen-like atom, or alternatively it can capture a proton to produce a bound state called neutralCHAMP. The different behaviors of CHAMPs and neutralCHAMPs lead to different bounds on their abundance. Note also that De Rújula *et* al. concluded that X^- would emerge from Big Bang Nucleosynthesis preferentially in the form of neutralCHAMPs [132].

Galactogenesis models provide constraints on the Dark Matter interactions, in particular of CHAMPs. The energy loss timescale in this case is in fact dominated by Coulomb scattering off electrons and protons, and it must be longer than the dynamical timescale for galaxy formation. In Ref. [132], the authors concluded that only CHAMPs heavier than 20 TeV are able to remain suspended in the halo, and to be therefore rare on Earth. This estimate disagree with that obtained by Dimopoulos *et* al who found, for the same considerations, the limit $M_X > 10^5$ TeV [133]. The discrepancy is due to the different choice of the target of CHAMPs scattering in the computation of the energy loss rate, respectively protons and electrons for De Rujula *et* al and Dimopoulos *et* al.

It has also been proposed that shock accelerations in supernovae could eject CHAMPs from the disk and reinject them back to the halo or out of the galaxy. The latter possibility is energetically disfavored, while in the former case, it may lead to a dangerous heating of the disk [133]. Recently this scenario have been reexamined and it has indeed been proposed that the disk formation may have been different in CHAMPs models, possibly leading a solution to the angular momentum problem[134].

One of the most stringent bounds on the CHAMPs abundance comes from searches of anomalous heavy water: CHAMPs, being chemically identical to heavy hydrogen, can be trapped in oceans and lakes in the form of HXO. If one assumes, as in Ref. [132], that CHAMPs heavier than 20 TeV remain suspended in the Galactic halo and they provide the Galactic DM, taking an accumulation time of 3×10^9 yr, comparable with the age of

oceans, the abundance of CHAMPs in sea water is predicted to be [135]:

$$\left(\frac{n_X}{n_H}\right)_{Earth} \sim 3 \times 10^{-5} \left(\frac{\text{GeV}}{m_X}\right) \Omega_X h^2.$$

If instead CHAMPs are present in the Galactic disk, taking in account the density and velocity of the interstellar gas, mostly hydrogen, the expected concentration is [135]:

$$\left(\frac{n_X}{n_H}\right)_{Earth} \sim 6 \times 10^{-5} \left(\frac{\text{GeV}}{m_X}\right) \Omega_X h^2.$$

All the searches of anomalous hydrogen in sea water have failed so that the abundance of CHAMPs, for masses in the range 100 GeV-1000 GeV is constrained to be

$$\left(\frac{n_X}{n_H}\right)_{Earth} \sim 10^{-28} - 10^{-29},$$

while it raises to $(n_X/n_H) < 10^{-20}$ for $M_X \sim 10$ TeV (see [136] for a compilation of upper bounds of heavy hydrogen from sea water searches). As a result, CHAMPs as DM candidates are ruled out in the mass range $M_X \sim 10 - 10^4$ GeV.

NeutralCHAMPs would preferentially bind on Earth to nuclei to form anomalous heavy isotopes. Null searches for these elements, covering a variety of nuclear species, constrain the NeutralCHAMPs abundance to be $< 10^{-20} - 10^{-16}$ for $M_X \sim 100 - 1000$ GeV [137] (for further details see [136] and references therein). The authors of Ref. [137], concluded that stable X^- Dark Matter in the mass range $10^2 - 10^4$ GeV is thus to be considered unlikely.

CHAMPs are also constrained by balloon or satellites experiments for Cosmic Rays studies. Perl *et* al, taking in account data from different experiments [133, 139, 140], excluded CHAMPs as Galactic Dark Matter in the mass range $2.4 \times 10^3 - 5.6 \times 10^7$ GeV and neutralCHAMPs for $10^5 - 4 \times 10^7$ GeV [138]. The lower limit comes from the requirement that particles penetrate the solar wind and the energy deposition is above the experimental threshold. The upper bound is obtained comparing the maximum CHAMP flux at the top of the atmosphere allowed by the CR experiments, with the local DM flux, which is typically assumed to be $\phi \sim 10^7 (\text{GeV}/M_X)$ cm^{-2}s^{-1}.

In the atmosphere, a proton in a neutralCHAMP gets replaced very quickly by a ^{14}N atom, and the exchange is followed by a MeV γ-ray emission from the excited $^{14}NX^-$ status. With the same argument explained above, the observational limits on γ-rays flux imply that neutralCHAMPs should be heavier than 10^6 GeV if they are to be the DM[133]. Further constraints on CHAMPs come from deep underground experiments. The responses of scintillators to monopoles and CHAMPs are expected to be similar, since they are both slowly moving, highly ionizing and penetrating. In Ref. [138], the authors applied the upper limit on monopole flux, obtained from MACRO experiment, to the CHAMP case, excluding the mass range $10^8 - 10^{20}$ GeV.

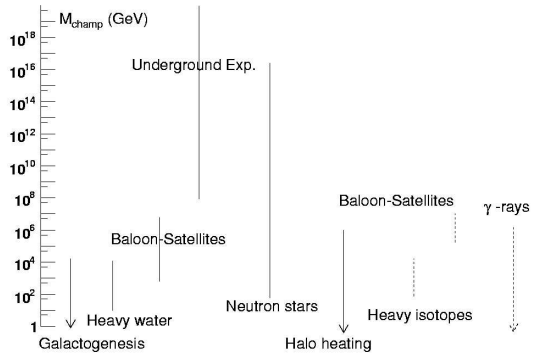

Figure 2.2: Exclusion plot for CHAMPs (solid lines) and NeutralCHAMPs (dotted lines). See text for more details.

Further constraints come from stellar evolution, in particular it has been shown that CHAMPs can disrupt a neutron star in a short timescale, falling into its center and producing a Black Hole. This argument excludes CHAMPs with masses $10^2 - 10^{16}$ GeV [597]. In addition, the properties of diffuse interstellar clouds constrain the interactions of halo particles with atomic hydrogen: the rate of energy deposition due to collisions must be smaller than the cooling rate, for clouds in equilibrium. It results that CHAMPs with masses below 10^6 GeV are ruled out because, for these particles, the expected cross section with hydrogen is higher than the maximum allowed value [142].

The various constraints on CHAMPs that we have discussed are summarized in Fig. 2.2. Even if the bounds are not completely model-independent, the combination of them basically rules out CHAMPs as DM, expect for the case of exotic scenarios [134].

The above limits apply to particles with integer electric charge, but theoretical frameworks have been proposed where particles with fractionary electric charge exist, also known as milli-charged particles [145, 147, 143, 144, 146, 148]. For example, adding a new unbroken $U(1)^{'}$ gauge group, the photon and paraphoton can mix, and particles charged under $U(1)^{'}$ can have a small coupling with photons [143]. Moreover, realistic extensions of SM motivated by string theory exist, that naturally implement this mechanism [145].

Constraints on mass and charge of milli-charged particles come from a variety of observations, and in Fig. 2.3 we show the excluded regions in the parameter space (m_q, ϵ), with $\epsilon = q/e$, obtained by Davison *et* al. [149].

Milli-charged particles can also affect CMB anisotropies, and for this reason WMAP data can severely constrain their cosmological abundance, at least in some regions of the

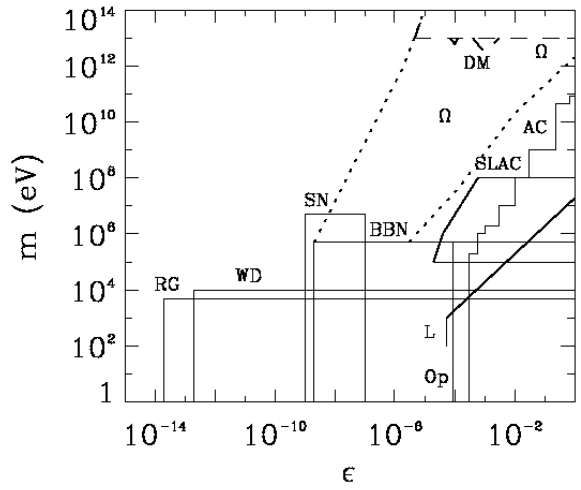

Figure 2.3: Excluded regions in the mass-charge plane for milli-charged particles. The constraints are relative to: RD plasmon decay in red giants; WD plasmon decay in white dwarfs; BBN big bang Nucleosynthesis; SN Supernova 1987A; AC accelerator experiments; SLAC SLAC millicharged particle search; L Lamb Shift; Op invisible decay of ortho-positronium; DM Dark Matter searches. From Ref. [149].

milli-charged particle parameter space [150].

Furthermore, searches of neutrino magnetic moment with reactor experiments exclude Dark Matter particles with $q > 10^{-5}e$, for masses $m_q \lesssim 1$ keV [151].

The result of the PVLAS collaboration [152] have been tentatively interpreted in terms of milli-charged particles with masses $m_q \sim 0.1$ eV and fractional electric charge $\epsilon \sim 10^{-6}$ [145, 146, 154], but the experimental result was not confirmed after an upgrade of the PVLAS apparatus [153].

Light milli-charged particles may largely affect sub eV Cosmology. In particular, processes such as $\gamma\gamma \to q\bar{q}$ can distort the CMB energy spectrum, which has been measured with high sensitivity by FIRAS. A detailed analysis has been performed in Ref. [155] and the authors reported the conservative upper bound $\epsilon \lesssim 10^{-7}$, for $m \lesssim 1$ eV, excluding in this way also the light milli-charged particles proposed in Ref. [145, 146, 154].

In principle, DM particles could have a $SU(3)_c$ charge. For example, "colored" candidates are naturally predicted in SUSY models if the LSP is a squark [156] or a gluino [157, 158], or in gauge mediated SUSY breaking models, where messengers can be colored and stable [159], or in mirror models [160]. These "heavy partons", after the deconfinement

temperature, $T \sim 180$ MeV, are surrounded by a QCD cloud and confined inside hadrons forming a color neutral bound state [161]. These particles can be actively searched for by underground experiments, indirect detection experiments or through the search of rare anomalous isotopes.

Since the proposal that DM might interact strongly with ordinary matter (SIMP), regardless of the nature of the interaction [132, 133, 162], many candidates have been put forward, but also many constraints on the scattering cross section off nuclei, $\sigma_{\chi N}$.

For example, the SIMPs interactions with baryons may disrupt the disk of spiral galaxies [162, 163]. Moreover, they may dissociate the light elements produced during Big Bang Nucleosynthesis, while SIMPs collisions with Cosmic Rays can produce an observable γ-ray flux [164]. The scattering of SIMPs off baryons also produces substantial distortion of CMB anisotropies and of the large scale structure power spectrum [165]. The SIMPs abundance for the mass range $\sim 1 - 10^3$ GeV, is also constrained by searches in terrestrial samples of gold and iron [166].

Atmospheric and satellite experiments, originally intended for other purposes, have been used to investigate high DM cross sections with baryonic matter. In particular, the results of the X-ray Quantum Calorimeter experiment (XQC) allow to rule out a large portion of the SIMP parameter space (M_χ, $\sigma_{\chi N}$), as discussed in Refs. [167, 168] and (more recently and with substantial changes with respect to previous analyses) in Ref. [169].

Complementary constraints are obtained by underground experiments, which are sensitive to DM particles with small interactions. In fact, they are able to detect SIDM particles if their interactions with ordinary matter are high enough to trigger a nuclear recoil in the detector but at the same time low enough to allow the particles to penetrate the Earth crust to the detector [170].

Recently, Mack *et* al. have analyzed the effect of SIMP annihilations on Earth, showing that a substantial heating of the Earth's core may occur, if the capture rate is efficient [171]. This argument rules out the regions of the parameter space lying between astrophysical and underground detector constraints.

To summarize the constraints on the SIMP scenario, Fig. 2.4 shows the excluded areas in the SIMP parameter space. The bounds leave no room for SIMPs as Dark Matter candidates in a very large mass range. Since the neutron-neutron scattering cross section is of order $10^{-25} - 10^{-24}$ cm^2 and the expected value for colored Dark Matter candidates is not far from this range (see e.g. [172]), DM particles are thus unlikely to bring color charge.

However, these constraints can be evaded by very massive composite dark matter candidates. For example macroscopically large nuggets of ordinary light quarks and/or anti-quarks, with masses in the range $m \sim 10^{20} - 10^{33}$ GeV, can behave as collisionless cold dark matter, without contradicting observations [173].

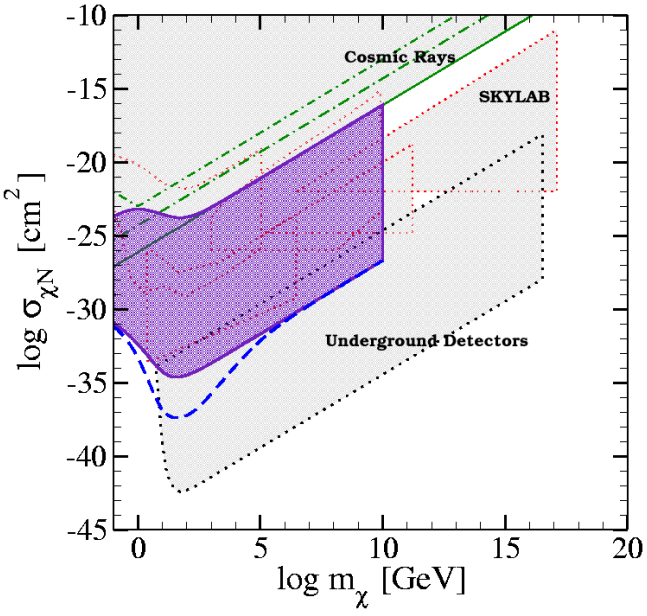

Figure 2.4: Excluded regions in the SIMP mass versus SIMP-nucleon cross section plane. The Violet area is excluded by the Earth's heat argument. See Ref.[171] and references therein.

2.5 Is it consistent with BBN?

Big Bang Nucleosynthesis (BBN) is one of the most impressive successes of the Big Bang Cosmology (See [15, 174] for reviews). It predicts the abundances of light elements produced in the first 3 minutes after the Big Bang, in agreement with the observations over a range spanning nine order of magnitudes.

The model is based on a set of coupled Boltzmann equations relating the number densities of protons, neutrons and light elements, through a network of nuclear chemical reactions. The weak interactions maintain the neutron-proton ratio to its equilibrium value until the freeze-out, that occurs at roughly 0.7 MeV. Later, nearly all neutrons are captured in the nuclei producing principally the most stable element ^{4}He. Smaller amount of ^{2}H, ^{3}H, and ^{7}Li are synthesized but the production of heavier elements is suppressed by the large Coulomb barriers. Looking for astrophysical environments with low metallicity, it is possible to infer the primordial abundance of light elements in order to test the predictions of BBN.

In the framework of the Standard Model, BBN depends only on the baryon to photon ratio η, and observations of the abundance of different elements agree with predictions in the range [15]

$$4.7 \leq \eta \cdot 10^{10} \leq 6.5 \text{ (95\% CL)}.$$

The agreement between predictions and measurements is a powerful success of the model

and it is remarkable that the inferred abundance of baryons quoted above is also consistent with the estimate of CMB experiments like WMAP [13]. BBN also provides a test of physics beyond the Standard Model, and it also constraints deviations from Standard Cosmology. In fact, the primordial abundance of ^{4}He is proportional to the ratio n/p and its value is related to the freeze-out temperature of the weak interactions and it is therefore sensitive to the expansion rate at that time.

Since $H \propto g_*^{1/2} T^2$, an increase of the relativistic degrees of freedom g_* with respect to the SM value leads to a faster expansion rate, thus to an earlier freeze out of the neutron to proton ratio and consequently to a higher ^{4}He abundance (and in general it also affects the abundance of the other light elements). At T$\sim$ 1 MeV, the relativistic species in the Standard Model are photons, electrons and neutrinos so with N_ν neutrino family $g_* = 5.5 + \frac{7}{4} N_\nu$ and for $N_\nu = 3$ this gives 43/4.

New relativistic particles can be accounted for through the introduction of an effective number of neutrinos:

$$\frac{7}{4}(N_\nu - 3) = \sum_{i=\text{extra b}} g_i \left(\frac{T_i}{T}\right)^4 + \frac{7}{8} \sum_{i=\text{extra f}} g_i \left(\frac{T_i}{T}\right)^4 ,$$

where T_i parametrizes the energy density of the relativistic species and b (f) stands for bosons (fermions).

A likelihood analysis, taking η and N_ν as free parameters, and based on the abundance of ^{4}He and ^{2}H, constrains the effective number of neutrinos to be [175]:

$$1.8 < N_\nu < 4.5 \text{ (95\% CL)}.$$

Assuming the value of η inferred by CMB experiments, the limit is further strengthened to [175]:

$$2.2 < N_\nu < 4.4 \text{ (95\% CL)}.$$

These bounds on N_ν can be applied to new species affecting the expansion rate during nucleosynthesis, such as gravitons [176], neutrinos with only right-handed interactions [175] or millicharged particles [149]. For a large class of supergravity models with a light gravitino, the requirement $N_\nu < 4$ rules out gravitino masses below 1 eV [177]. However, particles coupled to photons or to neutrinos during BBN, with masses in MeV range, have a non trivial impact on BBN, that cannot be accounted for with an equivalent number of light neutrinos [178].

For instance, it has been suggested that MeV Dark Matter, with masses in the range 4-10 MeV and coupled with the electromagnetic plasma, can lower the helium and deuterium abundances, contrary to what one naively expects, and it can therefore improve the agreement between the predicted and measured ^{4}He abundance [179].

In addition, the predictions of BBN can be dangerously modified by the decays of particles during or after BBN. For example, radiative decays induce electromagnetic showers and the subsequent photon-photon processes can destroy the light elements. In the early stages of BBN, $t < 10^2$ sec, hadronic decays may modify the interconversion of protons and neutrons, increasing the n/p ratio and consequently enhancing the ^{4}He and ^{2}H abundance. The opposite effect occur for late hadronic dacays, $t > 10^2$ sec, when the energetic hadrons trigger the ^{4}He dissociation.

Accurate calculations, with the use of BBN codes, restrict the primordial abundance of the decaying particle, depending on its lifetime, mass and hadronic branching ratio [180, 181, 182, 183, 184]. These results can be applied for instance to NLSP gravitinos: BBN requires an upper limit to the reheating temperature, which controls the primordial gravitino abundance, and in some cases the restrictions could lead troubles to thermal leptogenesis and inflation models [181, 183]. The difficulties can be circumvented for example in the case of a heavy gravitino, which decays well before BBN [185, 186].

Alternatively, the gravitino could be stable and play the role of Dark Matter. In this case, the NLSP particle is typically long-lived, because of the extremely weak interactions of gravitino, and its late decays can affect BBN. Moreover, it has been pointed out that if the long-lived particles are charged, e.g the stau, they can form bound states with light elements, potentially overproducing ^{6}Li and ^{7}Li [187, 188, 189, 190, 191]. However, these elements can also be destroyed, alleviating the severe bounds on the CHAMPs abundance during BBN.

A neutralino NLSP is excluded [192, 193, 194], while sneutrino NLSP poorly affects BBN [195]. A stop NLSP is viable in some regions of the parameter space [196].

We note that these BBN bounds can be circumvented if the NLSP abundance is diluted due to a significant entropy production [197].

2.6 Does it leave stellar evolution unchanged?

Stellar evolution provides a powerful tool to constrain particle physics, providing bounds that are often complementary to those arising from accelerator, direct and indirect Dark Matter searches.

If Weakly interacting particles are light, they may be produced in the hot plasma in the interior of stars, and if they escape without further interactions, they represent an energy loss channel for the star, possibly modifying the stellar evolution. Such particles may also be detected on Earth, as was the case for neutrinos from SN 1987A, or they can be indirectly searched for through their decay products. Here we describe the most important observational consequences (see Refs. [198, 199] for extensive reviews).

Stars as the Sun can be described as self-gravitating gas in hydrostatic equilibrium, such

that the gas pressure equilibrates the gravitational force. A significant energy loss produces a contraction of the system and an increase of the burning rate of the stellar fuel, reducing the lifetime of the star and enhancing the neutrino flux. Moreover, exotic energy losses would modify the sound speed profile, which is accurately measured in the interior of the Sun by means of helioseismic measurements.

Globular Clusters are alternative interesting probes of stellar evolution models because they are gravitationally bound systems of up to a million stars, formed at the same time, with the same chemical composition and differing only for their masses. The ignition of helium in Red Giant stars is sensitive to the temperature and density of the helium core, and any energy loss channel inevitably tends to delay it, resulting in more massive cores and producing observational consequences, such as an enhancement of star brightness. Therefore, observations of Red Giants in Globular Clusters allow to derive an upper limit on the energy loss rate of the helium plasma, ϵ, [198]:

$$\epsilon \lesssim 10 \text{ erg g}^{-1}\text{s}^{-1} \text{ at T} \approx 10^8 \text{ K}, \rho \approx 2 \times 10^5 \text{g cm}^{-3},$$

where the value of temperature and density are appropriate for Red Giant cores. In Horizontal Branch stars, energy losses speed up the helium burning rate, decreasing their lifetimes, that can be measured by number counting in Globular Clusters. This argument provides another bound on ϵ [198]:

$$\epsilon \lesssim 10 \text{ erg g}^{-1}\text{s}^{-1} \text{ at T} \approx 0.7 \times 10^8 \text{ K}, \rho \approx 0.6 \times 10^4 \text{g cm}^{-3}.$$

In addition, the cooling rate of White Dwarfs, inferred by their luminosity functions, is in agreement with the predictions and therefore any new cooling channel has to be subdominant.

It is remarkable that the total number of neutrino detected from SN 1987A, their energy and their time distribution, is in agreement with expectations from the standard model which describes the core collapse of a star. Any further energy loss mechanism reduces the duration of the neutrino burst and can in principle spoil the success of the model, leading therefore to the following bound on ϵ [198]:

$$\epsilon \lesssim 10^{19} \text{ erg g}^{-1}\text{s}^{-1} \text{ at T} = 30 \text{ MeV}, \rho = 3 \times 10^{14} \text{g cm}^{-3}.$$

All the arguments listed above provide upper limits to any additional energy loss rate and can be applied to constrain, for instance, the neutrino properties, the graviton emission in theories with extra dimensions, as well as models with right-handed neutrinos, sterile neutrinos, milli-charged particles, axions and other pseudoscalar particles. For instance, updated limits on axions from stars are reviewed in Ref. [200] and the implications of light Dark Matter or sterile neutrino Dark Matter on Supernovae core collapse are discussed in Ref. [201, 202]. More details and references for other particle physics scenarios can be found in [198, 199].

As we have seen in Sec.2.4, the most restrictive bounds on the fractional charge of $\sim$ keV milli-charged particles come from stellar physics, as it was shown in Fig.2.3.

The bounds discussed above apply to particles that are produced in the core of stars and that escape without losing energy, thanks to their weak interactions. However, if the particles interact strongly, they undergo multiple scattering, providing a mechanism for energy transport, in competition with photons, electrons or convection. This effect has been studied for keV-mass scalars produced in the Sun, Horizontal Branch stars and Red Giants, constraining the interactions of these particles [203, 204].

Moreover, the energy transport channel, provided by the WIMPs trapped in the Sun, may cool its interior and decrease the neutrino flux. This idea was proposed in the past as a solution of the solar neutrino problem and WIMPs with masses and cross sections suitable for this purpose ($m \sim 4 - 10$ GeV $\sigma \sim 10^{-36}$ cm^{-2}) were called cosmions [205, 206, 207].

Stars in which the heat transport is dominated by core convection may be dramatically affected by WIMPs in the case of effective transport of energy. In fact, in this case, the convection is suppressed, and the core is not replenished with nuclear fuel from outer regions, leading to a reduced stellar lifetime and a modification of its evolution [208, 209]. As a consequence, main sequence stars would present an anomalous mass-to-luminosity relation and Horizontal Branch stars would develop thermal pulses [209, 210, 211]. However, taking in account the current limits on the WIMP-nucleon cross section inferred from direct searches, these effects seems to be hardly detectable for the Sun [212, 213].

Dark Matter annihilations may provide an important source of energy, which, for stars orbiting in high Dark Matter density regions, can even be comparable or overwhelm that originated by nuclear reactions. This scenario has been investigated in Ref.[214], in the case of main sequence stars orbiting close to the galactic center and more recently, by means of numerical simulations, in Ref.[215, 216, 217] The most recent analysis show that the most pronounced effects are on low-mass stars following elliptical rather than circular orbits [217]. These "WIMP burners" could be found in regions where a recent star formation is inhibited, looking for populations of stars appearing oddly younger then higher mass ones. Presently only high-mass stars have been observed on such tight elliptical orbits, but as observations improve over the next few years, any low-mass counterpart population may become observationally accessible.

The effect of DM decays and annihilations on the formation of first structures have been investigated for light DM candidates [130, 221]. Recently, it has been pointed out that even standard DM candidates, such as the neutralino, may substantially modify the evolution of Population III stars, which may even be supported by DM annihilations rather than nuclear reactions, during part of their evolution. We will discuss about this possibility in details in Chapter 5.

2.7 Is it compatible with constraints on self-interactions?

The collisionless and cold nature of Dark Matter, has been questioned during the last decade, because of apparent discrepancies between the results of CDM simulations and observations. Two remarkable problems, as mentioned in Sec. 2.3, are the conflict between the cuspy DM halos predicted by N-body simulations and the constant core profiles inferred by LSB and dwarfs [96, 97] and the excess of substructures in CDM halo with respect to the observed number of galaxy satellites [94, 95].

Although astrophysical explanations exist for the observed discrepancies, [102, 103, 108, 109, 110, 111], many attempts have been made to modify the properties of DM particles in order to reproduce the appropriate astrophysical phenomenology. A possible solution is that DM is *warm* rather than *cold*, as mentioned before. Alternatively, DM might be self-interacting (SIDM), as proposed by Spergel and Steinhardt, with large scattering cross section (and small enough annihilations cross sections, in order to be consistent with the bounds from indirect detection) [112]. The net effect, under these assumptions, is that the central cusp reduces to an almost constant core. Moreover, subhalos can be destroyed by interactions with the surrounding halo particles, because they are excessively heated or because particles are scattered out of the them [112, 167]. Suitable SIDM candidates include Q-balls [112, 222], a quark-gluino bound state [223, 167] and scalar gauge singlets coupled with Higgs field [224].

Semi-analytical calculations and N-body simulations have been developed to study the effect of SIDM interactions on halo structures, especially for what concerns the formation of flat cores. Different solutions are obtained, depending on the ratio between the mean free path of the Dark Matter particle ($\lambda_{mfp} \propto (\rho\, \sigma/m)^{-1}$, with n the number density and σ/m the scattering cross section per unit mass of the SIDM) and the virial radius of the halo. A cross section per unit mass in the range $\sigma/m \sim 0.5 - 5\mathrm{cm}^2\mathrm{g}^{-1}$ was found to correctly reproduce the observed profile of galaxies [225, 226, 227, 228]. More recently, Ahn and Shapiro have found a much higher value, $\sigma/m \simeq 200\mathrm{cm}^2\mathrm{g}^{-1}$, as the best fit to LSB rotation curves [229].

Several constraints exist on SIDM interactions. For instance, Gnedin and Ostriker have shown that, for $0.3 \lesssim \sigma/m \lesssim 10^4$ cm^{2}g^{-1}, galactic halos in clusters would evaporate in a timescale shorter than an Hubble time [230]. Following the suggestion of Furlanetto and Loeb [231], Natarajan *et* al. compared the predicted truncation radii of SIDM halos with those of observed galactic halos in clusters, inferred by gravitational lensing, excluding $\sigma/m > 42$ cm^{2}g^{-1} [232].

An upper limit of $\sigma/m < 0.1$ cm^{2}g^{-1}, has been obtained by Arabadjis *et* al. comparing the results of simulations with the profile of the cluster MS 1358+62 [233]. Hennawi and

Ostriker ruled out $\sigma/m \gg 0.02$ cm^{2}g^{-1}, pointing out that the supermassive black holes at the center of galaxies would be more massive than observed [234]. The evidence of ellipticity in DM halos has been used to rule out $\sigma/m > 0.02$ cm^{2}g^{-1} because self-interactions tend to produce more spherical halos [235]. The limits reported above rule out the range of cross sections required to explain the mass profiles of galaxies, although the underlying simplifying assumptions and incomplete statistics suggest to take them with a grain of salt (see e.g. [229, 236]).

More robust results are obtained from the analysis of the 1E 0657-56 cluster of galaxies [9], which actually consists of a bullet-like gas sub-cluster, exiting the core of the main cluster at high velocity, $v \sim 4700$ Km s^{-1}. The combination of optical and X-ray images with the weak lensing map, shows that the centroid of the collisionless subcluster galaxies is ahead of the subcluster gas distribution and coincident with that of the Dark Matter clump. This cluster not only provides a robust visual evidence for Dark Matter, but it is also provides a probe of its collisionless nature.

The subcluster DM halo would be dragged by the main halo in presence of DM self-interactions, leadig to an offset between the galaxies centroid and the total mass peak inferred through weak lensing measurements. Moreover, the measured high merger velocity implies that eventual drag forces, due to DM collisions, are small. Finally, the mass to light ratio of the subcluster is in agreement with that observed in other clusters and in the main cluster, while SIDM would tend to scatter out the particles from the subcluster.

Markevitch *et* al. found that the latter argument provides the most restrictive limit to the self interaction cross section, $\sigma/m < 1$ cm^{2}g^{-1} [236]. Making use of more recent observations and more accurate N-body simulations, this bound has been slightly improved, $\sigma/m < 0.7$ cm^{2}g^{-1} [237]. Since this constraint assumes an identical mass-to light ratio of cluster and subcluster before the merger, a more robust limit is inferred by the absence of an offset between galaxies and total mass peaks, which implies $\sigma/m < 1.25$ cm^{2}g^{-1} [237]. Almost the full range of cross sections needed to solve the discrepancies emerged in CDM models, $\sigma/m \sim 0.5 - 5$cm^{2}g^{-1}, is ruled out, thus disfavoring SIDM.

It has been suggested that the scattering cross section might be velocity dependent, thus smaller on average in clusters than in galaxies (e.g. [227, 230, 234, 238]). A possible functional form is

$$\sigma = \sigma_* \left(\frac{100 \text{ Km s}^{-1}}{v_{rel}} \right)^a .$$

In order to avoid a fast evaporation of the cluster or a core collapse, the parameters are restricted to be: $\sigma_* = 0.5 - 1$ cm^{2}g^{-1} and $a = 0.5 - 1$ [230, 234], and simulations have confirmed that in this range, predictions match the observed flat cores [227]. However, observations of the LSB galaxy NGC 5963 seem to require an effective cross section per unit mass $\sigma/m < 0.2$cm^{2}g^{-1}, in the low velocity regime ~ 150 km s^{-1}, at odds with the quoted range [239].

In addition to the bounds presented above, that constrain the cross section per unit mass, additional limits come from the unitary of the scattering matrix [39, 40]. This argument provides upper bounds on the total cross section and inelastic cross section. In the low energy regime, taking in account the range of SIDM elastic cross sections needed to the reproduce the observed halo profile, the constraint on the total cross section can be turned into an upper bound on the SIDM mass: $m < 12$ GeV [40]. Possible exceptions to unitarity bounds have been discussed in Refs. [39, 40].

Self-annihilating DM has also been proposed to solve the cold dark matter cusp crisis [113] This scenario is however ruled out by the comparison of the neutrino flux from the Galactic center with the measured rate of (atmospheric) neutrinos, i.e. the least detectable among the final states produced in DM annihilations [240]. For the mass range $10^{-1} - 10^5$ GeV, $\langle \sigma_{ann} v \rangle$ has to be less than roughly 10^{-21} cm^{3}s^{-1}.

2.8 Is it consistent with direct DM searches?

Direct DM searches aim at detecting DM particles through the measurement of nuclear recoils produced by DM scattering. Despite the large DM flux expected at Earth, $\Phi \sim 10^5 (100 \text{ GeV}/m_{DM})$ cm^{-2}s^{-1} assuming a local density of $\rho_0 \sim 0.3$ GeVcm^{-3} and mean velocity of $\bar{v} \sim 220$ km s^{-1}, the weakness of WIMP interactions with nuclei makes direct detection challenging (see e.g. [241] for a review of direct searches).

The coupling between a WIMP and a nucleon receives contributions from both scalar (spin independent) and vector (spin dependent) interactions. The cross section for spin independent (SI) coupling with a nucleus (N) cross section is coherently enhanced with respect to the case of single nucleons:

$$\sigma_N^{SI} \simeq A^2 (M_{red}(N, M_\chi)/M_{red}(p, N_\chi))^2 \sigma_p^{SI}$$

where A is the atomic number and M_{red} is the reduced mass of the system WIMP (χ) - nucleus (proton) [242].

Although heavy nuclei are used in current DM direct detection experiments, the results are often given in terms of scattering cross section off protons in order to allow easy comparison between different experimental settings, involving different target materials. For spin dependent (SD) couplings, there is no coherent enhancement, and the cross section is determined by unpaired neutrons or protons in the target nucleus. For this reason, SI interactions usually dominate the cross section in current experiments, which exploit heavy nuclei. However, in region of parameter space where scalar coupling is suppressed, spin dependent couplings may represent the leading contribution to the direct detection event rate [243, 244].

The signature of DM elastic scattering off nuclei are nuclear recoils, characterised by an exponential recoil spectrum with typical energies of $\mathcal{O}(10)$ keV or less, for WIMP masses

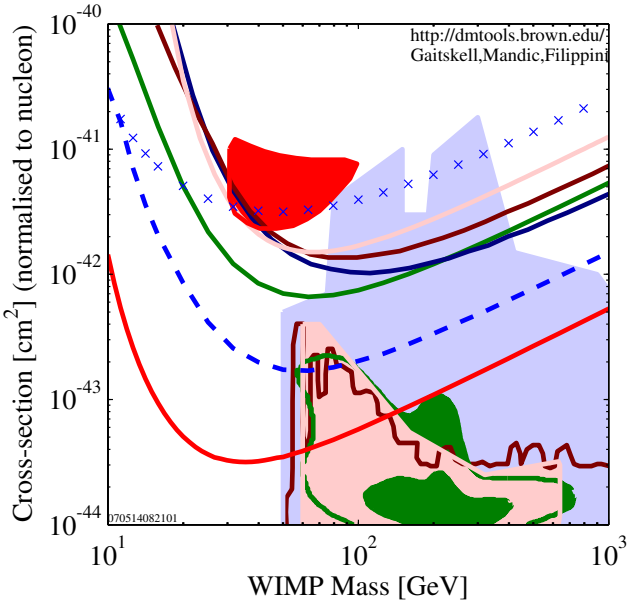

Figure 2.5: Upper limits on the spin independent WIMP-nucleon cross section, versus WIMP mass. The blue dashed (points) line is the Ge (Si) CDMS bound [255]. The dark red, pink, green and dark blue curves are the experimental limits respectively from EDELWEISS [258], CRESST 2004 [259], ZEPLIN II (Jan. 2007) [260] and WARP [261]. The lowest red solid line shows the first results from XENON 10 [256]. The red shaded region is the parameter space favored by DAMA experiment [252]. Supersymmetric models allow the filled regions colored: pink [262], green [263], dark red [264] and blue [265]. This figure has been obtained with the use of the interface at http://dendera.berkeley.edu/plotter/entryform.html.

between 1 and 100 GeV (see for more details e.g. [4]). In the case of inelastic scattering off nuclei or orbital electrons, the recoil is followed by a decay photon from the excited state [245, 246]. However, the natural radioactivity background makes the detection of this signal very problematic.

Current experiments exploit a variety of detection techniques, focusing on signals such as scintillation, phonons, ionization or a combination of them, as well as a variety of targets, e.g. NaI, Ge, Si and Xe.

In order to discriminate a DM signal against the natural background, some experiments have been searching for an annual modulation of the measured event rate [247]. In fact, the Earth rotation around the Sun is expected to produce a modulation of the relative velocity of DM particles given by

$$v_E = 220 \text{ Km/s } \{1.05 + 0.07 \cos[2\pi(t - t_m)]/1 \text{ year}\}$$

where t_m is approximatively the begin of June. The variation of the WIMP flux is actually

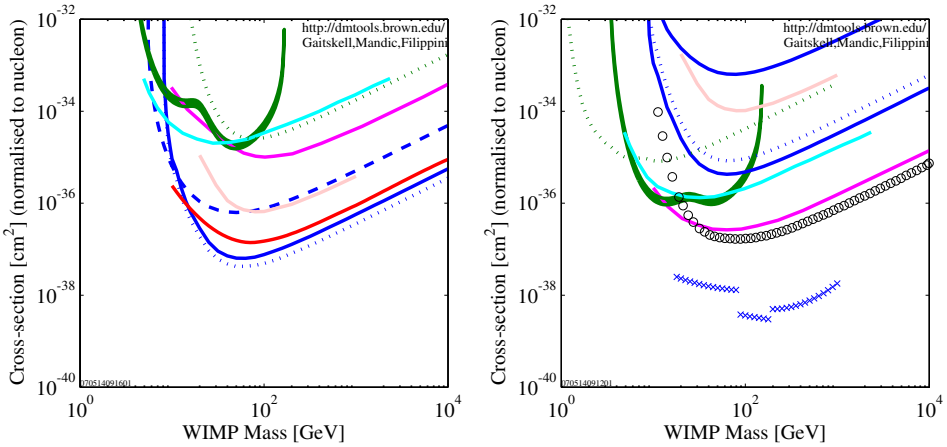

Figure 2.6: Upper limits on spin-dependent WIMP cross section as a function of the WIMP mass, in the case of a pure neutron (proton) and proton (left) coupling. The blue solid (dashed) line is the Ge (Si) CDMS bound [244]. The blue dotted line is the CDMS limit with an alternative form factor [244]. The light red, cyan, magenta and red curves are the experimental limits respectively from EDELWEISS [270], PICASSO [268], NAIAD 2005 [267] and ZEPLIN I [269]. The dark green shaded region shows the parameter space favored by DAMA experiments [266]. Finally the green points represent the CRESST results [266], the black crosses stand for Super-Kamiokande [271] and the black circles for KIMS 2007 [272]. The figures have been obtained with the use of the interface at http://dendera.berkeley.edu/plotter/entryform.html.

small $\approx$ 7%, so that a large number of events has to be collected and therefore a large detector is needed.

In 1998, the DAMA collaboration obtained evidence for a modulation of the event rate, that was later confirmed with a confidence level of 6.3 σ (see [248] for a recent discussion).

If interpreted in terms of a SI scattering of a WIMP off NaI, and further assuming an isothermal sphere DM halo, with a characteristic velocity of the Maxwell-Boltzmann distribution of $v_0 = 270$ Kms^{-1}, with a local DM density of $\rho = 0.3$ GeV cm^3, and with a slope $\rho \propto r^{-2}$, the DAMA result is compatible with the detection of a DM particle with a mass around 50 GeV and a WIMP-nucleons scattering cross section of order $10^{-41} - 10^{-42}$ cm^2.

Other experiments, such as CDMS and EDELWEISS, have explored the region of parameter space allowed by the DAMA modulation signal, finding null results [249, 250]. The comparison between the DAMA annual modulation and the other mentioned experiments is however model-dependent. Taking into account astrophysical uncertainties, the DAMA allowed region is sensibly increased, with masses extending up to $\sim$ 250 GeV and spin independent WIMP-proton cross section down to 10^{-43} cm^2 [251, 252, 253]. Nevertheless,

null searches of recent experiments make the most naïve interpretation of the DAMA signal problematic [254, 255, 256].

Recent investigations have shown that if the DAMA signal is interpreted in terms of WIMP elastic scattering off the target material, there still exist surviving small regions of the parameter space at low mass compatible with the results of the other experiments [274, 275]. Small windows are also found if one assume that the DAMA modulation is due to an inelastic scattering from a WIMP ground state to a slightly exited mass WIMP [276].

It should be stressed therefore that the DAMA signal should not be dismissed without further investigation, also in view of the fact that further theoretical scenarios (despite exotic) are still viable (see references in [274, 275, 276] for a complete bibliography on the subject).

The upper bounds on the WIMP spin-independent coupling inferred by several experiments are summarized in Fig. 2.5. The most stringent result (as of November 2007) was obtained by the XENON collaboration. The limits on SD cross section are far weaker and the best constraints, plotted in Fig. 2.6, come from CDMS [244], NAIAD [267], Super-Kamiokande [271] and KIMS [272]. A better sensitivity to spin dependent couplings is expected for the COUPP experiment, a heavy liquid bubble chamber under development in the NuMi gallery at Fermilab [273].

In comparison, the theoretical predictions of neutralino elastic scattering off nucleons, for different SUSY scenarios, show that current direct searches have begun to explore a relevant portion of the parameter space, while improved sensitivities are needed to perform a complete scan [277, 278].

Direct detection constraints exclude the left-handed sneutrino in the MSSM as dominant Dark Matter component. However, the right-handed sneutrino, in extensions of the MSSM, is a viable Dark Matter candidate, compatible with direct searches [279, 280].

2.9 Is it compatible with gamma-ray constraints?

Aside from direct and accelerator searches, one may search for DM through the detection of its annihilation products, such as photons, anti-matter and neutrinos.

In particular, since the energy scale of the annihilation photons is set by the DM mass, and since some of the most studied DM candidates, such as the supersymmetric neutralino and the LKP in UED models, are expected to lie in mass in GeV-TeV region, exotic gamma-ray sources are among the primary targets of indirect searches (see e.g. [281] for a review about DM searches though gamma-ray astrophysics). Significant emissions at other wavelengths is however predicted in most cases, due to the interactions of the annihilation products with ambient photons or magnetic fields, making multi-wavelength searches possible. Emission at different energy scales has also been discussed in the context of other DM

candidates, e.g. X-rays from the decay of sterile neutrinos (see Sec.2.10).

The gamma-ray flux from WIMP annihilations in a DM halo depends on the particle physics parameters as well as on cosmological quantities, such as the profile of DM halos. More precisely, the gamma-ray flux at earth (if the WIMP is not its own antiparticle a factor 1/2 must be added) is given by

$$\phi(\psi, E_\gamma) = \frac{\langle \sigma_{ann} v \rangle}{8\pi m_\chi^2} \frac{dN_\gamma}{dE} \times \int_{l.o.s.} ds \rho^2(r(s,\psi)),$$

where m_χ and $\langle \sigma_{ann} v \rangle$ are respectively the mass and the cross section annihilation times relative velocity of the DM particle. From Eq. 2.1 in Sec. 2.2 it follows that, to match the correct DM density, it is necessary for a cold thermal relic $\sigma_{ann} v \sim 10^{-26}$ cm^{3}s^{-1}, although this value is just indicative because, for instance, coannihilations can substantially modify the picture, plus the cross section in the non relativistic limit may substantially differ from the one at decoupling (e.g. in the case of p-wave annihilations). $\frac{dN_\gamma}{dE}$ is the photon spectrum from DM annihilations, that depends on the nature of DM candidate. Finally, the last term in the equation is the integration along the line of sight of the dark matter density squared. The quadratic dependence on ρ, suggests that ideal targets of indirect searches are regions where the DM density is strongly enhanced such as the Galactic center (e.g. [282, 283, 284, 285, 286, 287, 288, 306]), halo substructures (e.g. [289, 290, 291, 292, 293, 294]) and the core of external galaxies (e.g. [295, 296, 297, 298]). Prospects for detecting gamma-rays have been discussed also for overdensities in DM halos called caustics (e.g. [299, 300, 301, 302, 303]). Much steeper profiles, called *spikes*, may form due to adiabatic growth of black holes, for example around the Super Massive black hole at the Galactic center (see e.g. [464, 305, 306] for a discussion about the prospect for detecting DM annihilation gamma-rays in this scenario). Although in this case the spike is likely disrupted by astrophysical processes [464, 307, 308], a moderate enhancement, called crest, may form again due to gravitational interactions with the observed stellar cusp [309]. More promising targets may be mini-spikes around intermediate massive black holes, since they are not affected by dynamical processes that tend to lower the density enhancement [310, 311].

Although conclusive evidence for Dark Matter annihilations has not been obtained so far, gamma-ray experiments have nonetheless provided a wide range of observations that can be used as upper bounds of gamma-ray fluxes from DM annihilations, in order to constrain existing DM scenarios. In particular observations in the soft gamma-ray energy band, between roughly 50 keV and 1 MeV, have been performed by the Osse experiments [317] and more recently by INTEGRAL in the range 20-8000 keV (see [318, 319]). All-sky observations have been performed by COMPTEL in the energy range 3 MeV - 30 MeV [320], and EGRET from 30 MeV to over 30 GeV [321]. In Fig.2.7 we show the spectrum of the inner Galactic plane as measured by these experiments.

Current Air Cherenkov Telescopes such as CANGAROO [312], HESS [313], MAGIC

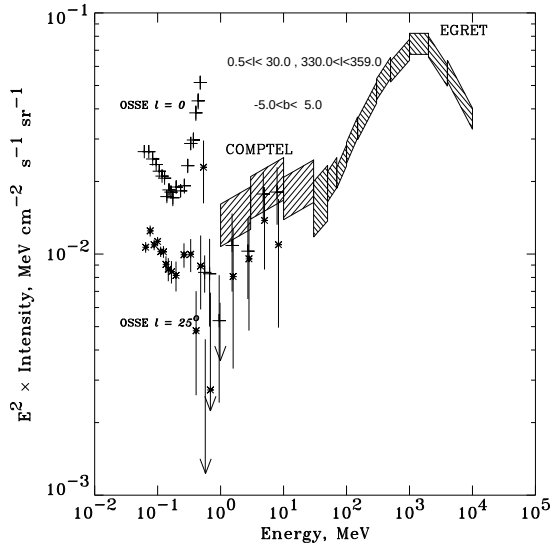

Figure 2.7: Spectrum of the inner Galactic plane for $|b| < 5^\circ$ measured by different experiments for energies ranging from sub MeV up to tens of GeV. From Ref. [320]

[314] and VERITAS [315] are collecting data at higher energies and the FERMI-GLAST satellite [316], which is now taking data, will allow much deeper observation in the energy range 20 MeV - 300 GeV.

As we have seen, there is no conclusive evidence of DM annihilations, but many claims of discovery, or hints of detection, have been been put forward in recent years. For example the gamma-ray source been detected by EGRET in the direction of the Galactic center, has been interpreted in terms of DM annihilations (as discussed e.g. in [288, 284, 285, 287, 322]), although it was subsequently suggested that the source may be slightly offset with respect to the Galactic center [323].

The HESS experiment has discovered a very high energy source spatially coincident with Sgr A*, the compact radio source at the Galactic center, and the spectrum has been subsequently confirmed by the MAGIC collaboration. Even in this case, however, the bulk of the signal can hardly be interpreted in terms of the annihilation of common DM candidates, since the shape of the energy spectrum is close to a perfect power-law over two decades in

energy, a circumstance that rather points towards ordinary astrophysical sources [282, 286].

Hints of a DM signal may hide in the cosmic gamma-ray background (CGB) which is is inferred from EGRET observations, after subtraction of the galactic component(see e.g. [330, 331, 332, 333, 334, 335]). The existence of a bump in the CGB spectrum at few GeV [324, 325] has been tentatively interpreted in terms of DM annihilations [326, 327, 328]. This cannot be however considered as evidence for DM, since the freedom in the DM (cosmological and particle physics) parameters allow enough freedom to explain almost any excess observed in the GeV-TeV range (see the discussion in [329]). In order to obtain conclusive answers, a more robust evidence could be provided by the power spectrum of the CGB anisotropies as can be obtained e.g. by FERMI [336, 337, 338].

Another observation awaiting for a (not necessarily exotic) interpretation is the INTEGRAL detection of an intense 511 keV emission line, due to positron annihilations, towards the galactic center. Many astrophysical sources of positrons have been proposed, for example interactions of cosmic-rays with the interstellar medium [339], pulsars [340], gamma-ray bursts [342], microquasars [343] or radiactive nuclei expelled by stars such as supernovae, Wolf-Rayet and red-giants [341] (see [281, 318] and references therein). However, conventional astrophysical scenarios, can hardly explain the size and morphology of the emitting region, that coincides roughly with the Galactic bulge and that exhibits a fainter disk component [318, 319]. Other more exotic interpretations are again open, in particular the positron source may be provided by DM annihilations. DM candidates with masses close to the electroweak scale have been excluded because the concomitant photon emission would violate the gamma-ray bounds. However, this problem may be circumvented in models where the WIMP shares a quantum number with a specie nearly degenerate in mass, with a splitting in the MeV-range [344, 345].

It has been shown that a DM candidate in the MeV range may successfully explain the 511 keV line, while remaining compatible with other observational constraints [346]. A list of alternative candidates include axinos [323], sterile neutrinos [348], cosmic strings [349], moduli [350], Q-balls [351] and scalars coupled to leptons with gravitational strength [348].

Upper limits on the WIMP mass, in order to be consistent with the EGRET and COMPTEL bounds, can be derived by comparing the gamma-ray emission from internal bremsstrahlung processes and in-flight annihilations with existing gamma-ray data [352, 353, 354], that set an upper limit on the mass of the DM particle of about 3-7 MeV (but see also [355]). This would be in conflict with the lower bound on the MeV DM particle mass (~ 10 MeV) inferred by the cooling rate and neutrino emission of the SN 1987A [201], unless the coupling of these particles with neutrinos is suppressed.

Anyway, all the Dark Matter interpretations of the 511 keV line are today disfavored by recent observations of the emission [356].

It is thus important to search for clear, smoking-gun signatures of DM. The first, and

maybe foremost, would be the detection of mono energetic gamma-ray lines, produced e.g. by neutralino or LKP annihilations via loop-diagrams with $\gamma\gamma$ or γZ as final states (see e.g. [285, 357, 330, 358, 359]) or also in models with scalar dark matter [360, 361]. A number of alternative strategies have been proposed over the years, see e.g. Ref. [362] for a recent review.

2.10 Is it compatible with other astrophysical bounds?

Neutrinos

Neutrinos can be produced in DM annihilations either directly or via the decay of other annihilation products, and may be detected with high-energy neutrino telescopes, that measure the Cherenkov light emitted by secondary muons propagating in water or ice.

The Sun and the Earth have been proposed as targets for indirect DM searches, since a large number of WIMPs could accumulate in their interior, releasing a large number of neutrinos. The neutrino flux depends on the capture rate of WIMPs in the Sun or in the Earth, thus on the elastic cross section of these particles.

The spin-dependent cross section is far less constrained than the spin-independent one (see Sec.2.7). Since in the Earth the abundance of nuclei with odd atomic numbers is very small, the capture rate is dominated by the strongly constrained spin independent coupling, contrary to what happens in the Sun. The prospects for detecting neutrinos from the center of the Earth are therefore not particularly promising, at least for current and upcoming experiments [364]. The null searches of AMANDA have been used to derive an upper limit on neutrino flux from WIMP annihilations, for example in the framework of neutralino Dark Matter [365]. In the framework of MSSM, however, the most optimistic neutralino scenarios will be probed by kilometer size neutrino telescopes such as IceCube [366].

The prospects for detecting neutrinos from the annihilation of Kaluza-Klein Dark Matter in the Sun are more promising, because of its large axial coupling, and the annihilations of B^1 particles to neutrino and tau leptons pairs, respectively forbidden and subdominant in the case of neutralino, dominate the neutrino spectrum, producing a large number of high energy neutrinos. The event rate in kilometer scale detectors is expected between 0.5 and 10 events per year [368].

The Galactic Center (GC), a well studied site for gamma-ray DM searches, offers instead poor prospects for detecting Dark Matter annihilations though neutrinos. An upper limit on neutrino flux from GC, in the case of neutralino Dark Matter, has been obtained by requiring that the associated gamma-ray emission would not exceed the flux measured by EGRET [369]. Unfortunately this bound is below the sensitivity of present and upcoming experiments, such as ANTARES, unless extreme scenarios are considered.

The prospects for detecting neutrinos from so-called *mini-spikes* around Intermediate

Mass Black Holes (see the discussion in Sec.2.9) appear more promising. The strong enhancement of the DM density around these objects induces a substantial boost of the DM annihilation rate, leading to neutrino fluxes within the reach of ANTARES and IceCube [370].

A combination of data from different neutrino telescopes can already be used to set an upper bound on the total DM annihilation cross section in the non-relativistic limit, for WIMP masses between 100 MeV and 10^5 GeV, which is stronger than the unitarity bound. [240].

Furthermore, neutrino experiments, as we have seen in Sec.2.8, can put strong limits on the spin-dependent WIMP-nucleon cross section, as those provided by Super-Kamiokande under the assumption that the equilibrium between WIMP capture and self-annihilation is reached in the Sun [271].

Antimatter

Indirect searches of Dark Matter can be performed by looking at an exotic contribution in the spectra of positrons and antiprotons in cosmic-ray fluxes. These charged messengers, contrary to gamma-rays and neutrinos, do not provide information on the location of their source because of the interaction with the interstellar magnetic field.

Positrons and antiprotons in cosmic-rays mostly originate from the interaction of cosmic ray protons and nuclei with interstellar gas. Analytic treatments and numerical codes have been developed to describe the propagation of cosmic rays, and to compute the amount of secondary cosmic rays, including positrons and antiprotons, produced by collisions of primary particles with the interstellar medium (see e.g. [377] for a review about the cosmic-ray propagation in the Galaxy). The measurement of the positron fraction, i.e. the ratio of the positron flux over the sum of the positron and electron fluxes and the antiprotons-to-proton flux ratio provide interesting tools to search for exotic positron/antiproton sources, for example Dark Matter annihilations. We will discuss in more details this interesting possibility in Chapter 4.

Here we just notice that current measurements of comic rays fluxes have not yet shown straightforward evidences for Dark Matter annihilations, even if very recent results look particulary promising for this purpose (See Chapter 4). Furthermore, cosmic-ray observations cannot be easily translated into constraints on DM candidates, due to the large uncertainties on the antimatter fluxes induced by the propagation parameters.

However, this is possible for specific DM scenarios. For instance, Bergström et al. have investigated the DM annihilation model of Ref.[378], proposed to explain the EGRET excess of the diffuse galactic gamma ray background, by computing the associated primary antiproton flux from WIMP annihilations. They were then able to rule out the scenario since the anti-proton flux was found to grossly exceed the measured anti-proton flux [379].

The model of Ref.[378] might still be made compatible with observations allowing for an anisotropic diffusion of cosmic rays [380].

Multi-wavelength approach and X-Rays emission

More in general, a multi-messenger, multi-wavelength analysis provides more robust results than the simpler *fit-the-bump* approach. For example, when interpreting the origin of a gamma-ray source, one may study the associated synchrotron, bremsstrahlung and Inverse Compton emission, produced by electrons and positrons inevitably produced along with gamma-rays in DM annihilations. These signals can in principle extend over a wide range of wavelengths, all the way from radio to gamma-rays. The limited field of view of radio and X-ray experiments makes it easier to perform multi-wavelength studies of a restricted number of candidate sources, such as the Galactic center [306, 381, 382, 383, 384] galaxy clusters [385, 386, 387, 388], and dwarf galaxies [389, 390, 391]. Radio and X-ray observations are powerful techniques to search for WIMP annihilations and they can provide constraints even more restrictive than those inferred from gamma-rays (e.g. [383, 384, 390, 382]).

X-ray observations provide useful constraints also on DM candidates other than WIMPs. For example, sterile neutrinos (see Sec. 2.3) can decay into active neutrinos ν_α and photons with energies in the X band: $\nu_s \rightarrow \nu_\alpha + \gamma$, $\mathrm{E}_\gamma = m_s/2$. Therefore, X-rays observations constrain the sterile neutrino mass m_s and their mixing angle with active neutrinos. Assuming then a production mechanism (see e.g. [76]), these limits can be turned into an upper bound on the particle mass. The observation of the cosmic X-ray background requires $m_s < 8.9$ keV (95 % C.L.) [392], but more stringent constraints are obtained from individual objects, such as galaxies or clusters of galaxies. For example the XMM-Newton observations of Virgo A impose $m < 10.6$ keV (95 % C.L.) [393] and an analysis of the Virgo and Coma cluster data further restrict the bound to $m < 6.3$ keV (95 % C.L.) [393, 394]. A significant improvement has been obtained from X-ray observations of the Andromeda Galaxy: $m < 3.5$ keV (95 % C.L.) [395]. These results, combined with the lower limit on the sterile neutrino mass inferred by measurements of small scale clustering (see Sec. 2.3), rule out sterile neutrinos in this scenario as the dominant Dark Matter component, constraining their fraction on the total Dark Matter amount to be $f_s \lesssim 0.7$ at the 2 σ level [396].

However, sterile neutrinos remain viable for alternative production mechanisms, such as Higgs decays in models with an extended Higgs sector [397], or a resonant production in presence of a very large lepton asymmetry in the Universe, $\mathrm{L} >> 10^{-10}$ [78, 77].

2.11 Can it be probed experimentally?

The last requirement for a particle to be a good DM candidate, is that such particle can be probed experimentally, in the sense that it can be directly detected or that convincing

evidence for it, or for the theoretical scenario it arises from, can be obtained with present or future experiments. The nature of this requirement is different from that of the nine other conditions discussed above, where we have essentially required that DM scenarios are not in conflict with existing experiments and observations. Here we add the requirement of "discoverability", that reflects our prejudice on what can be considered a *good* theory in science.

2.11.1 Probing SuperWimps

DM particles may interact far less than weakly, and they could evade all conventional dark matter searches. For example, the supersymmetric gravitino, which only couples gravitationally, has been proposed as a well motivated Dark-Matter candidate. The LKP graviton in UED, axions and axinos are other examples of super-weakly interacting massive particles (or super-WIMPs), i.e. Dark Matter candidates that can be extremely difficult or impossible to observe in direct and indirect Dark Matter searches because of their very suppressed interactions [34, 398, 399].

However, the next to lightest supersymmetric particle (NLSP) could be long-lived, for example the stau NLSP lifetime is of order 10^6 sec, for gravitino masses of 10 GeV [400]. If the NLSP is a neutralino, this scenario may have an interesting collider signature, similar to the case of neutralino LSP, because the decays of the NLSP neutralino may occur outside the detector. In this case, the sparticle spectrum may allow the discrimination between gravitino and neutralino LSP through the analysis of selected decay channels [401], or spins [402], even if this programme may be challenging for the LHC.

A stau NSLP scenario, as possibly realized in supergravity models [401], offers a more promising opportunity to uncover gravitino Dark Matter models at colliders. The charged NLSP particle particle would have distinctive time-of-flight and energy-loss signatures that might enable to reconstruct its mass with high accuracy, at a level of per cent or even smaller [401, 403, 404]. A stau would be produced at the end of every supersymmetric cascade and being strongly ionizing, if it is sufficiently slow moving, it may be stopped inside the detector or in a surrounding water tank or calorimeter detector. In particular, it has been suggested that up to $\mathcal{O}(10^3)$ and $\mathcal{O}(10^4)$ charged NLSP can be trapped per year at LHC and ILC respectively, by placing a 10 Kton trap around the detector [400, 405, 404].

Collecting a large number of stau, it would be possible to measure the stau lifetime and kinematically determine the gravitino mass, from the dominant decay $\tilde{\tau} \rightarrow \tau + \tilde{g}$. The measurements of gravitino and stau masses would allow to compute the stau lifetime predicted by the supergravity model and if it matches the experimental value, one would obtained a strong evidence for supergravity and for gravitino LSP [402, 400, 405].

Detailed simulations have been performed to study the gravitino Dark Matter scenario at LHC and ILC (e.g. [401, 403, 406]). In particular, at ILC, with an integrated luminos-

ity of 200 fb^{-1} at $\sqrt{s} = 420$ GeV, thousands of stau will be stopped within the hadron calorimeter, allowing a reconstruction of the gravitino mass with an accuracy of few GeV and a determination of the Planck mass, for a test of supergravity predictions, at a level of 10 % [406].

As discussed in Sec.2.5, for NLSP and gravitino masses in the GeV range, BBN bounds severely constrain the case of neutralino and stau NLSP, while a sneutrino NLSP is perfectly viable. In the latter case, the NLSP decay is invisible, but the predicted small sneutrino-stau mass splitting may produce interesting collider signatures, with soft jets or leptons in the final states [407]. Finally, models of gravitino DM with broken R-parity, may also be searched for in accelerators [408, 409, 410], but also through indirect detection [412, 411].

Axinos

Axinos appear in supersymmetric models implementing the Peccei-Quinn mechanism for solving the strong CP problem, and correspond to the fermionic superpartner of the axion. Their mass ranges between the eV and the GeV scale, and they can be efficiently produced through thermal and non-thermal processes in the early Universe under the form of cold, warm or even hot Dark matter (see e.g. Refs. [413, 398, 414, 415] and references therein).

In particular, axinos cold Dark Matter is achieved for masses $m \geq 100$ keV and for low reheating temperatures $T_R \leq 10^6$ GeV, in contrast with gravitino CDM that can allow for higher values of T_R, such as $T_R \sim 10^{10}$ GeV for $m_{\tilde{g}} \sim 1$ TeV.

Axino couplings are suppressed by the inverse of the Peccei-Quinn breaking scale, $f_a \geq 10^9$ GeV, and therefore these particles are extremely weakly interacting. As a consequence, similarly to the case of gravitino LSP, the lifetime of the NLSP can be long, and the strong bounds from Big Bang Nucleosynthesis avoided [415].

The direct production of axinos at colliders is strongly suppressed but they can be profusely produced by the decays of the NLSP particles. As in the case of gravitino, a large number of sleptons NLSP could be collected, in order to measure the NLSP lifetime and to reconstruct the axino mass and the Peccei-Quinn scale f_a (see [414] and references therein).

However, the problem may arise of discriminating between axino and gravitino LSP models. For instance, a stau NLSP with a lifetime within the range 0.01 s - 10 h is predicted in both scenarios, while shorter or longer lifetime are possible only with a gravitino LSP. To solve this ambiguity, one may consider the three body decay $\tilde{\tau} \rightarrow \tau + \gamma + \tilde{g}/\tilde{a}$. For at least $\mathcal{O}(10^4)$ observed stau decays, a clear distinction between the two models can be achieved through the angular distribution of the decay products and/or measuring its branching ratio [416, 404].

Axion

Axions have been proposed as a viable CDM candidate and the suppression of their interactions by the Peccei-Quinn scale makes them very weakly interacting (see e.g. [54, 55] and references therein for more information). Their relic abundance matches the Dark Matter cosmological density for masses around 10 μeV but significant deviations from this value can occur because of the large uncertainties in the production mechanisms.

One of the most prominent phenomenological properties is the two photon interaction that allows axion-photon conversions in presence of an electromagnetic field:

$$\mathcal{L}_{a\gamma} = g_{a\gamma}\mathbf{E} \cdot \mathbf{B}\, a.$$

Here, $\mathbf{E}$ and $\mathbf{B}$ are respectively the electric and magnetic fields, a is the axion field and $g_{a\gamma}$ is the coupling constant.

This coupling constant is linearly related to the mass of the axion and connected to measured properties of the pions and to details of the underlying particle physics model. However, in some cases this relation can be relaxed postulating the existence of axion-like particles with unconnected masses and couplings. The Primakoff process that converts axions into photons is at the basis of most axion searches (see e.g. [417, 55] for a discussion about axion searches).

For example, galactic Dark Matter axions could be resonantly converted into microwave photons in the magnetic field permeating a cavity. The signal would carry information on the mass as well as the axion distribution in the galactic halo. The ADMX experiment[418] has already started to explore the region of parameter space favored for Dark Matter axions, while a larger portion will be probed by the upgraded version of the same project and upcoming microwave cavity experiments.

Complementary searches are dedicated to axions produced by photon conversion in the electromagnetic field of the Sun, probing regions of the parameter space where axions are unlikely the dominant component of Dark Matter.

Solar axions can be searched for with axion helioscopes, through the reconversion to X-rays in external magnetic fields. The strongest bound is obtained by the null searches of the CAST experiment $g_{a\gamma} < 8.8 \cdot 10^{-11}$ GeV^{-1} for $m_a \lesssim 0.02$ eV [419].

In addition, one may look for the axion Primakoff conversion into photons in the intense Coulomb field of nuclei in a crystal lattice. However the inferred limits are less restrictive with respect to the previous strategy.

Axions could also affect the polarization of a laser beam propagating through a magnetic field. If the light is linearly polarized with a non vanishing angle with the magnetic field direction, the polarization plane rotates because the polarization component parallel to the magnetic field is depleted by the photon-axion conversion processes whereas the perpendicular component does not. In addition to the rotation of the polarization plane (dichroism),

an ellipticity is developed (birefringence) because of the different refractive indexes of the parallel and transverse polarization components. A positive signal of dichroism and birefringence was initially claimed by the PVLAS collaboration [152] and some models have been proposed to reconcile an axion-like interpretation with existing astrophysical bounds [146, 420, 421, 422]. However, recent observations, after an upgrade of the apparatus, appear to suggest that the signal was likely due to instrumental artefacts [153].

Axions can also be searched for with photon regeneration experiments, such as ALSP [423]. A laser beam propagates through a magnetic field where photons can be converted into axions. These particles, contrary to photons, can easily pass a opaque barrier wall and they can be subsequently reconverted in photons by the use of a second magnetic field. Finally, gamma-ray experiments could be sensitive to axion-like particles because the photon-axion conversions in the galactic magnetic field or in the photon production sites could induce detectable signatures in the spectra and fluxes of high-energy gamma ray sources [424, 425, 426, 427].

2.11.2 UED or SUSY?

Even if a detailed discussion is beyond the scope of this work, we briefly mention the important role of electroweak measurements on constraining DM models. In fact, accelerator bounds can severely reduce the parameter space of particle physics models and even rule out Dark Matter candidates. As an example, a light left-handed sneutrino is excluded as dominant Dark Matter candidate from the measurements of the invisible width of the Z gauge boson [428, 429].

The constraints from collider experiments are highly model-dependent and their impact have been extensively studied on selected models, for example for a large class of supersymmetric models [430, 431, 432, 433, 434, 435, 436], and for UED [437, 438] and Little Higgs [439] theories.

We conclude this section with a comment on the discrimination between different DM scenarios. In fact, even in the case of the most well studied DM candidates, i.e. the supersymmetric neutralino and the LKP in UED, the experimental signatures may not easily allow an unambiguous identification. As we have seen, neutralinos could be pair-produced at LHC and escape the detector leading to an imbalance of measured momentum. The discovery reach depends on the rate of such missing energy events, that is strongly related to the squarks and gluino masses. The discovery potential of LHC and the ability to determine the SUSY parameters and masses for given supersymmetric models have been extensively studied [440, 441, 442, 443, 444, 445, 446, 447, 448] and for squarks and gluino lighter of 1 TeV the necessary integrated luminosity will be available at LHC already in the first year of operation [440]. In Fig. 2.8 we show the reach of LHC to TeV scale SUSY, for different channels.

An important role, in the discovery and understanding of SUSY, may be played by the planned positron-electron International Linear Collider (ILC) that should allow a more precise reconstruction of the supersymmetric parameters.

The interplay of LHC and ILC might be crucial for Dark Matter studies, because it would allow to measure the particle physics cross sections and sparticle masses with enough accuracy to infer the neutralino relic density and to test whether the LSP really constitutes the Dark Matter [449] (see also [450] for a broader discussion on the complementarity of LHC and ILC).

The prospects for discovery of Universal Extra Dimension at LHC are also promising. The most abundantly produced states are those strongly interacting, i.e. the first level quarks and gluons, with very large production cross sections for masses in the range of few hundreds GeV [451]. The first excitation of the hypercharge gauge boson, B^1, can be the LKP and, thanks to KK parity conservation, a good Dark Matter candidate. Similarly to R-parity conserving SUSY, the first level KK states have to be pair produced, and they subsequently decay into SM particles and into B^1 LKP, with the latter escaping from the detector and leading to a missing energy signature. At LHC, the signature with the largest rate is $E_T^{miss} + (N \geq 2)$ jets, but a more promising channel for UED discovery is that of multilepton final states, with the signature $4l + E_T^{miss}$. The LHC should then probe an inverse compactification radius of $R^{-1} \simeq 1.5$ TeV [452].

However, if a signal of new physics will be detected at LHC, the problem will arise of discriminating between UED and SUSY [452]. In addition, also restricting to SUSY models, LHC will leave degeneracies in the parameter space as it has been shown in Ref. [453, 454]. Some specific features may simplify the task [455, 456, 457, 458], also for a discrimnation between SUSY and Little Higgs model [459].

For example, the spins of KK states are the same as their SM partners while in SUSY they differ by 1/2. The spin determination at LHC will be an extremely difficult task, but a charge asymmetry in the lepton-jet invariant mass distributions from particular cascade decays could be used to discriminate UED and SUSY. In particular, quasi-degenerate mass spectra, such as those expected in UED, tend to wash out the spin-correlations and therefore the prospect to exclude a UED pattern given a SUSY spectrum are much better than vice-versa [456, 457, 458].

Another difference between the two models is the structure of the Higgs sector: in the Minimal UED model the analogues of the heavy Higgs bosons in MSSM, $H^0, A^0, H^\pm$ are absent. Even if the first level of Higgs boson has the same quantum numbers, it appears more similar to the higgsino, since it carries KK parity. However, this is not a robust criterium of discrimination at LHC because there are regions of the SUSY parameter space where only the SM higgs bosons can be detected, and therefore SUSY and UED could be confused [452].

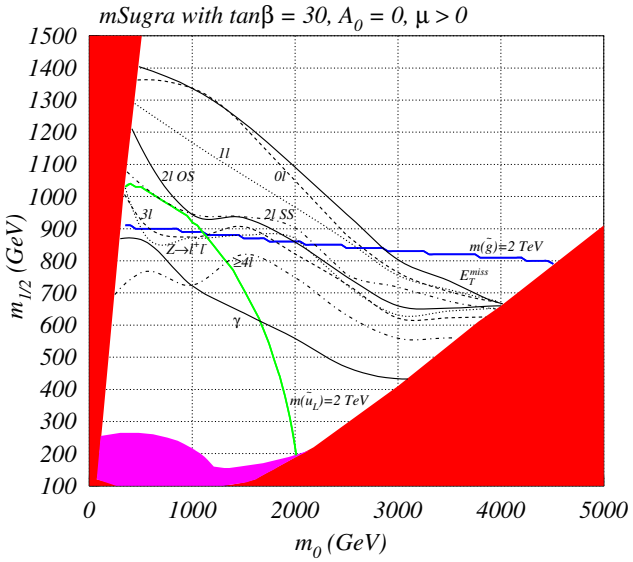

Figure 2.8: An example of the reach of LHC to TeV-SUSY for different channels in the plane m_0 vs $m_{1/2}$ in mSUGRA model. The channels taken in account are: zero leptons (0l), one lepton (1l), leptons with opposite charge (OS), leptons with same charge (SS), three leptons (3l), four or more leptons (≥4l), any numer of leptons plus one photon (γ), at least 2 opposite sign leptons with the invariant mass within an optimized interval around the Z mass ($Z \to l^+l^-$) and the inclusive missing transverse energy channel. The solid lines are the 2 TeV mass contours for squark and gluinos. The red region is excluded by theoretical arguments and the magenta region is excluded experimentally. An integrated luminosity of 100 fb^{-1} is assumed. From Ref. [441]

A smoking gun signature of UED models is instead provided by the detection of second level particles. The γ^2 and Z^2 offer the best prospect for discovery and their resonances can be separately detected for $R^{-1} \leq 1$ TeV [456]. However, this is not a probe of UED because the resonance could be interpreted as an extra Z boson. A quasi-degenerate B^1-Z^1 double resonance is instead a more robust feature of UED, being an accidental mass degeneracy of extra-Z bosons unmotivated. However, this double peak structure would be very difficult to observe at LHC (see Ref.[456] for more details).

In conclusion, it is likely that LHC alone will leave the door open to several models. Anyway, ILC, with $\sqrt{s} = 3$ TeV, will provide a more adequate tool to effectively distinguish UED and SUSY. In particular the angular distribution of the events and the threshold shape in the KK muons/smuons pairs production are the most convincing evidences for UED/SUSY discrimination [455].

DM candidate	**I.** Ωh^2	**II.** Cold	**III.** Neutral	**IV.** BBN	**V.** Stars	**VI.** Self	**VII.** Direct	**VIII.** γ-rays	**IX.** Astro	**X.** Probed	**Result**
SM Neutrinos	×	×	✓	✓	✓	✓	✓	✓	✓	✓	×
Sterile Neutrinos	∼	∼	✓	✓	✓	✓	✓	✓	✓!	✓	∼
Neutralino	✓	✓	✓	✓	✓	✓	✓!	✓!	✓!	✓	✓
Gravitino	✓	✓	✓	∼	✓	✓	✓	✓	✓	✓	∼
Gravitino (broken R-parity)	✓	✓	✓	✓	✓	✓	✓	✓	✓	✓	✓
Sneutrino $\tilde{\nu}_L$	∼	✓	✓	✓	✓	✓	×	✓!	✓!	✓	×
Sneutrino $\tilde{\nu}_R$	✓	✓	✓	✓	✓	✓	✓!	✓!	✓!	✓	✓
Axino	✓	✓	✓	✓	✓	✓	✓	✓	✓	✓	✓
SUSY Q-balls	✓	✓	✓	✓	∼	✓	✓!	✓	✓	✓	∼
B^1 **UED**	✓	✓	✓	✓	✓	✓	✓!	✓!	✓!	✓	✓
First level graviton UED	✓	✓	✓	✓	✓	✓	✓	×	×	✓	×[a]
Axion	✓	✓	✓	✓	✓	✓	✓!	✓	✓	✓	✓
Heavy photon (Little Higgs)	✓	✓	✓	✓	✓	✓	✓	✓!	✓!	✓	✓
Inert Higgs model	✓	✓	✓	✓	✓	✓	✓	✓!	[b]	✓	✓
Champs	✓	✓	×	✓	×	✓	×	✓	∼	✓	×
Wimpzillas	✓	✓	✓	✓	✓	✓	✓	✓	✓	∼	∼

Table 2.1: Test performance of selected DM candidates. The ✓symbol is used when the candidates satisfy the corresponding requirement, and it is accompanied by a ! symbol, in the case that present and upcoming experiment will soon probe a significant portion of the candidate's parameter space. If the requirement can be satisfied only in less natural, or non-standard scenarios, or in the case of tension with observational data, the symbol ∼ is used instead. Candidates with a ∼ symbol in the last column, where the final result is shown, should still be considered viable. If one of the requirements is not satisfied, then the symbol × is used, and since these requirements are *necessary* conditions, the presence of a single × is sufficient to rule out the particle as a viable DM candidate. Footnotes: [a] It is possible to reconcile a graviton LKP scenario with CMB and diffuse photon background measurements, if the minimal UED model is extended with right-handed neutrinos, Ref.[460]. [b] There are not yet studies on neutrino or antimatter signals potentially produced by this Dark Matter candidate.

2.12 Summary

In this chapter, we have presented a set of requirements that a particle has to fulfil in order to be considered a viable DM candidate. The requirements are presented in the form of a ten-point test, and we have discussed each of them in a dedicated section that describes the nature of the requirement and guides the reader through the relevant literature.

The test performance of a small subset of DM candidates proposed over the years is shown in Tab.2.1. The ✓symbol is used when the candidates satisfy the corresponding requirement, and it is accompanied by a ! symbol, in the case that present and upcoming experiment will soon probe a significant portion of the candidate's parameter space. If the requirement can be satisfied only in less natural, or non-standard scenarios, or in the case of tension with observational data, the symbol $\sim$ is used instead. Candidates with a $\sim$ symbol in the last column, where the final result is shown, should still be considered viable. If one of the requirements is not satisfied, then the symbol $\times$ is used, and since these requirements are *necessary* conditions, the presence of a single $\times$ is sufficient to rule out the particle as a viable DM candidate.

Chapter 3

Indirect detection with gamma-rays

Mini-spikes are large Dark Matter over-densities expected to form around Intermediate Mass Black Holes (IMBHs) and due to pair WIMPs annihilations they can appear as bright gamma-ray emitters. Focusing on a population of IMBHs in the Andromeda galaxy, we study the prospects for detection with FERMI and ACTs. We then compute the contribution of cosmological mini-spikes to the cosmic gamma-ray background. We study its angular correlations and investigate the prospects for detection of Dark Matter annihilations in the CGB anisotropy data.

This chapter is based on [311] and [338].

3.1 Introduction

WIMPs are among the best motivated DM candidates, due to their connections with several, independently formulated particle physics theories beyond the Standard Model, and also in view of their intriguing phenomenology (see Refs. [4, 5, 6, 7] for reviews). These particles are actively searched for with underground detectors, with searches for related signatures with the Large Hadron Collider, and, *indirectly*, through the detection of their annihilation products such as photons, neutrinos, positrons and antiprotons. The annihilation rate being proportional to the square of the DM density, ideal targets of indirect searches include all those regions where the DM density is strongly enhanced, due to gravitational clustering, as in the case of the Galactic center and halo substructures or because of energy losses capture in large celestial bodies, as in the case of the Sun and the Earth (see Sec.2.9 for references).

Large DM overdensities can also form as a consequence of astrophysical processes, such as the adiabatic growth of Supermassive [461, 306, 572] or Intermediate Mass Black

Holes [463, 310]. In fact, DM halos inevitably react to the growth of black holes, leading, in the case of adiabatic growth, to the formation of large DM overdensities called *spikes* [461]. A DM cusp with a power-law density profile $\rho \propto r^{-\gamma}$, gets redistributed after the BH growth into a steeper profile $\rho_{sp} \propto r^{-\gamma_{sp}}$, with $\gamma_{sp} = (9 - 2\gamma)/(4 - \gamma)$, within the radius of gravitational influence of the Black Hole (BH) (see below for further details). BHs can thus be thought as *annihilation boosters*, because the annihilation rate after their growth is boosted by several orders of magnitude, making these objects ideal targets for indirect DM searches. Even in absence of mergers [307], and ignoring a possible off-center formation [308], a spike around the Supermassive BH at the Galactic center would inevitably be destroyed by the combined effect of gravitational scattering off the *observed* stellar cusp at the GC, and DM annihilations [464]. The very same gravitational processes can still lead to the formation of moderate enhancements called *crests* (Collisionally REgenerated STructures), but these structures do not lead to significant enhancements of the annihilation signal [309]. *Mini-spikes* around Intermediate Mass Black Holes (IMBHs) are more promising targets of indirect detection, since they would not be affected by these dynamical processes, and they should appear as bright point-like sources, which could be easily detected by large field of view gamma-ray experiments as the Fermi Gamma-ray Space Telescope (formerly known as GLAST) [316] and further studied with ground-based Air Cherenkov telescopes (ACTs) such as CANGAROO [312], HESS [313], MAGIC [314] and VERITAS [315]. A search for these objects based on a HESS survey of the Galactic plane region has already allowed to set some interesting constraints on the mini-spikes scenario [465]. In addition, mini-spikes in the Milky May or nearby galaxies could be detected with neutrino telescopes [466] or boost anti-matter fluxes [467].

In this chapter, we explore the mini-spikes scenario. In the first sections we focus on the population of IMBHs in the Andromeda Galaxy (also known as M31), a spiral galaxy very similar to the Milky Way (MW), whose center is located 784 kpc away from us. We compute gamma-ray fluxes from DM annihilations around IMBHs in M31, and study that the prospects for detection with FERMI and ACTs [311].

Then, we move to "cosmological mini-spikes". We compute their contribution to the cosmic gamma-ray background (CGB) and we study the prospect for detection in the CGB angular power spectrum with FERMI [338].

3.2 Intermediate Mass Black Holes

3.2.1 IMBHs formation scenario

IMBHs are compact objects with mass larger than $\approx 20 M_\odot$, the heaviest remnant of a stellar collapse [468], and smaller than $\approx 10^6 M_\odot$, the lower end of the mass range of SuperMassive

Black Holes (SMBH) [469]. The theoretical and observational motivations for IMBHs were recently reviewed in Ref. [470]. For instance, Ultra-Luminous X-ray point sources (ULXs) could be interpreted as accreting IMBHs, since alternative explanations in terms of AGNs, neutron stars or SMBHs appear to be problematic or even ruled out [470, 471].

From a theoretical point of view, a population of massive seed black holes could help to explain the origin of SMBHs. In fact, observations of quasars at redshift $z \approx 6$ in the Sloan Digital survey [472, 473, 474] suggest that SMBHs were already in place when the Universe was only ~ 1 Gyr old, a circumstance that can be understood in terms of rapid growth starting from massive seeds (see e.g. Ref. [475]).

In fact, a generic prediction of scenarios that seek to explain the properties of the observed SuperMassive Black Hole population, is that a large number of "wandering" IMBHs should exist in DM halos [476, 478, 477]. Despite their theoretical interest, it is difficult to obtain conclusive evidence for the existence of IMBHs. A viable detection strategy could be the search for gravitational waves produced in the mergers of the IMBH population [479, 480, 481, 482, 483, 484], with space-based interferometers such as LISA [485].

In Ref. [310], two scenarios for IMBHs formation have been considered. The first posits IMBHs as remnants of the collapse of Population III stars. These are stars with very low metallicity, that do not experience any metal line cooling, leading to a higher mass scale with respect to more recent stars. Moreover, they do not have significant winds, and have weak pulsations, so that they lose comparatively little of their mass during the evolution. Stars heavier than $250 M_\odot$ collapse directly to a BH without any mass loss [470], and under some simplifying assumptions, a population of roughly 1000 IMBHs with mass of $10^2 - 10^3 M_\odot$ is predicted to wander in the MW DM halo [310].

Here, we will focus only on the second scenario, based on Ref. [477], where IMBHs form at high redshift from gas collapsing in mini-halos. If the latter are massive enough, proto-galactic disks form at the center of each halo, composed by baryons lying in the low values tail of the angular momentum distribution. Gravitational instabilities introduce an effective viscosity that causes an inward mass and an outward angular momentum flow. The process goes on until it is interrupted by feedback from star formation (1-10 Myrs) that heats the disk. Then the so-formed object undergoes gravitational collapse into a black hole. A characteristic mass scale of $10^7 M_\odot$ is imprinted to the mini-halo by the requirements that it is heavy enough to form a gravitational unstable disc and that the black hole formation timescale is shorter than the typical major mergers one. The resulting black holes have a mass log-normally scattered, with a $\sigma_\bullet = 0.9$, around the mean value of [477]:

$$M_\bullet = 3.8\times10^4 M_\odot \left(\frac{\kappa}{0.5}\right)\left(\frac{f}{0.03}\right)^{3/2}\left(\frac{M_{vir}}{10^7 M_\odot}\right) \times\left(\frac{1+z}{18}\right)^{3/2}\left(\frac{t}{10\ \mathrm{Myr}}\right), \tag{3.1}$$

where κ is that fraction of the baryonic mass which loses its angular moment that remains in the remnant black hole. f is the fraction of the total baryonic mass in the halo that has fallen into the disc, M_{vir} is the halo virial mass, z is the redshift of formation and t the timescale for the evolution of the first generation of stars.

Although our analysis is performed in the context of this specific scenario, it is by no means assured that this is the actual mechanism for IMBHs formation. The recipe for halo population and spike formation can nevertheless be generalized to any IMBHs formation scenario.

Reference [310] studied the population of IMBHs in our own Galaxy. Specifically, the authors simulated the formation of a Milky-Way-like DM halo starting from mini-halos at high redshifts, following the hierarchical merger history of the latter until $z = 0$ in the context of a ΛCDM model for structure formation. In that analysis, the formation of IMBHs in a given halo follows the prescription given in Ref. [477], and pair BH mergers occur if the pair distance is lower than 1 kpc. IMBH formation is absent after reionization, $z < z_{re}$, since most of the molecular hydrogen, the main baryonic coolant, is ionized. In the simulation of Ref. [484], the authors find that IMBHs formation is highly suppressed for $z > z_{re}$ since the suitable hosts for BH formation become increasingly rare as redshift increases. Therefore, according to Ref. [484], the formation redshift distribution is peaked at z_{re}.

The authors performed 200 statistical realizations of the IMBH population providing for each IMBH its distance from the center of the galaxy, its mass and the surrounding DM distributions. The average number of unmerged IMBHs is $N_{BH} = 101 \pm 22$. The radial distribution of the IMBH population is described by the volume probability, $g(r)$, shown in Fig. 3.1 for an average realization among the 200 realizations of the IMBH population in the Milky Way. The function $g(r)$ is simply defined as the probability to find an IMBH at a radial distance r from the Galactic center, in a spherical shell of thickness dr. The volume probability function is normalized to 1 between 1 kpc and the maximal distance from the Galactic center at which an IMBH is found, i.e.roughly 300 kpc. The error bars in the plot reflect the scatter among the 200 realizations.

The distribution is well fitted by the analytical function

$$g(r) = 5.9610^{-2}\left[1+\left(\frac{r}{9.1\ \mathrm{kpc}}\right)^{0.51}\right]^{-10.8}\ \mathrm{kpc}^{-3}.$$

The logarithmic slope, $\gamma = d\log g/d\log r$, is 1.5 at 1 kpc and 4.5 at 200 kpc, and therefore the resulting distribution is cuspier than a Navarro-Frenk-White profile (NFW) [486], shown in Fig. 3.1 for comparison.

3.2.2 DM distribution around IMBHs

Following earlier work on the dynamics of stars and DM around compact objects (see Ref. [487] and references therein), Gondolo and Silk have shown that the adiabatic growth of a massive black hole in the center of a dark halo modifies the distribution of the surrounding DM, inducing an enhancement of the density called "spike" [461]. They focused their attention on the SMBH at the center of our Galaxy, but the same formalism can be applied also to IMBHs. The initial DM distribution in all mini-halos is taken to be with a NFW profile:

$$\rho(r) = \rho_0 \left(\frac{r_s}{r}\right)\left(1+\frac{r}{r_s}\right)^{-2}, \tag{3.2}$$

where r_s, called the scale radius, sets the radius at which the profile slope changes. The new profile after the adiabatic growth, will be [461]:

$$\rho_{sp}(r) = \rho(r_{sp})\left(\frac{r}{r_{sp}}\right)^{-7/3}, \tag{3.3}$$

where ρ is the density function of the initial NFW profile. r_{sp} gives the upper limit inside which Eq. 3.3 is considered valid and is related to the radius of gravitational influence of the black hole r_h: $r_{sp} \approx 0.2 r_h$ [488], where r_h is implicitly defined as:

$$M(r < r_h) \equiv \int_0^{r_h} \rho(r) r^2 dr = 2M_\bullet$$

with $M_\bullet$ is the mass of the black hole.

After the formation of the BH, the DM number density decreases because of DM pair annihilations as: $\dot{n}_\chi = -(\sigma v) n_\chi$ with (σv) the annihilation cross section times velocity. The solution to this equation gives an upper limit to the DM density $\rho_{lim} = m_\chi \times (\sigma v)^{-1}(t - t_f)^{-1}$ where m_χ indicates the DM mass and $t - t_f$ is the time elapsed since BH formation. We denote r_{lim} the radius where this maximum density is reached. The density is considered to be constant within a cut-radius defined as $r_{cut} = \mathrm{Max}[4R_{Schw}, r_{lim}]$ where R_{Schw} is the BH Schwarzschild radius.

Although we perform our calculations in the context of NFW profiles, we note that spike slope γ_{sp} depends weakly on the initial slope γ:

$$\gamma_{sp} = \frac{9 - 2\gamma}{4 - \gamma}. \tag{3.4}$$

Varying γ between 0 to 1.5, γ_{sp} thus ranges between 2.25 to 2.4. Furthermore, although the spike depends quite strongly on the density normalization at r_{sp}, most alternative

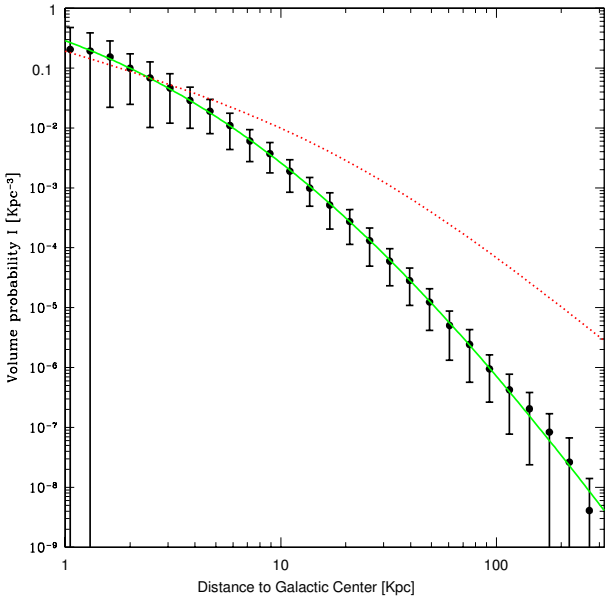

Figure 3.1: Radial distribution of the IMBH population in the Milky Way from the numerical results of Ref. [310]. The points refer to an average among the 200 Monte Carlo realizations of the Milky Way halo and error bars show the scatter among realizations. The solid line is an analytical fit and the dotted line is a NFW profile.

profiles deviate from NFW on scales smaller than r_{sp}. We have for instance checked the case of the Navarro et al. profile proposed in Ref. [489] and found that the corresponding annihilation flux from each spike gets rescaled only by a factor 1.6, which is well within the other uncertainties in our calculations.

3.3 Gamma-Rays from IMBHs in M31

3.3.1 IMBHs in M31

Although similar, the Milky Way and Andromeda do not have exactly the same properties. The mock catalogs of IMBHs built for our Galaxy, thus have to be modified to account for the different average number and different spatial distribution in the host halo. A comparison between the properties of Andromeda and of the Galaxy is shown in Table 3.1.

We start from the mock catalogs obtained in Ref. [310] and we rescale the total number of objects by the ratio between the host halo masses, since the number of unmerged IMBHs scales linearly with the host halo mass, and the galactocentric distance by the ratio of virial radii. We obtain for M31 an average number of IMBHs per realization $N_{M31} = 65.2 \pm 14.5$.

The mass spectrum remains unchanged, with an average mass around $10^5\ M_\odot$, while the average distance from the center of the galaxy is 32.31 kpc. We have verified that our rescaling procedure reproduces in a satisfactory way the properties of the IMBHs population in Andromeda, by comparing our results with a limited number of mock catalogs obtained as an exploratory study in Ref. [310].

3.3.2 Gamma-rays flux from IMBHs in M31

Once the mock catalogs of IMBHs in M31 have been obtained, the gamma-ray flux from each IMBH in every realization is computed as:

$$\begin{aligned}\Phi(E) &= \frac{\sigma v}{2m_\chi^2}\frac{1}{d^2}\frac{dN_\gamma(E)}{dE}\int_{r_{cut}}^{r_{sp}}\rho^2(r)r^2dr \\ &= \Phi_0\frac{dN_\gamma(E)}{dE}\left(\frac{\sigma v}{10^{-26}\mathrm{cm}^3/\mathrm{s}}\right)\left(\frac{m_\chi}{1\ \mathrm{TeV}}\right)^{-2} \\ &\quad\times\left(\frac{d}{780\ \mathrm{kpc}}\right)^{-2}\left(\frac{\rho(r_{sp})}{100\ \mathrm{GeV/cm}^3}\right)^{2} \\ &\quad\times\left(\frac{r_{sp}}{5\ \mathrm{pc}}\right)^{14/3}\left(\frac{r_{cut}}{10^{-3}\ \mathrm{pc}}\right)^{-5/3},\end{aligned} \tag{3.5}$$

where $\Phi_0 = 2.7\times10^{-14}\ \mathrm{cm}^{-2}\mathrm{s}^{-1}$, d is the IMBH distance to the observe. r_{cut} and r_{sp}, represent the inner and outer size of the spike, as discussed in the previous section.

Adopting the same notation as in Sec.2.9, σv is the DM annihilation cross section times relative velocity and m_χ is the DM particle mass. $dN_\gamma(E)/dE$ is the differential photon yield per annihilation, that can be expressed as:

$$\frac{dN_\gamma(E)}{dE} = \sum_a B^a\frac{dN_\gamma^a(E)}{dE}. \tag{3.6}$$

	Milky Way	Andromeda
Distance to the center [kpc]	8.5	784.0
Virial Radius [kpc]	205	180
Virial Mass [$M_\odot$]	1.0×10^{12}	6.8×10^{11}
r_s [kpc]	21.75	8.18
ρ_0 [$\frac{M_\odot}{kpc^3}$]	5.376×10^6	3.780×10^7

Table 3.1: Distance from the Sun (in kpc), virial radius (defined as the radius within which the density reaches 200 times the critical density, in kpc), virial mass (in solar masses) and the two NFW density profile parameters (in kpc and $M_\odot\mathrm{kpc}^{-3}$ respectively), both for the MW and the Andromeda Galaxy [322, 490].

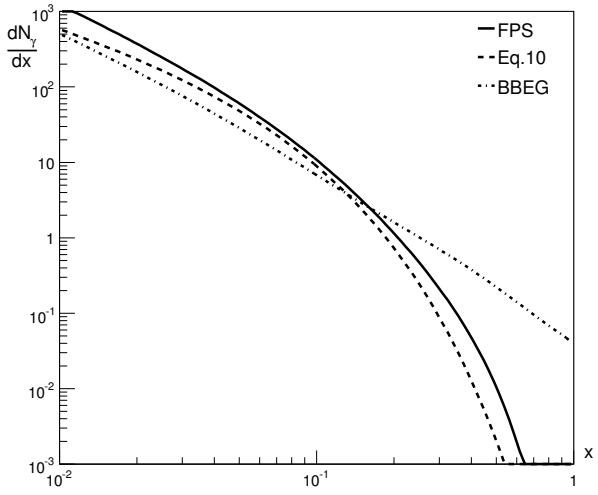

Figure 3.2: Differential photon spectrum per annihilation. Different parametrizations and annihilation channels are shown. Solid line (FPS) is an analytic fit relative to the $b\bar{b}$ channel, as obtained in Eq. 3.7. Dashed line (Eq. 3.10) is relative to the same annihilation channel $b\bar{b}$, but with a different parametrization of the FFs (see Eqs. 3.9 and 3.10). Dotted line (BBEG) is relative to B^1 annihilations and includes final state radiation from annihilation to charged leptons (see text for more details)

Common DM candidates can annihilate into a pair of SM particles $a\bar{a}$ where a stands for a fermion or a gauge or Higgs boson. The ratio of the annihilation rate into a particular channel $a\bar{a}$ over the total annihilation rate is the Branching ratio B^a. dN_γ^a/dE is the secondary photon spectrum due to the annihilation channel $a\bar{a}$. The latter term is thus a purely Standard Model calculation, while branching ratios have to be derived in the framework of new theories beyond the Standard Model, such as SUSY or UED.

We review here different parametrizations of the photon yield that have been recently proposed in literature. The first parametrization we focus on, has been obtained in Ref. [322], and it is relative to annihilations into $b\bar{b}$. The authors have parametrized the results obtained with the event generator PYTHIA [492] as follows

$$\frac{dN_\gamma^b(x)}{dx} = x^a \mathrm{e}^{b+cx+dx^2+ex^3}, \tag{3.7}$$

where the parameters depend on the neutralino mass, and for the specific case $m_\chi = 1$ TeV, $(a, b, c, d, e) = (-1.5, 0.37, -16.05, 18.01, -19.50)$. While for annihilation to τs

$$\frac{dN_\gamma^\tau(x)}{dx} = x^a(bx + cx^2 + dx^3)\mathrm{e}^{ex}, \tag{3.8}$$

and for $m_\chi = 1$ TeV, $(a, b, c, d, e) = (-1.31, 6.94, -4.93, -0.51, -4.53)$.

Alternatively, one can start from the most recent Fragmentations Functions (FFs) (e.g. [493]), describing the hadronization of partons into the particles of interest. The FF of b quarks hadronizing in neutral pions has been fitted with a simple analytic form that captures in a satisfactory way the behavior of the FF at large x finding the following analytic fit

$$f(x) = \frac{7.53}{x^{0.87} e^{14.62x}}. \tag{3.9}$$

Convolving the spectrum pions with their decay spectrum into photons one finally obtains the differential photon yield

$$\frac{dN_\gamma(x)}{dx} = \int_x^1 f(x') \frac{2}{x'} dx'. \tag{3.10}$$

We have also considered an example inspired from theories with Unified Extra-Dimensions, where the role of DM is usually played by the first excitation of the hypercharge gauge boson, and referred to as $B^{(1)}$. Since the $B^{(1)}$ annihilation into fermions does not suffer from chirality suppression, as in MSSM, we also include the contribution from annihilation to $l\bar{l}\gamma$, as calculated in Ref. [494], as well as the contribution from τ fragmentation, and usual from annihilations to $b\bar{b}$, with the appropriate branching ratio. The final state radiation arising from annihilation to charged leptons has a characteristic, very hard, spectral shape [352, 494]

$$\frac{dN^l_\gamma(x)}{dx} = \sum_{l=e,\mu} \frac{\alpha}{\pi} \frac{x^2 - 2x + 2}{x} \ln \left[\frac{m^2_{B^{(1)}}}{m^2_l} (1 - x) \right]. \tag{3.11}$$

The three prescriptions for the annihilation spectrum are plotted in Fig. 3.2 (for $m_\chi = 1$ TeV). As expected, all spectra are very similar up to $x \equiv E/m_\chi \sim 0.1$, but the spectrum relative to $B^{(1)}$ annihilations is harder at large x, and exhibits a distinctive sharp cut-off at $x = 1$.

To show the small effect that the adoption of different annihilation spectra has on the prospects for indirect detection, we have calculated the DM annihilation flux from the smooth component of the M31 halo, assuming a NFW profile with the parameters described in Tab. 3.1 above. The results are displayed in Table 3.2, and as one can see, differences are

	M31 flux [$\mathrm{cm}^{-2}\mathrm{s}^{-1}$]
FPS [322]	1.33×10^{-14}
Eq. 3.10	9.79×10^{-15}
BBEG [494]	1.60×10^{-14}

Table 3.2: Gamma-ray flux over 100 GeV from Andromeda (in $\mathrm{cm}^{-2}\mathrm{s}^{-1}$) for a smooth NFW, and for the different parametrizations discussed in the text. Differences among the predicted fluxes are within a factor of 2.

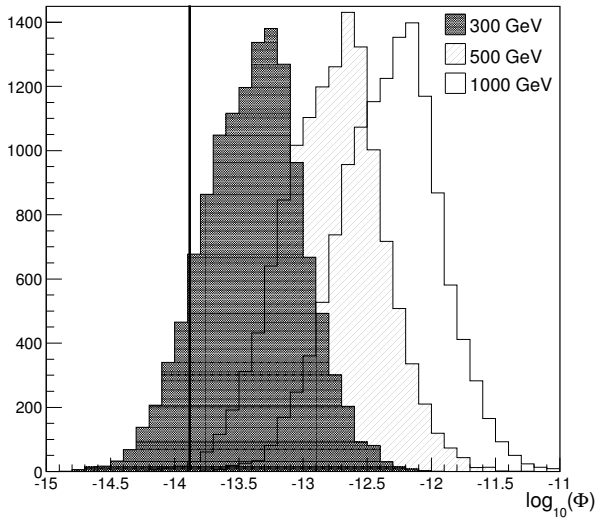

Figure 3.3: Luminosity function of IMBHs (fluxes are in $\mathrm{cm}^{-2}\mathrm{s}^{-1}$), for $m_\chi = 0.3, 0.5$ and 1 TeV. Energy threshold is equal to 100 GeV and $\sigma v = 3 \times 10^{-26}\mathrm{cm}^3 s^{-1}$. The vertical line shows the contribution of the smooth component of the M31 halo, assuming a NFW profile and $m_\chi = 1$ TeV.

within a factor of 2. In the next sections, we will thus work only with the first analytic fit, since the uncertainties associated with other astrophysical and particle physics parameters are significantly larger.

By calculating the gamma-ray flux in Eq. 3.5 for IMBHs in all realizations, we obtain the luminosity function of IMBHs (sum of all realizations), for different values of the DM particle mass (see Fig. 3.3). The distribution is approximately gaussian, and the average flux of IMBHs is larger than emission due the smooth component. The dependence from the mass results in due to a balance between the $m_\chi^{-9/7}$ dependence in Eq. 3.5, and the m_χ dependence of the upper limit in the integral of the energy spectrum. Having set in the

	Average flux $[\mathrm{cm}^{-2}\mathrm{s}^{-1}]$
$m_\chi = 50$ GeV	5.26×10^{-11}
$m_\chi = 150$ GeV	7.65×10^{-11}
$m_\chi = 300$ GeV	6.92×10^{-11}
$m_\chi = 500$ GeV	5.81×10^{-11}

Table 3.3: Average flux from IMBHs in all 200 realizations (in $\mathrm{cm}^{-2}\mathrm{s}^{-1}$), for different values of DM mass, $\sigma v = 3 \times 10^{-26}\mathrm{cm}^3\mathrm{s}^{-1}$ and $E_{thr} = 4$ GeV.

figure an energy threshold $E_{thr} = 100$ GeV, the luminosity flux towards higher fluxes when the mass increase. We will come back later to this threshold effect, that leads to higher fluxes for higher masses when $m_\chi \sim E_{thr}$ despite the explicit $m_\chi^{-9/7}$ dependence of the annihilation flux. Meanwhile we note that this effect disappears when $m_\chi \gg E_{thr}$, as can be seen from Table 3.3.

3.4 Prospects for detection

As we shall see the prospects for detection depend on the expected or measured experimental performances, but also on the atmospheric and astrophysical backgrounds. We perform separate analysis for Air Cherenkov Telescopes and the upcoming gamma-ray satellite FERMI.

3.4.1 Prospects for ACTs

The calculations in this section are performed for a generic ACT, but they are particularly relevant for two specific experiments: MAGIC and VERITAS. As for HESS, being located in Namibia, it cannot detect gamma-rays from the direction of Andromeda.

To determine the significance of the signal from an individual mini-spike, as calculated in the previous section, we compare the number of signal photons, to the fluctuations of the background

$$n = \frac{n_\gamma}{\sqrt{n_{bk}}} = \sqrt{T \cdot \Delta\Omega} \frac{\int A_{eff}(E,\theta) \frac{d\Phi}{dE} dE d\theta}{\sqrt{\int A_{eff}(E,\theta) \frac{d\Phi_{bk}}{dE} dE d\theta}}, \tag{3.12}$$

where T is the exposure time, A_{eff} the effective area, $\Delta\Omega$ the solid angle, $d\Phi_{bk}/dE$ is the total background differential flux.

For Air Cherenkov Telescopes, the main background is due to hadrons interacting with the atmosphere and producing electromagnetic showers. Following Ref. [495] [298], we consider

The ratio of the number of hadrons misinterpreted as gamma-rays, over the total number of cosmic ray hadrons, ϵ_h, provides an estimate of the telescope potential to discriminate the gamma-ray signal from the hadronic background. We adopt a typical value $\epsilon_h = 10^{-2}$, following Refs. [298] [496]. The electronic contribution to the background is [298]:

$$\frac{d\Phi_e}{d\Omega dE} = 6.9 \times 10^{-2} \left(\frac{E}{\text{GeV}}\right)^{-3.3} \frac{\text{e}}{\text{cm}^2\text{s GeV sr}} \tag{3.13}$$

and it is typically subdominant at the energies of interest.

In Figure 3.4 we compare the DM annihilation signal with the different sources of background, as a function of the field of view. The minimum flux for a 5σ detection

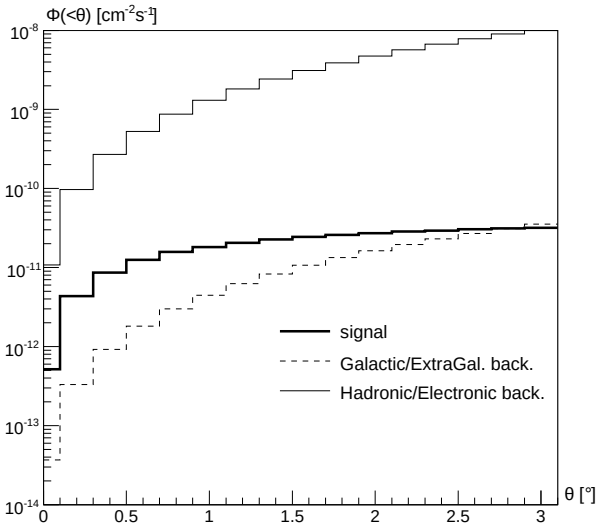

Figure 3.4: Gamma-ray flux (in $\mathrm{cm}^{-2}\mathrm{s}^{-1}$) from DM annihilation around IMBHs (solid thick line), integrated over a cone of size θ towards the center of M31, as a function of θ. We show for comparison the hadronic/electron background, assuming $\epsilon_h = 10^{-2}$ (solid thinner line) and the diffuse extragalactic background (dashed line).

with an effective area of $A_{eff} = 3 \times 10^4$ m^2 [314] and an exposure time of 100 hours, is $\phi_{min} = 1.6 \times 10^{-12}\mathrm{cm}^{-2}\mathrm{s}^{-1}$.

To produce this estimate we have considered values of effective area and angular resolution similar to MAGIC and the result is consistent with earlier estimates of the MAGIC sensitivity [6]. An actual estimate of the instrument performance suggests that the minimum flux can be up to an order of magnitude higher [497].

A sky-map for Andromeda (like in the left panel of Fig. 3.5) is obtained computing the fluxes from the mini-spikes in a random realization among the 200 of the mock catalogue. The pixel size matches the angular resolution of Ground Based Telescopes such as VERITAS and MAGIC, and of FERMI. For the map, a DM mass of 1 TeV and an annihilation cross section $\sigma v = 3 \times 10^{-26}\mathrm{cm}^3 s^{-1}$ have been adopted. Black circles highlight the position of objects brighter than the experimental sensitivity (indicated in the color scale by the black line).

The number of detectable IMBHs (averaged above the 200 realizations) for $m_\chi = 1$ TeV is $N_{5\sigma} = 5.2 \pm 3.1$, where the error is relative to the 1-σ scatter in the computation of the average.

We note that current simulations indicate that the next-generation Cherenkov Tele-

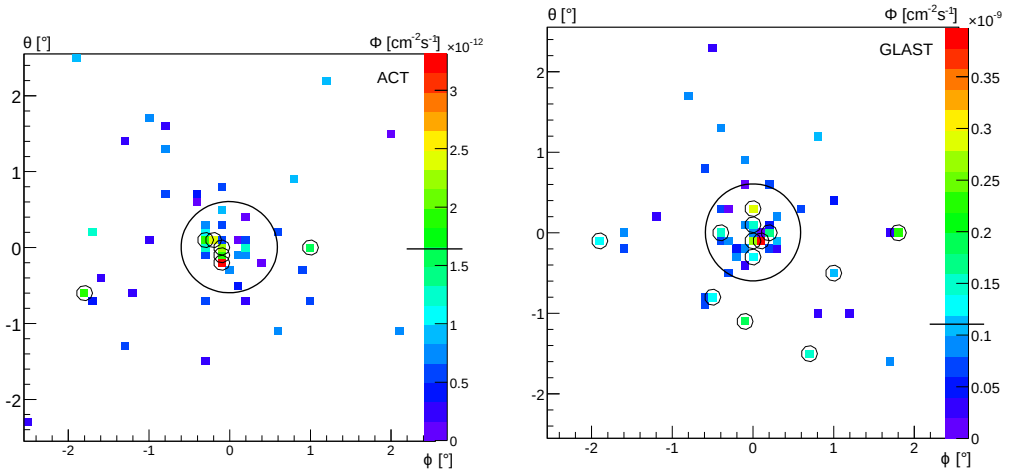

Figure 3.5: Color online. Left (right) panel shows a map of the gamma-ray flux in units of photons $\mathrm{cm}^{-2}\mathrm{s}^{-1}$, from DM annihilations around IMBHs in M31, relative to one random realization of IMBHs in M31. The size of the bins is 0.1° and the threshold for the left (right) panel is 100 GeV (4 GeV) as appropriate for ACTs (FERMI). The circles highlight IMBHs within the reach of current ACTs for a 5σ detection in 100 hours (within the reach of FERMI for a 5σ detection in 2 months). The big circle shows for comparison the M31 scale radius r_s.

scopes Array (CTA)[498], may significantly improve the sensitivity, down to $\phi_{min} \approx 10^{-13}\mathrm{cm}^{-2}\mathrm{s}^{-1}$, thus leading to a substantial improvement in the prospects for detection.

3.4.2 Prospects for FERMI

The space satellite FERMI is expected to play a crucial role in indirect DM searches [499], thanks both to its ability to perform observations at energy scales comparable to the mass of common DM candidates and to its potential of making deep full-sky maps in gamma-rays, thanks to its large ($\sim$ 2.4 sr) field of view [316]. Despite the smaller effective area, it is not affected, being a satellite, by the atmospheric hadronic and electron background. Furthermore, its lower energy threshold (30 MeV) allows to probe lighter DM particles, typically leading to higher fluxes. The angular resolution of FERMI is $\approx 3°$ in the energy range 30 MeV-500 MeV, becomes 0.5° from 500 MeV to 4 GeV, and reaches 0.15° above 4 GeV [316].

As in the case of ACTs, we compare the expected fluxes with the photon background, which in this case, since FERMI will perform observations above the atmosphere, is mainly due to diffuse gamma-ray emission. The galactic and extragalactic background has been measured in [500, 501] by EGRET in the energy range between 30 MeV and 10 GeV and

we extrapolate it to higher energies by fitting with a power-law with spectral index of -2.1. The resulting formula is

$$\frac{d\Phi_{extra/gal}}{d\Omega dE} = 2.3 \times 10^{-6} \left(\frac{E}{\mathrm{GeV}}\right)^{-2.1} \frac{\gamma}{\mathrm{cm^2 s\ GeV\ sr}}. \tag{3.14}$$

The sensitivity above 30 MeV, i.e. the minimum detectable flux for a 5σ detection with an exposure of 2 months, is found to be $\phi_{min} = 3.2 \times 10^{-8}\mathrm{cm}^{-2}\mathrm{s}^{-1}$. This value is derived from Eq. 3.12, adopting values of the energy dependent effective area provided by [502], and is consistent with FERMI sensitivity maps obtained in Ref. [503]. The integral flux above threshold from IMBHs, averaged among realizations and integrated in a 3° cone towards M31, is $\phi_{30} = 1.3 \times 10^{-7}\mathrm{cm}^{-2}\mathrm{s}^{-1}$.

In the right panel of Fig. 3.5, we show the results of our analysis relative to a random realization, and adopting $m_\chi = 150$ GeV, and $\sigma v = 3 \times 10^{-26}$ cm^3 s^{-1}. Mini-spikes appear as high emission peaks, and can be easily resolved by selecting photons above 4 GeV, so that the angular resolution of FERMI approaches 0.1 degrees. Black circles highlight those objects that produce a flux detectable at 5σ with FERMI, with a 2 months exposure.

3.5 Summary

$$\frac{d\Phi_h}{d\Omega dE} = 1.5 \times \left(\frac{E}{\mathrm{GeV}}\right)^{-2.74} \frac{\mathrm{p}}{\mathrm{cm^2 s\ GeV\ sr}}. \tag{3.15}$$

Although we have performed the analysis of the prospects for detection with FERMI and ACTs for 2 different benchmark scenarios (essentially high DM particle mass for ACTs, low m_χ for FERMI), the analysis can be easily extended to any value of the particle physics parameters of the annihilating DM particle. To explore the dependence on m_χ, we show in the left panel of Fig. 3.6 the number of objects that can be detected with the aforementioned experiments, as a function of the DM particle mass. Near the experiment threshold, fluxes increase with mass. When $m_\chi \gg E_{thr}$ this threshold effect disappears and one recovers the expected behavior (smaller fluxes for higher masses).

Similarly, one can plot the number of detectable objects as a function of the angular distance from the center of M31, to estimate the region where most mini-spikes can be found. This is shown in the right panel of Fig. 3.6 where the total number of objects is also shown for comparison. Vertical lines denote the angular size of the region that contains 90% of the detectable IMBHs for the various experiments, which has a characteristic size of $\theta = 3.3°$.

We stress that, while in the case of Galactic IMBHs the identification of mini-spikes will require a case-by-case analysis of their spectral properties, variability and multi-wavelength counterparts, as discussed in [504], for the IMBHs around Andromeda, the detection of a

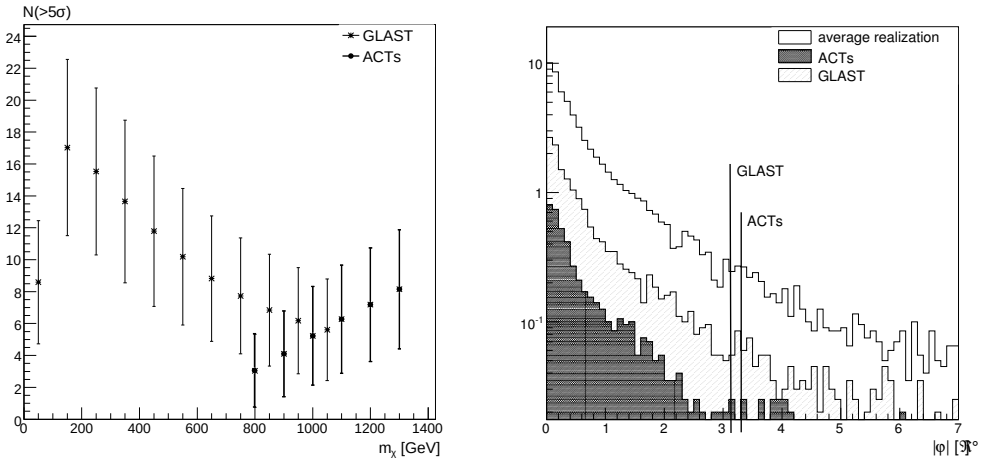

Figure 3.6: Number of detectable mini-spikes in M31 with FERMI (2 months) and ACTs (100 hours) as a function of the DM particle mass (left) and as a function of the angular distance from the center of M31 (right). In the left panel, error bars denote the $1-\sigma$ scatter among different realizations. In the right panel, the total number of objects is shown as an empty histogram, while the vertical lines denote the size of the region that contains 90% of the detectable IMBHs.

cluster of sources around the center of the galaxy would *per se* provide a hint on the nature of these sources, since other astrophysical sources, e.g. gamma-ray pulsars, will tend to lie in the disk and bulge of M31, while IMBHs would be isotropically distributed around its center, within a region of $\sim 3^\circ$.

In conclusion, we have computed gamma-ray fluxes from DM annihilations in mini-spikes around IMBHs in the Andromeda Galaxy. We have studied the prospects for detection with Air Cherenkov telescopes like MAGIC and VERITAS and with the FERMI satellite, and found that a handful of sources might be within the reach of current ACTs, while the prospects for the planned CTA are more encouraging. The obvious advantage of the proposed scenario with respect to mini-spikes in the MW, is that they are not randomly distributed over the sky, but they are contained, at 90%, within 3 degrees from the center of Andromeda, and can thus be searched for with ACTs by performing a deep scan of this small region.

The prospects for FERMI appear more promising, since an exposure time of 2 months allows the detection of up to of ≈ 20 mini-spikes, that would be resolved as a cluster of point-sources with identical spectra, within a $\sim 3^\circ$ region around the center of Andromeda. Such a distinctive prediction cannot be mimicked by ordinary astrophysical sources. As in the case of IMBHs in the MW, null searches would place very strong constraints on the proposed scenario in a wide portion of the DM parameter space.

3.6 Cosmic gamma-ray background and DM annihilations

The origin of the cosmic gamma-ray background (CGB) measured with EGRET [505] is currently uncertain and the the most favored explanation calls for the existence of an unresolved population of active galactic nuclei (AGNs). Recent determinations of the gamma-ray luminosity functions (GLF) show however that unresolved blazars alone can explain only 20-50% of the measured CGB [506], therefore leaving room for other gamma-ray emitters. Besides other standard astrophysical sources, e.g. unresolved gamma-ray emission from clusters of galaxies [507, 508] or normal galaxies [509], cosmological WIMPs annihilation could also contribute to the CGB [330, 308, 331, 326].

Assuming a smooth profile for DM halos, the absence of intense gamma-ray emission from the center of our galaxy constrain the DM contribution from cosmological halos to be rather low [333], but it has been shown that the presence of substructures can largely boost this signal without being in conflict with galactic bounds [334, 510]. For instance, taking into account the contribution from cosmological mini-spikes, DM annihilations can largely contribute to the measured CGB [334], while spikes around SMBHs can provide only moderate boosts [335].

In previous sections, we have shown the prospects for detection of mini-spikes in our or nearby galaxies such as M31 are encouraging and the simultaneous detection of several sources with the same energy spectra, showing a cut-off at the DM mass, would be a smoking gun for WIMPs annihilation. On the contrary, it is difficult to extract straightforward evidences for DM annihilation from the study of the CGB spectrum itself. However, additional information can be extracted by the anisotropy data [336, 337, 511, 512, 513, 514]. In particular, the CGB angular power spectrum from blazar and from DM annihilation in halos or subhalos are quite different, due to their different energy spectra, cosmological distribution, and radial emissivity profiles. Therefore, the study of the CGB angular power spectrum provides, in principle, a robust and direct tool to discriminate between the two different scenarios. Assuming the unresolved blazar contribution as a "known" background, DM annihilation could be detected with roughly 2 years of Fermi data, provided they contribute a fraction $\gtrsim 0.3$ of the CGB at 10 GeV [337].

In the next sections we perform the angular anisotropy analysis for the case of cosmological DM mini-spikes around black holes. We compute the angular power spectrum for different DM benchmark setups, varying the particle mass and the annihilation channel, and for different gamma-ray energies, showing that the results are quite sensitive to all of these variables. We also discuss the possibility to distinguish with Fermi data the mini-spike scenario from the case of substructure-dominated emission.

The remainder of the chapter is organized as follows: in Sec. 3.7 we compute the contri-

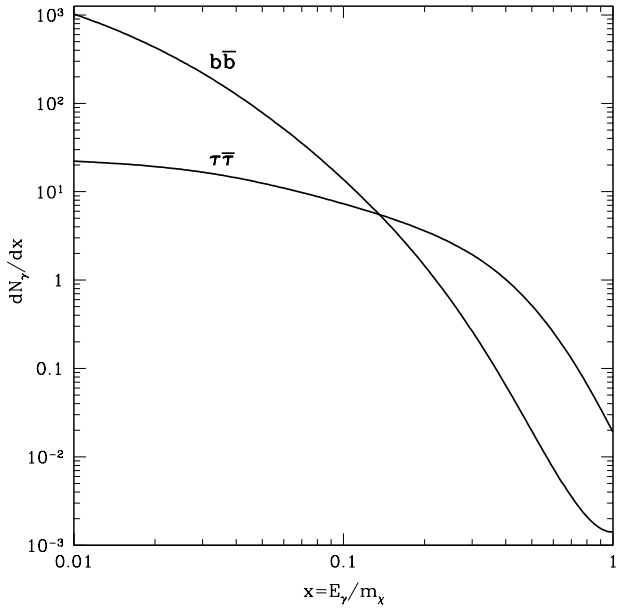

Figure 3.7: Photon spectra for DM annihilation into $b\bar{b}$ and $\tau^+\tau^-$. The DM particle mass is set to $m_\chi = 100$ GeV

bution to the CGB mean intensity from DM annihilation in cosmological mini-spikes and from blazars. Sec. 3.8 is devoted to the computation of he angular power spectrum for the two cases. A mixed scenario is presented in Sec. 3.9, where we also discuss prospects for detecting DM annihilation with the Fermi Telescope and the effect of changing particle DM parameters and the gamma-ray energy at which the anisotropy is studied. Finally, conclusions are presented in Sec. 3.10. Throughout this chapter, we adopt a flat ΛCDM model with the cosmological parameters from WMAP 5-year data [13].

3.7 Cosmic Gamma-Ray Background

3.7.1 Dark Matter Annihilations

DM annihilation contribution to cosmic gamma-ray background

Following Ref. [334], the CGB gamma-ray flux from cosmological DM mini-spikes, defined as the number of photons per unit area, time, solid angle and energy, is then obtained as:

$$\langle I(E)_{DM} \rangle = \int dr \; W\left(E[1+z], z\right), \tag{3.16}$$

where

$$W(E,z) = \frac{(\sigma v)}{8\pi m_\chi^2}\frac{dN_\gamma}{dE}\left(E[1+z]\right)e^{-\tau(E[1+z],z)}\Delta^2(z). \tag{3.17}$$

The absorbtion of gamma-rays due to interaction with the diffuse extragalactic background light is parametrized through the effective optical depth τ as in Ref. [330]. The comoving distance r and the redshift z are interchangeably used and the element dr is simply $dr = c/H(z)dz$ with $H(z)$ the Hubble function. The function $\Delta^2(z)$ in Eq. (3.17) is

$$\Delta^2(z) = n(z)\int_{r_{cut}}^{r_{sp}} \rho_{sp}^2(r) d^3r,$$

with $n(z)$ the comoving number density of IMBHs.

As reminded in Sec.3.3, the gamma-ray annihilation spectrum dN_γ/dE depends on the DM particle physics model; i.e., it determines the branching ratios for annihilation in Standard Model final states. Given these branching ratios (which can be computed for any specified particle DM model), the quantity dN_γ/dE can be reconstructed via Monte Carlo simulations. This is how, for instance, dN_γ/dE is computed in codes like `DarkSUSY` [22] which, in particular, makes use of `Pythia` [515, 516] Monte Carlo simulations.

From the discussion above, it is clear that the specific DM annihilation spectrum depends critically on the particle physics model. In the present study we wish to consider a particle dark matter setup as model independent as possible. As such, we consider two representative standard model final states, and assume that the DM particle annihilates 100% of the time in one of those two final states. For definiteness, we consider the final states $b\bar{b}$ and $\tau^+\tau^-$. The choice is motivated by both theoretical and phenomenological considerations: first, in the context of supersymmetry, perhaps the best motivated extension to the standard model encompassing a DM candidate, these final states are ubiquitous; second, the resulting DM annihilation spectra dN_γ/dE cover the two extreme cases of a soft photon spectrum ($b\bar{b}$) and of a relatively hard spectrum ($\tau^+\tau^-$). Even harder photon spectra are in principle possible, for instance in the context of universal extra dimensions [7], or in other models with a large branching ratio in charged leptons. This is not critical to us, since we only focus on a single gamma-ray energy in our analysis; our results for the $\tau^+\tau^-$ are conservative with respect to even harder photon spectra, and the comparison with the soft spectrum we picked is a solid guideline to what would change with an even harder spectrum.

In supersymmetry, in the large $\tan\beta$ regime favored by Higgs searches at LEP, the dominant annihilation final states for the lightest neutralino include gauge bosons (if kinematically open) and down-type fermion-antifermion final states. The role of gauge bosons depends on the higgsino fraction of the lightest neutralino. Supersymmetric models with radiative electroweak symmetry breaking and gaugino unification at the grand unification scale feature generically a small higgsino fraction. In any case, the spectrum resulting from gauge boson final states resembles closely the $b\bar{b}$ spectrum [6, 322, 503]. If down-type

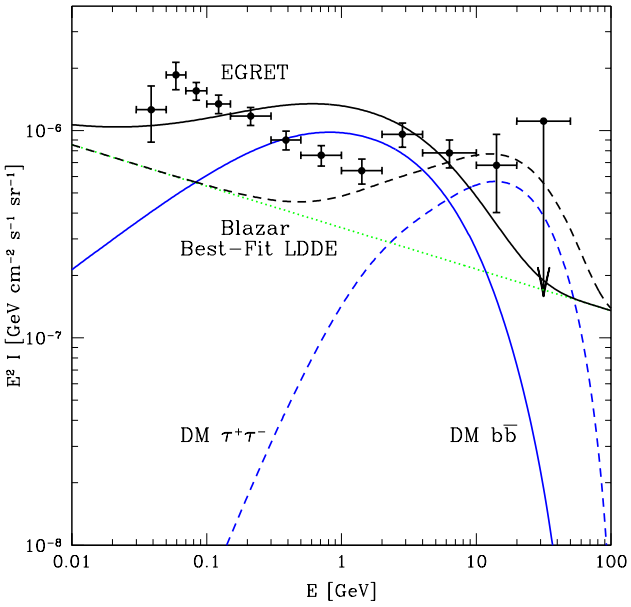

Figure 3.8: Cosmic gamma-ray background spectrum from DM annihilation in mini-spikes (dashed) and blazars with the best fit LDDE GLF model(dotted). The sum of the two signals is shown as a solid line and the data points are from EGRET data [521].

fermion-antifermion final states dominate, pair annihilation into $b\bar{b}$ is the dominant channel, possibly competing with $\tau^+\tau^-$ but winning over it by a factor 3 from color and by the square of the bottom-to-tau mass ratio (see e.g. [286]). In some cases, however, supersymmetry predicts a large branching ratio in $\tau^+\tau^-$, for instance when the lightest neutralino relic abundance is driven by coannihilation with the lightest stau, which then also mediates the dominant pair-annihilation channel. Several supersymmetric models feature $\tau^+\tau^-$ as the dominant annihilation channel. In addition, other models [7] where for instance the quantum numbers of the DM particle weigh favorably charged leptons over quarks, naturally feature a hard photon spectrum, close to $\tau^+\tau^-$.

In summary, in the present study we restrict ourselves to the two final states $b\bar{b}$ and $\tau^+\tau^-$ as representative WIMP annihilation final states bracketing a wide range of model-dependent predictions. The input spectra, shown in Fig. 3.7, are the results of the numerical study of Ref. [517].

Modeling the mini-spikes number density

The IMBH number density is parametrized following the numerical study of Ref. [484]. We consider that one IMBH is formed at redshift z_{re} in every DM halo with a mass higher

than $M_{min} = 10^8 M_\odot$. As mentioned in Sec. 3.2, IMBHs cannot be formed at more recent epochs and the formation at higher redshifts is negligible. In any case, the prescription we have adopted provides a lower limit to the CGB mean flux from mini-spikes, also in view of the fact that more than one IMBH could be formed in larger halos as well.

The comoving number density at the formation redshift, is obtained as:

$$n(z_{re}) = \int_{M_{min}}^{\infty} dM \frac{dn}{dM}(M, z = z_{re}). \tag{3.18}$$

We employ here the halo mass function $dn/dM(M, z)$ given in Ref. [518], with the transfer function of Ref. [520].

After formation, IMBHs get redistributed in halos during their hierarchical mergers. At the present epoch, the comoving number density of unmerged IMBHs is given by:

$$n(0) = \int_{M_{min}}^{\infty} dM \frac{dn}{dM}(M, z = 0) N_{bh} \frac{M}{10^{12.1} h^{-1} M_\odot}, \tag{3.19}$$

with the average number of IMBHs in the Milky Way halo N_{bh} obtained from the simulation of Ref. [484]. Here we assume a linear dependence of the number of unmerged IMBHs on their host halo mass. As noticed in Ref. [334], reasonable deviations from the this linear interpolation produce small changes on the final CGB flux.

At intermediate redshift, we follow the prescription of Ref. [334], and compute $n(z)$ assuming a redshift power-law behavior, with the index β obtained by fitting $n(z)$ at $z = 0$ and $z = z_f$:

$$n(z) = n(z_f) \left(\frac{1+z}{1+z_f} \right)^{\beta}. \tag{3.20}$$

Reference [484] found that a Milky-Way like galaxy would host a population of $N_{sp} = 101$ IMBHs at $z = 0$. For the same choice of the cosmological parameters and using Eqs. (3.25) and (3.20) we obtain $\beta = 0.3$, as in Ref. [334]. This computation can be updated by using the more precise measurements of the cosmological parameters from WMAP5 [13]. Keeping $\beta = 0.3$, we obtain a sensible decrease of the IMBH number density and for a Milky-Way like halo at z=0, we get $N_{sp} = 40$.

For the rest of the chapter we will therefore assume $N_{sp} = 40$ and $\beta = 0.3$ to parametrize the IMBH number density. Concerning the DM density distribution around IMBHs, the average parameters for the spikes found in the simulations of Ref. [310] are $r_{sp} = 6.8$ pc and $\rho_{sp} = 1.2\ 10^{10}\ M_\odot\ \mathrm{kpc}^{-3}$. We employ here these reference values throughout our analysis. Using Eq. (3.16) we can now compute the mean extragalactic gamma-ray flux from DM annihilation in cosmological mini-spikes. The integration over z is performed up to the formation redshift, i.e., z_{re}. The results are shown in Fig. 3.8 adopting $m_\chi = 100$ GeV and $(\sigma v) = 3 \times 10^{-26}\ \mathrm{cm}^{-3}\ \mathrm{s}^{-1}$ and for DM annihilation into $b\bar{b}$ and $\tau^+\tau^-$. In the same plot are shown the measurements of the CGB extracted from EGRET data [521]. The predictions largely depend on the annihilation spectrum, with the CGB flux peaking at higher

energies for harder spectra. For energies of the order $\mathcal{O}$(1–10) GeV, the contribution from DM annihilation is at the same level of the CGB intensity inferred from EGRET measurement, suggesting therefore that in this energy range DM annihilation could substantially contribute to the total CGB flux.

In our analysis, we have included also the contribution from low redshifts, where IMBHs are potentially detectable. In the previous sections we have shown that the Fermi satellite is expected to resolve mini-spikes in our galaxy [310] and maybe Andromeda [311] but not further. On the other hand, the contribution of IMBHs from $z < 10^{-5}$ to the extragalactic gamma-ray background is negligible.

3.7.2 Unresolved Blazars

The gamma-ray luminosity function (GLF) of blazars is obtained from the luminosity dependent density evolution (LDDE) model of Ref. [522].

The CGB flux from unresolved blazar is computed as:

$$E\langle I_B(E)\rangle = \int_0^{z_{max}} dz \frac{d^2V}{dz d\Omega} \int_{L_{min}}^{L_{max}(z)} dL \rho_\gamma(L,z) \mathcal{F}_E(L,z).$$

The functions in the Equation above are derived in Ref. [337] and references therein. The minimum blazar luminosity is taken to be $L_{min} = 10^{41}$ erg s^{-1} and the EGRET flux sensitivity above 100 MeV is 10^{-7} cm^{-2} s^{-1}. In Fig. 3.8 we show the results for the best-fit LDDE GLF model (details on the blazar model can be found in Ref. [337]).

3.8 Cosmic gamma-ray angular correlations

3.8.1 Dark Matter Annihilations

The angular power spectrum C_l of the CGB from DM annihilation in substructures has been computed in Ref. [337]. Here we adapt their formalism to the case of mini-spikes and we refer to the original reference for the derivation of the equations.

The angular power spectrum from mini-spikes is obtained as:

$$\langle I(E)\rangle^2 C_l = \int \frac{dr}{r^2} W\left([1+z]E, z\right)^2 P_{DM}\left(\frac{l}{r}, z\right), \tag{3.21}$$

where $P_{DM}(k)$ is the spatial power spectrum of mini-spikes and it can be divided into 1-halo

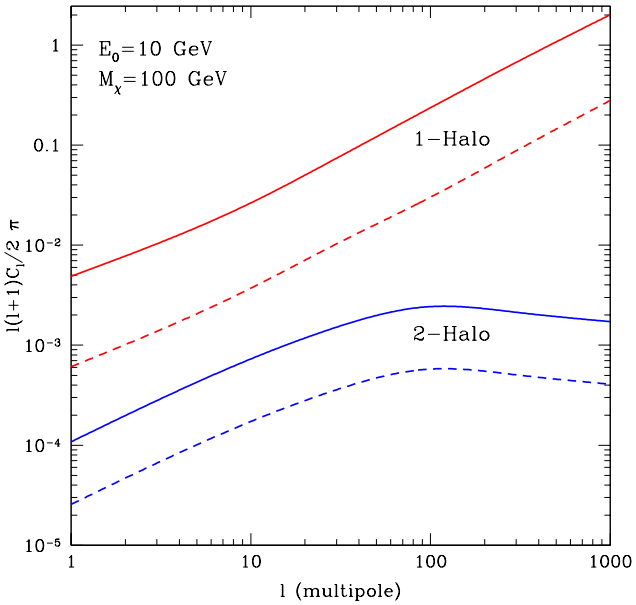

Figure 3.9: Angular power spectrum from DM annihilation in mini-spikes computed at $E_0 = 10$ GeV. We show separately the contributions from 1-halo (red) and 2-halo (blue) terms. The total angular power spectrum is the sum of the two curves. Solid lines refer to DM annihilation into $b\bar{b}$ and dashed ones are for $\tau^+\tau^-$ final states. We set the DM particle mass to $m_\chi = 100$ GeV.

and 2-halo terms:

$$P_{DM}(k) = P^{1h}(k) + P^{2h}(k), \tag{3.22}$$

$$P^{1h}(k) = \int_{M_{min}}^{\infty} dM \frac{dn}{dM} \left(\frac{\langle N|M \rangle}{n(z)} \right)^2 |u(k,M)|^2, \tag{3.23}$$

$$P^{2h}(k) = \left[\int_{M_{min}}^{\infty} dM \frac{dn}{dM} \frac{\langle N|M \rangle}{n(z)} b(M) |u(k,M)| \right]^2 \times P^{linear}(k,z). \tag{3.24}$$

These terms refer to correlations between two points in the same halo (1-halo) or in two different halos (2-halo). The function $u(k, M)$ is the Fourier transform of the IMBH volume probability, defined in Sec. 3.2. Following the scaling procedure adopted in Sec. 3.3, the volume probability distribution function of the IMBH population in a given galaxy, $u(r)$, is obtained from that for the Milky Way, as $u(r) = g(r/\kappa)/\kappa^3$, with κ the ratio between the virial radii. The virial radius for a halo of a given mass M at a given redshift is defined as the radius of a spherical volume within which the mean density is $\Delta_c(z)$ times the critical density at that redshift, $M = 4\pi r_{vir}^3 \Delta_c(z) \rho_c(z)/3$, with the virial overdensity $\Delta_c(z)$ as given in Ref.[519].

The linear power spectrum $P(k)$ is obtained using the transfer function of Ref. [520] and the bias parameter is taken from Ref. [523].

The function $\langle N|M\rangle$ gives the number of IMBHs in an halo of given mass at a given redshift and it is related to the IMBH comoving number density as:

$$n(z) = \int_{M_{min}}^{\infty} dM \frac{dn}{dM} \langle N|M\rangle. \tag{3.25}$$

As noticed in Sec. 3.2, at $z = 0$ $\langle N|M\rangle$ is well approximated by $\langle N|M\rangle_{lin} = N_{sp}(\frac{M}{10^{12.1}h^{-1}M_{\odot}})$ with N_{sp} corresponding to $N_{sp} = 40$, as appropriate for the Milky Way. On the other hand, at the formation redshift we assume that one BH is formed for every halo with mass above M_{min}. Formally, there is no unique expression for $\langle N|M\rangle$ which interpolates the two regimes above and that, at the same time, allows one to reproduce Eq. (3.20) from Eq. (3.25). We have explored different parametrization for $\langle N|M\rangle$ encompassing its limiting behaviors at $z = 0$ and $z = z_{re}$ and overestimating and underestimating $n(z)$ with respect to Eq. (3.20). Since the power spectrum computed in Eq. (3.21) is dominated by the contribution at small z, we have found that these different choices produce differences in C_l always between a factor 2, that are within other uncertainties in the calculations. This is also true also for the cross-correlation terms that we will introduce in Sec. 3.9.

From Eq. (3.21), we note that the multipoles C_l are independent of the value of (σv) and of the choice of DM density profile around each IMBH. We also find that they are weakly dependent on the normalization N_{bh}.

In Fig. 3.9 we show, for the two different WIMP annihilation channels, the contributions of 1-halo and 2-halo terms on the angular power spectrum. We picked a gamma-ray energy at which we compute the anisotropy power spectrum of $E = 10$ GeV, and fixed the particle DM mass to $m_{\chi} = 100$ GeV.

The 2-halo term turns out to be negligible at all angular scales. The slope of the 1-halo term lies between those of the 1-halo terms for annihilation in subhalos and smooth NFW halos computed in Ref. [337] (see their Fig. 2). This can be understood considering that the signal in the subhalo and in the smooth-halo-dominated cases follow respectively the density profile and its square and for the case of a NFW profile the two distributions are respectively shallower and steeper than the IMBH radial distribution. The increased normalization of the power spectrum with respect to the case of subhalos emission is explained by the same argument: the Fourier transform of the IMBH profile gets more power at high k with respect to that of NFW. The same tendency is found for the two choices of the annihilation spectra. The angular power spectrum for DM annihilation into $b\bar{b}$ is larger than that for $\tau^+\tau^-$ final states because at the energy of $E_0 = 10$ GeV, the former photon spectrum is significantly steeper than the latter.

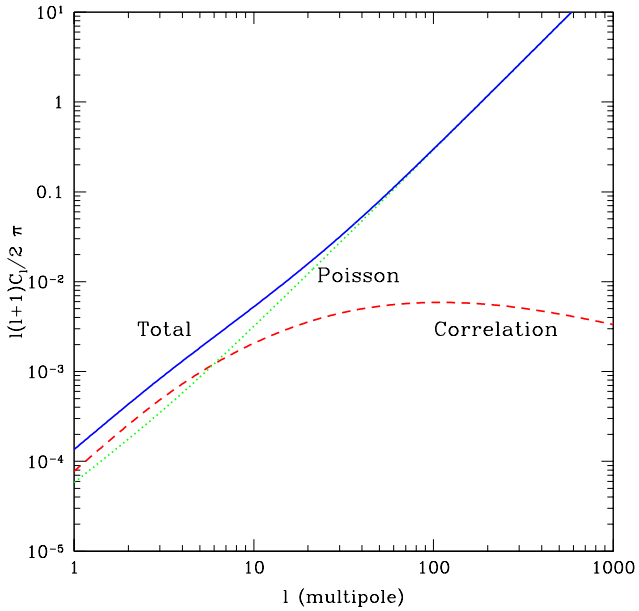

Figure 3.10: Angular power spectrum of the CGB from unresolved blazars expected for Fermi. We show separately the Poisson (dotted) and the correlation (dashed) terms. The total is simply the sum, and is shown as a solid curve. We assume here the best-fit LDDE GLF model.

3.8.2 Blazars

The angular power spectrum from unresolved blazar comes from the contributions of a Poisson term C_l^P and a correlation term C_l^C, respectively the 1-halo and 2-halo terms:

$$C_l = C_l^P + C_l^C, \tag{3.26}$$

$$C_l^P = \frac{1}{E^2\langle I_B(E)\rangle^2}\int dz \frac{dV}{dz d\Omega} \times \int_{L_{min}}^{L^{max}(z)} dL \rho_\gamma(L)\mathcal{F}_E(L,z)^2, \tag{3.27}$$

$$C_l^C = \frac{1}{E^2\langle I_B(E)\rangle^2}\int dz \frac{dV}{dz d\Omega} P_{lin}\left(\frac{l}{r(z)}\right) \times \left[\int_{L_{min}}^{L^{max}(z)} dL \rho_\gamma(L) b_B(L,z)\mathcal{F}_E(L,z)\right]^2. \tag{3.28}$$

The blazar bias b_B indicates how strong blazars are clustered with compared to the linear matter power spectrum. Presently, this value is uncertain, and different (generically inconsistent) estimates are inferred from different techniques. Current observations give an upper bound $b_B \lesssim 5$ (see Ref. [522]).

Reference [337] estimated the correlation term assuming either a bias model inferred

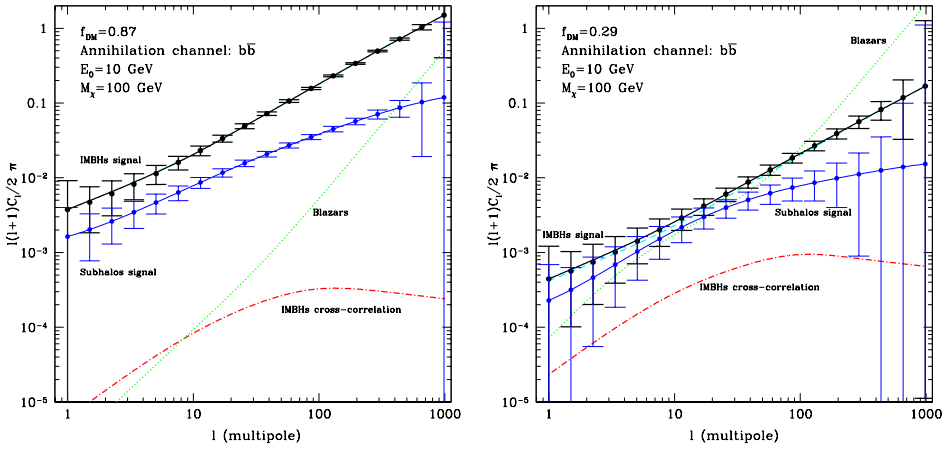

Figure 3.11: Angular power spectrum of the CGB from DM annihilations around IMBHs at a photon energy $E_0 = 10$ GeV. Dashed line shows the contribution from DM annihilation ($f_{DM}^2 C_l^{DM}$), dotted line is for blazars ($f_B^2 C_l^B$) and the dot-dashed line is the cross-correlation term $2 f_{DM} f_B C_l^{Cr}$. The total signal C_l^s is shown as a thick black solid curve. Error bars are for 2-years of Fermi data. The thin blue solid curve show the DM signal for DM annihilations in subhalos [337] (see text for more details).

from quasar observations or a simply constant $b_B = 1$. The results obtained are quite similar since the main contribution to the CGB comes from low-redshift blazars, which have bias close to 1. In addition, for $l \gtrsim 10$ the total angular power spectrum is dominated by the Poisson term.

We present in Fig. 3.10 our predictions for the angular power spectrum expected to be reconstructed from Fermi data, adopting the best-fit LDDE GLF model. We assume a Fermi point source sensitivity of 2×10^{-9} cm^{-2} s^{-1}, the value expected for energies above $E = 100$ MeV and two years of full sky survey mode, for sources with a spectral index equals to 2. We note that the power spectrum is independent of the gamma-ray energy, since we have assumed the same power-law spectrum for all blazars and these dependence exactly cancels when we divide by the mean intensity squared in Eq. (3.27) and Eq. (3.28).

3.9 Distinguishing Dark Matter Annihilation from Blazars

We outline here the prospects for distinguishing DM annihilation from blazar emissions in the angular power spectrum of CGB with Fermi.

3.9.1 Angular correlations of CGB in the two component case

The CGB background receives contributions from both DM annihilation and from ordinary astrophysical sources, with unresolved blazars being a representative candidate for the latter class of emitters. For the detection of DM annihilation in the CGB, blazars therefore constitute a background. Their contribution is currently uncertain but we expect it will be modeled rather precisely with the Fermi catalog of detected blazars. In addition, as mentioned in Sec. 3.8 the angular power spectrum for astrophysical sources is energy independent and therefore it could be calibrated at low energies where the contribution from DM annihilation is negligible and then subtracted from the total anisotropy data. For this analysis we therefore treat the blazar contribution as a known background, and we study the prospects for detecting DM annihilation on top of it.

In this two component analysis, the total CGB intensity is the sum of the DM and blazar contributions:

$$\langle I_{CGB}(E)\rangle = \langle I_{DM}(E)\rangle + \langle I_B(E)\rangle.$$

Labeling with f_{DM} the fraction of the total CGB coming from DM annihilation, $f_{DM} = \langle I_{DM}(E)\rangle/\langle I_{CGB}(E)\rangle$, the total angular power spectrum is:

$$C_l^{CGB} = f_{DM}^2 C_l^{DM} + 2 f_{DM} f_B C_l^{Cr} + f_B^2 C_l^B,$$

where C_l^{DM} and C_l^B are respectively the angular power spectrum from DM annihilation and blazars and f_B is simply $f_B = 1 - f_{DM}$.

The cross-correlation term C_l^{Cr} has been studied in Ref. [337] and is divided into 1-halo and 2-halo terms:

$$\begin{aligned} C_l^{Cr,1-halo} &= \frac{W([1+z]E,z)}{E\langle I_B(E)\rangle\langle I_{DM}(E)\rangle}\int_{L_{min}}^{L^{max}(z)} dL\rho_\gamma(L) \\ &\times \mathcal{F}_E(L,z)\frac{\langle N|M\rangle}{n(z)} u\left(\frac{l}{r}, M[L]\right), \qquad (3.29) \\ C_l^{Cr,2-halo} &= \frac{W([1+z]E,z)}{E\langle I_B(E)\rangle\langle I_{DM}(E)\rangle}\int_{L_{min}}^{L^{max}(z)} dL\rho_\gamma(L) \\ &\times \mathcal{F}_E(L,z) b_B(L,z)\int_{M_{min}}^{\infty}\frac{dn(M,z)}{dz)}\frac{\langle N|M\rangle}{n(z)} \\ &\times b(M,z) u\left(\frac{l}{r}, z, M\right) P_{lin}\left(\frac{l}{r}, z\right). \qquad (3.30) \end{aligned}$$

A relation between the blazar luminosity and its host halo mass, $M[L]$ is given in Ref. [522].

In this two component framework, the total signal C_l^s and the background noise C_l^b therefore read:

$$\begin{aligned} C_l^s &= f_{DM}^2 C_l^{DM} + 2 f_{DM}(1-f_{DM}) C_l^{Cr}, \qquad (3.31) \\ C_l^b &= (1-f_{DM})^2 C_l^B. \qquad (3.32) \end{aligned}$$

The GLF-LDDE blazar model in Ref. [522] basically depends on three parameters (γ_1, q, k) and as reminded in Sec. 3.7, the best-fit model only accounts for ∼15% of the CGB intensity at 10 GeV. However, varying the parameters of the blazar model allows to explain different fractions of the CGB. For example setting them to ($\gamma_1 = 1.36$, $q = 3.80$, $k = 3.15 \times 10^{-6}$) we obtain a blazar fraction $f_B = 0.71$. On the other hand, the contribution from DM annihilation in mini-spikes is largely affected by astrophysical and particle physics uncertainties. For example, in WIMP models the mass usually lies in the broad range $\mathcal{O}$(1–1000) GeV[1] and (σv) can largely differ from the thermal value $(\sigma v) = 3 \times 10^{-26}$ cm^3 s^{-1} in the presence of efficient coannihilations or Sommerfeld corrections, if the DM candidate is non-thermally produced or if a modified cosmological expansion rate is postulated at the time of WIMP freeze-out. Moreover, as discussed in Sec. 3.7, the number of mini-spikes in halos could differ from that found in simulations, since IMBH formation could have been underestimated or on the contrary IMBHs could have been more efficiently destroyed by astrophysical processes than what is expected. In addition, the DM density profile around each IMBH could be modified as well by feedback.

Motivated by these arguments we compute two different models of blazars, explaining respectively a small and an high fraction of the CGB at 10 GeV, and we assume that the remaining CGB intensity comes from DM annihilation in mini-spikes. As a benchmark model we fix the DM mass to $m_\chi = 100$ GeV and we refer to annihilation to $b\bar{b}$ pairs. Following Ref. [337], we choose an energy of observation $E_0 = 10$ GeV as a compromise between maximization of signal count and minimization of the Galactic emission. At lower energies, the galactic foreground becomes stronger, masquerading the extragalactic component, while at higher energies, the photon count is more suppressed. However, we perform our analysis also for different choices of DM parameters and energies of detection.

3.9.2 Prospect for detection with the Fermi Telescope

The Large Area Telescope (LAT) onboard the Fermi satellite is currently taking scientific data in a survey mode. The LAT has a more than one order of magnitude better sensitivity in the 20 MeV to 10 GeV region than its predecessor Energetic Gamma Ray Experimental Telescope (EGRET) onboard the Compton Gamma-ray Observatory [525]. In addition, the LAT extends the high-energy gamma-ray region up to around 300 GeV. In the present study, we consider a mean exposure of 1.2×10^{11} cm^2 s, corresponding, roughly, to 2 years of all-sky survey mode operation [526, 527, 316]. We assume an angular resolution for 68% containment of the point spread function of $\sigma_b = 0.115°$, appropriate for energies of around 10 GeV. Our choices reflect those described in Ref. [337]. The angular resolution improves at larger energies, and degrades at lower energies.

For the type of study hereby presented, a thorough knowledge of the gamma-ray galactic

[1] For a recent discussion of ultra-light WIMPs in supersymmetry see Ref. [524].

background will be warranted. In addition, disentangling the diffuse extra-galactic background from the mentioned galactic emission will also be challenging. Realistically, the 2 years of observations we consider refer not to the early stages of the mission but, rather, to a stage when these backgrounds are considered to be thoroughly under control.

Considering the Fermi specifications described above, the projected 1-σ error bars of the CGB power spectrum from DM annihilation is:

$$\delta C_l^s = \sqrt{\frac{2}{(2l+1)\Delta l f_{sky}}} \left(C_l^s + C_l^b + \frac{C_N}{W_l^2} \right). \tag{3.33}$$

We take a bin width $\Delta l = 0.5l$. The window function of a gaussian point spread function is $W_l = \exp(-l^2\sigma_b^2/2)$. C_N is the photon spectrum of the photon noise and it is given by $C_N = \Omega_{sky} N_{tot}/N_{CGB}^2$ with N_{tot} and N_{CGB} respectively the total and CGB photon numbers detected from a region of sky Ω_{sky}.

Following Ref. [337], we restrict the analysis to galactic latitudes $|b| > 20^\circ$. At lower latitudes, the galactic foreground dominates over the CGB flux, while the situation is expected to be reversed in the region we consider. After the cut of the galactic plane, the fraction of sky we consider is $f_{sky} = 0.66$. Using $N_{tot} \sim N_{CGB}$ we obtain $C_N \sim 4\pi f_{sky}/N_{CGB} = 8 \times 10^{-5} (E/10 \text{ GeV})$. Here we employ the total CGB flux as estimated from EGRET data. We note, however, that since Fermi is expected to detect a large number of blazars, the total GCB intensity will be in all likelihood reduced, possibly lowering our error estimations.

In Fig. 3.11, we present our predictions for two blazar models contributing a fraction $f_B = 0.13$ and $f_B = 0.71$ of the total CGB flux at $E_0 = 10$ GeV. We show the signal and the background power spectra that Fermi is expected to measure after two years of observations as well as the projected 1-σ signal error bars. The signal is detected if $C_l^s > \delta C_l^s$. We notice that this occurs even if the DM contribution is very small. In addition, the shape of the DM power spectrum is very different from the one corresponding to blazars. This feature could therefore help distinguish the two scenarios.

In Refs. [336, 337], the authors first studied the angular anisotropies of the CGB from DM annihilation. They focused their attention on two scenarios, the first assuming that the DM signal is dominated by annihilations occurring in cosmological DM halos and the latter considering that the dominant contribution comes from the populations of DM clumps hosted in the main DM halos. For each possibility they took into account the possible uncertainties on the minimum halo mass value and on the halo occupation distribution, i.e., the number of subhalos in a parent halo of given mass. For these frameworks, they computed the angular power spectrum from DM annihilation that Fermi is expected to measure. They concluded that provided DM annihilation contribute to the CGB at 10 GeV with a fraction $f_{DM} \gtrsim 0.3$, after two years of data taking Fermi will be able to detect the DM signal.

In Fig. 3.11, we show their results for the most promising case, i.e., when the DM signal is dominated by cosmological clumps with an halo occupation distribution $\langle N|M\rangle \propto M$. We consider that DM annihilations in subhalos contribute to a certain fraction f_{DM} to the CGB intensity at 10 GeV and the remaining flux comes from blazars. In each plot the DM fraction f_{DM} is the same for the mini-spike and clump scenarios. The signal for the subhalo case with the associated 1-σ error bars is plotted as a thin blue solid line. Comparing the DM signals in the mini-spike and subhalos scenarios we notice that provided that DM annihilations largely contribute to the CGB mean intensity, there are promising prospects for distinguish the two cases. This conclusion is further strengthened if we consider DM annihilation in cosmological smooth halos instead of clumps, since, as stated before, the expected angular power spectrum is smaller than when subhalos emission dominates.

3.9.3 Power spectrum dependence on energy of detection, annihilation spectrum and DM mass.

Even if the results discussed in the section above refer to a certain specific choice of DM parameters and energy of detection, we have also repeated the calculations for different cases. Rather than presenting all the plots, we just show in Fig. 3.12 what we obtained for some benchmarks and we try to summarize some general guidelines. A more complete analysis, for example dedicated to the optimization of the energy of detection as a function of the particle mass, is beyond the scope of this study.

First we show how our predictions change if we pick another energy of detection. At energies higher than 10 GeV the galactic foreground is sensibly suppressed but also the photon number from DM annihilation is reduced, since the interval of integration in energy is shrunk. Therefore, it is not trivial to infer which is the effect on the DM angular power spectrum and its error bars. We find that even if the CGB mean intensity at 20 GeV is reduced with respect to its value at 10 GeV, the power spectrum is increased. We remind that the power spectrum is normalized to the mean flux, as in Eq. (3.21). At an energy of 1 GeV the CGB mean intensity is comparable with the galactic foreground therefore in Eq. (3.33) we consider $C_N \sim 2\Omega_{sky}/N_{CGB}$. For this gamma-ray energy, the signal is sensibly reduced and the prospects for detection are degraded.

As pointed out in Sec. 3.8 for softer energy spectra, the normalization of angular power spectrum is decreased. We indeed find this behavior when we compare the results obtained for the $\tau^+\tau^-$ and for the $b\bar{b}$ DM annihilation final states. For the "pessimistic" case of annihilations into $\tau^+\tau^-$, assuming an energy of detection of 10 GeV and $m_\chi = 100$ GeV, DM annihilations have to contribute at least with a fraction $f_{DM} \sim 0.3$ to the mean CGB in order to be detectable in the CGB angular power spectrum with Fermi.

We finally show the results for $m_\chi = 1000$ GeV and $E_0 = 10$ GeV. The photon spectra from DM annihilation can in good approximation be scaled with the particle mass defining

the adimensional variable $x = E/m_\chi$, as in Fig. 3.7. Therefore, looking at Eq. (3.17) and Eq. (3.21), we note that there is an approximate scaling which links the angular power spectra computed at different energies of observations and for particle of different masses. For example, the choices ($E_0 = 10$ GeV, $m_\chi = 1000$ GeV) and ($E_0 = 1$ GeV, $m_\chi = 100$ GeV) actually correspond to the same value of dN_γ/dx, and should thus lead to identical angular power spectra. This scaling is broken by the dependence of the function $\tau(z)$ on E_0 in Eq. (3.17), which fortunately is not important at the energies of interest, and our qualitative considerations are still roughly valid. This can be seen noting that the power spectra in Fig. 3.12 for the two cases above are indeed very similar. Note however that, as already stressed, different energies of observations significantly affect the projected errors bars.

3.10 Summary

DM annihilation in mini-spikes around IMBHs is a promising scenario for indirect DM searches with gamma rays. In particular, Fermi is expected to detect a significant fraction of the IMBH population in the Milky Way and maybe a few sources in the Andromeda galaxy. The remaining cosmological mini-spikes will remain unresolved, but could leave their imprint in the CGB. As shown in [334], for a standard neutralino with a mass $m_\chi = 100$ GeV and a "thermal" annihilation cross section $(\sigma v) = 3\ 10^{-26}$ cm^{3}s^{-1} the predicted CGB flux from cosmological mini-spikes is comparable to the EGRET CGB flux at gamma-ray energies of $\mathcal{O}(1-10)$ GeV. We find that, for example, this corresponds to a fraction $f_{DM} = 0.35$ and $f_{DM} = 0.72$ of the CGB at $E = 10$ GeV, respectively for DM annihilation into $b\bar{b}$ and $\tau^+\tau^-$. Fermi is expected to resolve a much larger number of galactic and extragalactic gamma-ray sources compared to its predecessor EGRET, with the expectation of reducing the measured unresolved diffuse CGB flux. At the same time, only IMBHs very close to us will be resolved, therefore the DM contribution to the CGB could be increased with respect to our estimates, based on the mean CGB spectrum extracted from EGRET data.

However, in absence of characteristic spectral features, it will be problematic to distinguish DM annihilation and ordinary astrophysical emissions from the mean CGB intensity. Instead, Ref. [337] showed that gamma-ray anisotropy data could provide a more suitable tool to pursue this program. In fact, provided DM annihilation contributes substantially to the CGB mean intensity, it will be detectable in the CGB angular power spectrum by Fermi.

Motivated by these considerations, in the previous sections, we studied the anisotropies of the CGB in the mini-spikes scenario. Astrophysical and particle physics uncertainties largely affect the predictions for the mean CGB intensity from mini-spikes and also the blazar contribution is currently unknown. Considering these two sources as the main com-

ponents of the CGB, we computed their angular power spectra for different relative contributions and, treating the blazar component as a known background, we studied the prospects for DM annihilation detection in the CGB angular power spectrum with two years of Fermi observations. We expect that considering unresolved blazars as a background is a reasonable assumption, since their GLF and bias should be quite reliably reconstructed from the Fermi source catalog.

We repeated our computations for different detection energies, particle masses and annihilation modes, showing that our results are significantly affected by all these parameters. Interestingly, this could mean that information on these three quantities can actually be inferred from the measured DM-induced gamma-ray anisotropy power spectrum. However a more detailed analysis would be necessary to fully study the potential of the anisotropy technique to reconstruct these parameters. We found that the shape of the DM power spectrum is very different from that of blazars, providing a robust handle to disentangle the two signals. Astrophysical sources other than blazars could however also contribute to the CGB and, if spatially extended, as clusters of galaxies, the shape of their angular power spectrum could significantly differ from that of blazars, which is dominated at large multipoles by the Poisson term. We stress that even in this case we could calibrate the astrophysical power spectrum at low energies, where DM annihilations are negligible and subtract it from the measured total CGB power spectrum at the energies of interest. In fact, for sources with power-law energy spectra, the gamma-ray angular power spectrum is energy independent and this condition is common to almost any class of standard astrophysical gamma-ray emitter.

In conclusion, we showed that the prospects for detecting DM annihilation from cosmological mini-spikes in the angular CGB power spectrum with Fermi are promising, and that the analysis of the anisotropy power spectrum allows not only a discrimination of a DM component against astrophysical sources, but also a better understanding of the structures where the DM signal originates.

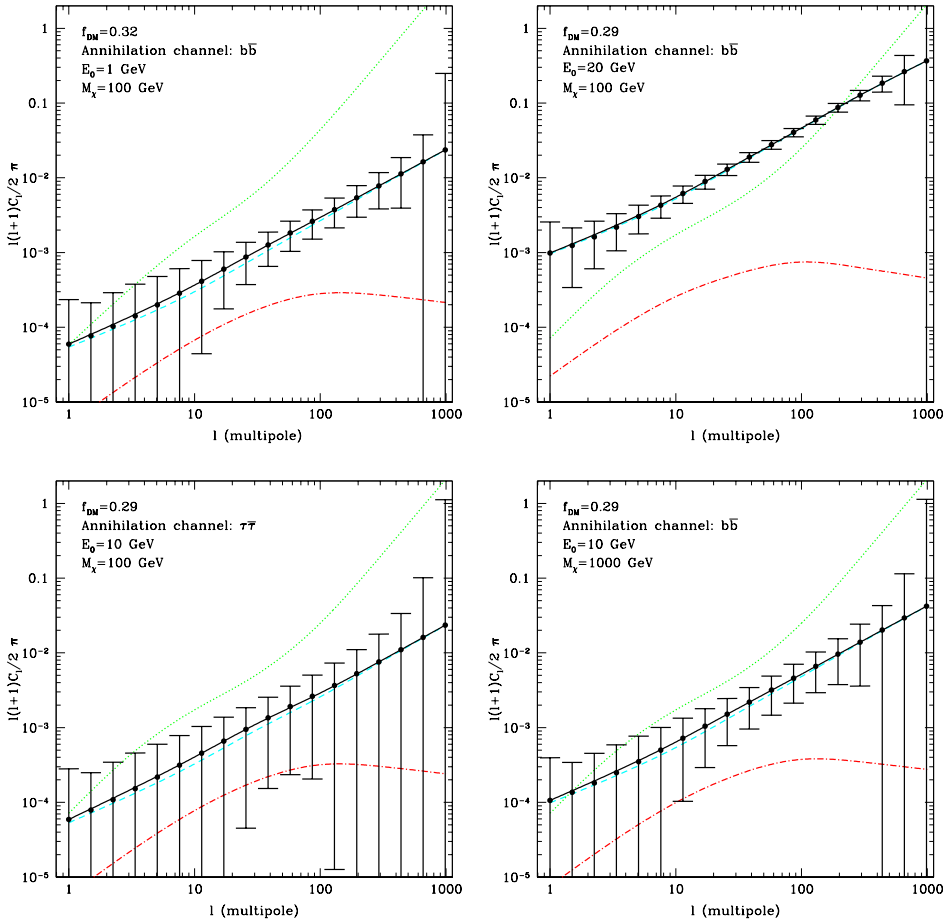

Figure 3.12: Angular power spectrum of the CGB from DM annihilation and for blazars. Lines are as in Fig. 3.11. Annihilation channel, energy of detection, DM mass and fractional contribution to the CGB mean intensity are specified for each panel.

Chapter 4

Indirect detection with antimatter

PAMELA and ATIC have recently reported an excess in $e^{\pm}$ cosmic rays that has been tentatively interpreted in terms of Dark Matter annihilations. We constraint this interpretation comparing the associated gamma-ray flux and the synchrotron emission produced by $e^{\pm}$ in the galactic magnetic field with HESS and radio observations of the galactic center and HESS observations of dwarf Spheroidals. For the most commonly adopted DM profiles, the models that provide a good fit to the PAMELA and ATIC data are ruled out, unless there are physical processes that boost the local anti-matter fluxes more than one order of magnitude, while not affecting the gamma-ray or radio fluxes.

This Chapter is partially based on [384] and [528].

4.1 Introduction

For cosmic-rays are generally intended charged particles propagating in the Universe. Antimatter particles constitute a small fraction of cosmic-rays that are mainly produced by the interaction of nuclei cosmic-rays with the interstellar medium. Measurements of electrons and positrons cosmic-rays spectra have however revealed a possible excess of the positron fraction,$(\phi(e^+)/(\phi(e^+) + \phi(e^-)))$, with respect to the theoretical predictions. A first hint have been observed at energies beyond 7 GeV by the HEAT experiments [529] and have been subsequently confirmed by further measurements obtained by HEAT [530] and by re-analysis of the AMS-01 data [531].

Recently, a much stronger evidence have been obtained by the more precise data from the PAMELA satellite which have reported [532] an excess in the positron fraction above 10 GeV with a steep rise of the spectrum up to 100 GeV, the highest energy currently

probed by the experiment. No excess is instead seen in the antiproton flux [533]. Moreover, the balloon-borne experiment ATIC-2 [534] have reported the detection of a peak in the undistinguished flux of positron and electrons, in the energy range between 300 and 800 GeV. The two signals are compatible and at low energy, the precise data from PAMELA confirm previous hints from HEAT and AMS-01 experiments.

Of course caution should be used when interpreting the data, as the background flux from conventional astrophysical processes carry big uncertainties, as large as one order of magnitude, so that even the very evidence for an excess in PAMELA data could possibly be jeopardized [535, 536].

The spectacural features in the PAMELA and ATIC-2 spectra have however stimulated a lot of theoretical works trying to interpret the excess in terms of a primary source of positrons and electrons.

A likely possibility is that the observed effects are due to some single astrophysical object, such as a pulsar or a collection of them. Indeed it is expected that pulsars produce a power law spectrum of mostly electron-positron pairs, with a cut-off in the multi-TeV range. The known nearby pulsars Geminga and B0656+14 are the main candidates, but unknown and past pulsars can contribute to the integrated flux [537]. Work is underway to assess more precisely the features of the expected fluxes from pulsars and discriminate from the DM hypothesis [538].

Dark Matter annihilations in the galactic halo are indeed another potential candidate to solve the positron excess puzzle. Specific Dark Matter models have been recently proposed for this purpose and more general studies have been done to determine the Dark Matter properties suggested by the cosmic-rays data. Given these tantalizing hints of Dark Matter annihilations in the charged particle signals, it is now crucial to consider the constraints on this interpretation that come from the photon fluxes that necessarily accompany such charged particles. The best targets to search for these annihilation signals are regions with high DM densities, such as the Milky Way Galactic Center (GC), the Milky Way Galactic Ridge (GR) and the Sagittarius Dwarf spheroidal satellite galaxy (Sgr dSph). The predicted photon fluxes can then be compared with observational data, in order to rule out combinations of astrophysical and particle physics parameters that violate observational constraints. The aim of this chapter is to compare the regions suggested by the PAMELA (and ATIC) data in the plane of annihilation cross section and DM mass $(\sigma v, M)$ with those excluded by photon observations.

4.2 Cosmic-rays overview

Cosmic rays (CR) are charged particles propagating in the Universe with energies from eV up to PeV-scale. They are composed by electrons, protons and fully ionized nuclei of

light elements. Small amounts of antimatter are also presents. Depending on their origin cosmic-rays can be classified as follows:

i) Solar cosmic-rays: they are produced by solar activity and their composition mimic that of the Sun itself.

ii) Galactic cosmic-rays: they enter the solar sistem from outside. They are the focus of this study.

iii) Extragalactic cosmic-rays: they are produced outside our galaxy. Little is known about their composition due to a lack of statistyics.

Natural sources of galactic cosmic-rays are the the supernovae. Shockwaves produced during their explosions allow to accelerate particles that after escaping propagate in the interstellar medium and modify their energy spectra and directionality in various processes. The composition of cosmic-rays is as well modify by the collisions of these high energy particles with the interstellar and intergalactic gas, leading to the production of the so called secondaries, for example rare nuclei, like antiprotons, and pions which decay into electron and positron pairs.

Beside supernovae further primary sources are possible, both standard astrophysical objects, like pulsars and exotic contributions like Dark Matter annihilations and the evaporation of primordial black holes.

The antimatter cosmic-rays are less abundant than their matter counterpart and their origin is not yet established even though a fraction of them is certainly produced by cosmic-rays spallation with the interstellar gas. A comparison between theoretical predictions and observations is therefore a strategy to look for primary sources, for example Dark Matter annihilations. In the next section we will review the current status of antiprotons and positrons observations.

4.3 Cosmic-rays observations

Observations of galactic cosmic-rays are performed by balloon and satellite-borne experiments. A useful way to present antiprotons and positron measurements is in terms of the antiproton-to proton flux ratio, $\bar{p}/p$ and the positron fraction, a ratio of positron and electron fluxes (ϕ) defined as $(\phi(e^+)/(\phi(e^+) + \phi(e^-)))$. The most recent determinations of these observable have been recently done by the PAMELA satellite, which have extended the energy range explored by previous experiments and significantly improved the existing statistics.

The current status of positrons and antiprotons observations is shown in Fig. 4.1.

The antiproton-to-proton flux ratio determinations are well in agreement among different experiments while the situation for the positron fraction is more complicated. At high energy

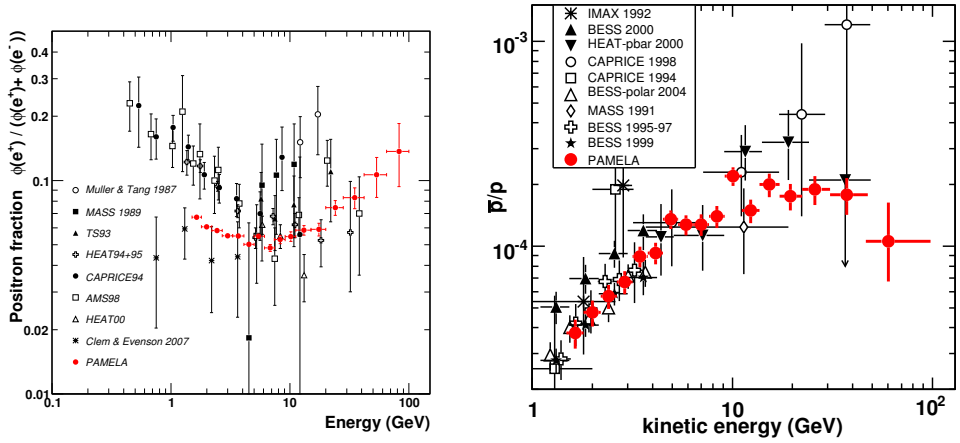

Figure 4.1: Left: positron fraction versus energy. From [532]. Right: antiproton-to-proton ratio as a function of the energy. From [533].

(above 10 GeV) the PAMELA data show a rise of the positron fraction with the energy, consistently with the results from other experiments. However, at lower energy (roughly below 5 GeV) the PAMELA data are systematically lower than previous determinations obtained during 1990's. These apparent discrepancy is probably explained by the solar modulation, e.g. the repulsion of the cosmic rays from the solar neighborhood produced by the solar wind. This effect depend on the solar activity, which is has approximately a sinusoidal time behavior with a complete period of 22 years and influences the fluxes of cosmic-rays with energies less than about 10 GeV.

In Fig. 4.2 the PAMELA results are compared with theoretical predictions for the antiprotons and positrons secondary production from cosmic-rays interactions with the interstellar gas. While antiproton-to-proton flux data follow the trend expected from the theoretical estimates, the prediction for the positron fraction significantly deviates at energies above 10 GeV. As reminded in the Sec. 4.1 this anomaly confirms previous hints from HEAT and AMS-01 data. It is important to remak that the positron fraction measured by PAMELA increases at energies above 10 GeV, therefore in an energy range where solar modulation effects on positron and electrons are not relevant.

Recently, the balloon-borne experiments ATIC-2 have detected a peak in the sum of positron end electron fluxes at energies of $\sim 300 - 800$ GeV [534]. Measurements at high energy (above 600 GeV) carried out by the HESS satellite [543] are compatible with the ATIC-2. The situation is shown in Fig. 4.3. These observations seem to indicate a bump in the positron and electron spectrum with a cut-off at ~ 1 TeV.

The origin of this "positron excess" is still under debate. Of course, a careful examination of the theoretical predictions is necessary, in order to single out a possible primary positron

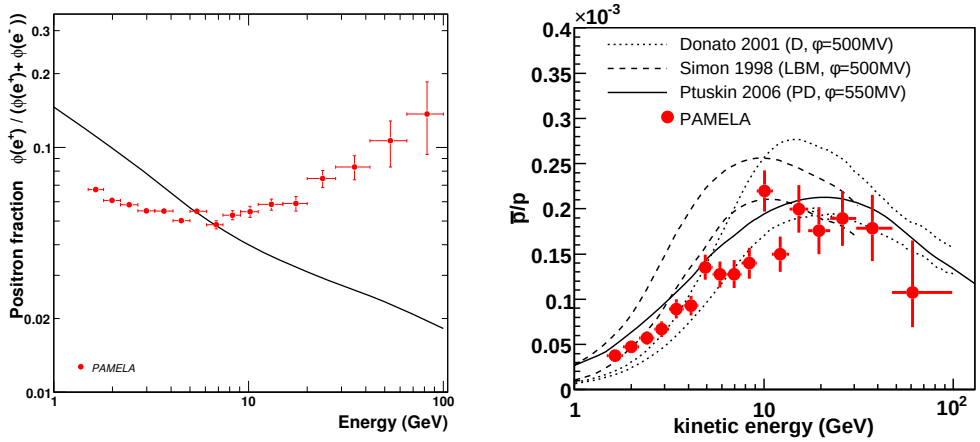

Figure 4.2: Left: PAMELA positron fraction compared with theoretical predictions for pure secondary production [539] From [532]. Right: comparison between PAMELA measurements of the antiproton-to-proton ratio with theoretical predictions for secondary production. The dashed lines show the upper and lower limits calculated by [540] , while the dotted lines show the limits from [541]. The solid line shows the calculation by [542]. The estimates have been obtained using a solar modulation parameter, ϕ, appropriate for the PAMELA data taking period. From [533].

component. The theoretical estimates of the secondary positron are in fact largely affected by the uncertainties in the propagation parameters, nuclear cross sections and primary cosmic-ray nuclei fluxes. Moreover, the positron fraction depends on the electron flux which is of course known only within the experimental accuracy. Considering all these sources of uncertainties, in Ref. [535] the authors have shown that, for the case of a soft electron spectrum, the predictions for the positron fraction are compatible with the PAMELA determinations, while a positron excess is present if an hard electron spectrum is considered (see [535] for more details). These considerations do not discard the possibility for a primary positron contribution in the cosmic-ray data, also because a single propagation model producing a good fit to the data have not yet been singled out. However, it has to be keep in mind that current observations cannot yet clearly demonstrate the presence of this exotic positron source.

On the other hand, if the PAMELA and ATIC-2 features are explained by the presence of a primary positron component an intriguing possibility is that Dark Matter annihilations are at the origin of these signals. This scenario is investigated in the next sections.

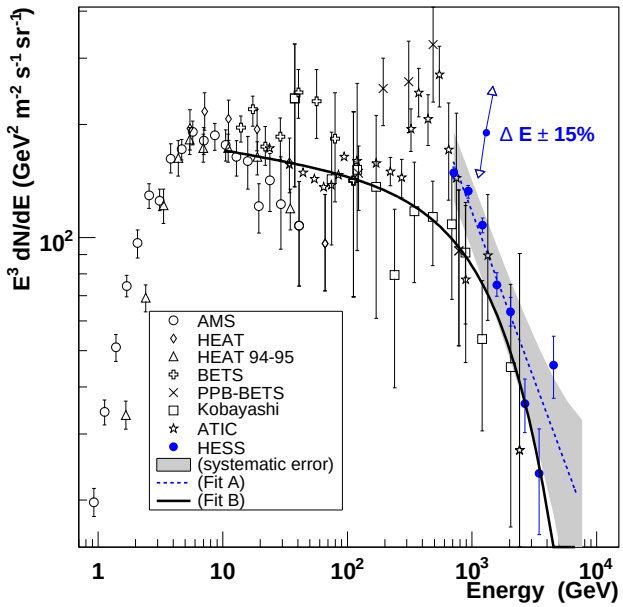

Figure 4.3: The energy spectrum E^3 dN/dE of CR electrons as measured by HESS, ATIC-2 and previous experiments. From [543]. See the original reference for the meaning of the solid curves.

4.4 Positrons and antiprotons from DM annihilations

4.4.1 Cosmic-rays propagation

Cosmic-rays propagating in our galaxy are affected by a large number of processes. The magnetic diffusion, induced by the galactic random magnetic field, modify the cosmic-ray energy spectrum and spatial distribution. Cosmic-rays can loose or gain energy in the interactions with the interstellar gas and new comic-rays species can be produced in these processes. Also the solar activity has to be considered since the associated solar wind tends to push the cosmic-rays outside the solar neighborhood and reduce their energy.

All these effects can be included in the Two-Zone Propagation Model, which describes the cosmic-ray propagation in a region of the galaxy called the Propagation Zone. The Propagation Zone is described by two cylinders, centered at the Galactic center and with a common radius $R = 20$ kpc, i.e. the galactic one. The thick cylinder has a height $2L$ with L describing the extension of the magnetic field. The second one sketches the galactic plane as a thin disk with a height 200 pc. This regions contains the interstellar medium and host supernovae explosions and shockwaves production, which are at the basis of cosmic-rays production and reacceleration.

The cosmic-rays density per unit energy, $\psi(E, \mathbf{x}, t)$, obey the transport equation:

$$\frac{\partial \psi}{\partial t} - \nabla \cdot \left\{ K(\mathbf{x}, E)\, \nabla \psi - \mathbf{V}_c \right\} - \frac{\partial}{\partial E} \left\{ b(E)\, \psi \right\} = q\left(\mathbf{x}, E\right), \tag{4.1}$$

Boundary conditions impose the vanishing of ψ at the surface of the thick zone, outside of which cosmic-rays freely propagate and escape.

In Eq. 4.1, $K(\mathbf{x}, E)$ is the diffusion coefficient which is usually assumed spatial independent and parametrized as $K(E) = K_0 \beta (\mathcal{R}/1\ \mathrm{GeV})^{\delta}$ with $\mathcal{R}$ the particle rigidity. The energy losses and gains are included in the coefficient $b(E)$ while $q\left(\mathbf{x}, E\right)$ is the cosmic-rays positron source. $\mathbf{V}_c$ is the vector field of the galactic wind. The cosmic-rays flux measured by the experiments is computed as $\phi(E, t) = \beta c / 4\pi \psi(\mathbf{x}_\odot, E, t)$ where $\mathbf{x}_\odot$ is the location of the solar system.

The positrons/antiprotons source term for DM annihilations is:

$$q_{e^+/\bar{p}}\left(\mathbf{x}, E\right) = \frac{1}{2} \left(\frac{\rho(\mathbf{x})}{m_\chi} \right)^2 (\sigma v) \frac{dN_{e^+/\bar{p}}}{dE}$$

where m_χ, (σv) and ρ are respectively the DM mass, annihilation cross section and density profile. The positron/antiproton energy spectrum per annihilation is denoted as $dN_{e^+/\bar{p}}/dE$.

4.4.2 Positrons

The main processes affecting the propagation of electrons and positrons with energies above 10 GeV are the the magnetic diffusion and the energy losses, due synchrotron radiation and Compton scattering on CMB and galactic starlight, which occur at a rate $b(E) = E^2/(\mathrm{GeV}\ \tau_E)$, with $\tau_E = 10^{16} s$.

Assuming steady-state, the transport equation Eq. 4.1 simplifies into:

$$K_0 \epsilon^{\delta} \Delta \psi + \frac{\partial}{\partial \epsilon} \left\{ \frac{\epsilon^2}{\tau_E} \psi \right\} + q = 0 \tag{4.2}$$

with $\epsilon = E/1$ GeV. Measurements of the boron to carbon ratio cosmic ray fluxes (B/C) constraint the parameter space of the propagation parameters, i.e. δ, K_0 and L.

In general it is not possible to single out, among all the configurations compatible with B/C data, a propagation model which maximize or minimize the positron signal, unless to restrict the attention to high energy positrons [544]. In Ref. [544], the authors have defined three sets of propagation parameters called MIN, MED and MAX. The MIN and MAX configurations lead respectively to minimum and maximum positron fluxes for energies above roughly 10 GeV, the exact value depending on the DM mass. The MED set defines a medium configuration.

4.4.3 Antiprotons

The propagation of antiprotons produced by DM annihilations in the galactic halo is described by the following simplified steady state transport equation:

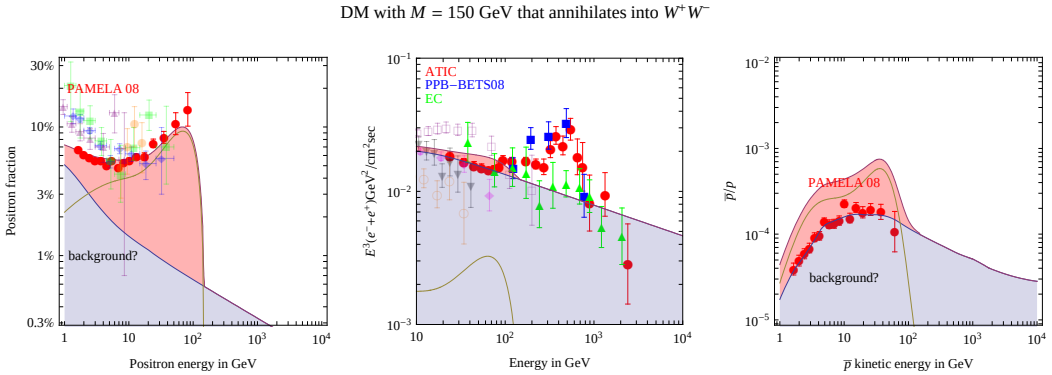

Figure 4.4: Fit of the positron fraction (left), $e^+ + e^-$ (center) and $\bar{p}/p$. Galactic DM profiles and propagation parameters models are varied to provide the best fit. From [517].

$$-K(E)\cdot\nabla^2\psi + \frac{\partial}{\partial z}\left(\mathrm{sign}(z)V_c\psi\right) = q - 2h\delta z\Gamma_{ann}\psi \tag{4.3}$$

The convective wind V_c is assumed constant and directed outside and perpendicular the galactic plane (z-direction). The last term in Eq. 4.3 describes the annihilations of antiprotons with interstellar proton at a rate $\Gamma_{ann} = \left(n_H + 4^{2/3}n_{He}\right)\sigma^{ann}_{p\bar{p}}v_{\bar{p}}$. Parametrization of the $p\bar{p}$ annihilation cross section and hydrogen (n_H) and helium (n_{He}) densities can be found in [545] and references therein. The height of the disk is $h = 100$ pc. Energy redistribution, including energy losses, reacceleration and tertiary redistribution can be safely neglected as antiprotons from DM annihilations rarely cross the thin disk (e.g. see the discussion in [546]).

As for positrons, the propagation parameters are constrained by the B/C observations. Sets of parameters which maximize/minimize the antiproton fluxes are given in [545].

4.5 Dark Matter annihilations and cosmic-rays data

In Ref.[517], the authors have studied the combinations of Dark Matter, mass m_χ, annihilation cross section σv and main annihilation mode, that can reproduce the PAMELA "positron excess", consistently with the PAMELA $\bar{p}$ data and ATIC-2 $e^+ + e^-$ measurements.

The primary positrons and antiprotons fluxes at Earth from DM annihilations are computed solving their respective transport equations, Eqs. 4.2 and 4.3, once the propagation model and DM particle physics parameters and density distribution are specified.

In their analysis they considered three different DM density profiles: Moore[547], NFW [486] and isothermal [548]. All of them are normalized in the same way at the Sun position ($\rho(r_\odot) = 0.3$ GeV/cm^3 with $r_\odot = 8.5$ kpc) but they largely differ at small ra-

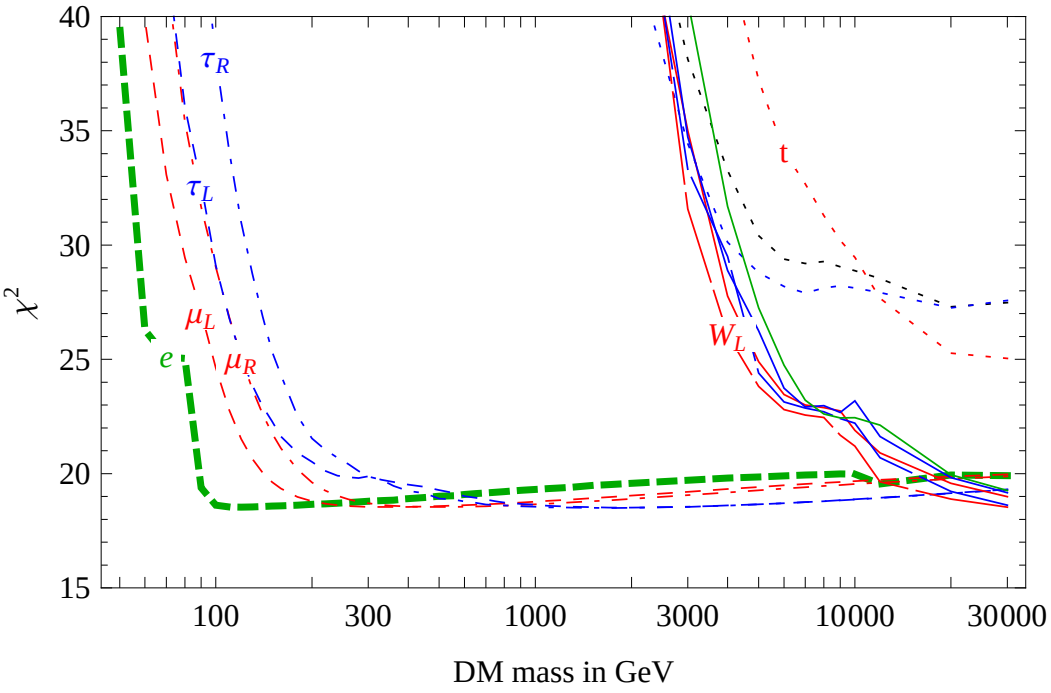

Figure 4.5: Combined fit to the PAMELA positron fraction and $\bar{p}/p$ data. The plot shows the χ^2 as a function of the DM mass for different annihilation channels. From [517].

dius. However the high energy primary positron and antiproton fluxes are not dominated by the far galactic center contribution therefore these different halo profiles don't make big differences. This is particulary true for positrons which cover shorter distances than antiprotons.

The propagation models considered are the MIN, MED and MAX configurations presented in the previous section. The astrophysical background, consisting on the e^- spectrum and $e^+, \bar{p}$ pure secondary spectra, are borrowed from [539, 549, 550], with free normalization and an independent uncertainty in their slope in order to mimic their astrophysical uncertainties (see discussion in [517]).

All the possible DM annihilation channels into two-body SM final states have been considered, $\chi\chi \to SM\ SM$,

$$SM = e, \mu_L, \mu_R, \tau_L, \tau_R, W_L, W_T, Z_L, Z_T, h, q, b, t$$

taking in account the allowed polarizations (Transverse, Longitudinal, Left, Right). The energy spectra of $e^\pm, p^\pm$, coming from the decays of DM annihilation products, are computed using Monte Carlo tools.

In Ref.[517], they fitted the PAMELA $e^+/(e^+ + e^-)$ and $\bar{p}/p$ data scanning over the DM

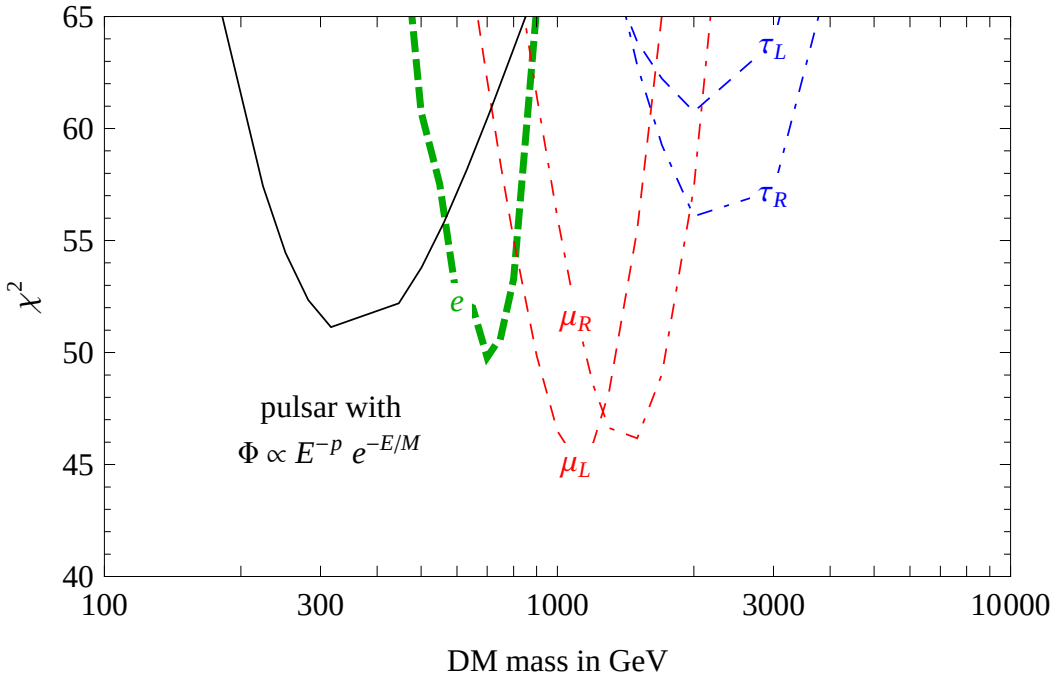

Figure 4.6: Combined fit to PAMELA and ATIC-2 data. From [517].

profiles, propagation parameters and background spectra in order to provide the best fit (see the original reference for further information on the fitting procedure). The presence of substructures is taken in account allowing an energy independent boost factor B, assumed to be equal for $e^{\pm}$ and $p^{\pm}$.

The result of the global fit for all the different annihilation modes is shown in Fig.4.5. Annihilations into quarks, Higgs and vector bosons are viable only for DM masses above 10 TeV otherwise the antiprotons produced in the annihilations would violate the PAMELA $\bar{p}/p$ data. An example is shown in Fig.4.4: even if the candidate gives a nice fit to the positron fraction this possibility has to be discarded because of the antiprotons constraints. This problem can be circumvented for large DM masses since the antiproton excess lays at energies unexplored by PAMELA. Of course, annihilations into leptons are not constrained by $\bar{p}/p$ data as they do not produce antiprotons. The inclusion of the ATIC-2 data changes the picture as shown in Fig.4.6.

On the basis of this analysis three main classes of models emerge:

a) From PAMELA e^+ and $\bar{p}$ data the Dark Matter can be:

   a1) a particle that dominantly annihilates into leptons, with no strong preference for the mass, if above a few hundred GeV;

a2) a particle that annihilates into W, Z or higgses and that has a mass $\gtrsim 10$ TeV. An example in this class is the fermion quintuplet in the predictive Minimal Dark Matter model [551], where DM has mass $m_\chi = 9.6$ TeV and annihilates into transversely polarized W^+W^-: this model predicted the PAMELA excess and predicts that the ATIC peak is not there;

b) adding the peak from ATIC-2, a clear indication for the mass emerges: DM has to be a particle with mass ~ 1 TeV that dominantly annihilates into leptons. We will exemplify this class of models referring to a generic candidate with $m_\chi = 1$ TeV and annihilations into $\mu^+\mu^-$.

The upcoming results of ATIC-4 [552], PAMELA, or the first data from the Fermi LAT calorimeter [553] or Air Cherenkov Telescopes [543] can soon check if a peak is really present in the $e^+ + e^-$ spectrum just below 1 TeV: if the peak is there b) is favored and a) is excluded; if instead the peak is not there, then a) is favored and b) excluded. Models with $m_\chi \ll 1\ TeV$ appear to be already disfavored.

For what concerns the magnitude of the annihilation cross section, the large flux above the background in the PAMELA and ATIC data indicates a very large σv. In Figures 4.9 and 4.10 the green (red) bands show the region allowed by PAMELA (PAMELA and ATIC combined) in the plane $(\sigma v) - m_\chi$, varying the $e^\pm$ propagation models between the MIN/MED/MAX sets of parameters. We do not show the subleading $\lesssim 20\%$ experimental and background uncertainty. It appears that, considering for instance a candidate in class b), a value of the order of few $10^{-23}\mathrm{cm}^3\mathrm{sec}^{-1}$ is needed to fit the data. This is much larger than the typical thermal cross section $\sigma v = 3 \cdot 10^{-26}\mathrm{cm}^3\mathrm{sec}^{-1}$ suggested by the cosmological DM abundance. As discussed in [517, 554], the two values can be reconciled if a Sommerfeld enhancement is at work: this effect, in fact, depends on the DM velocity in an important way and so it would be present at $v \sim 10^{-3}$ (the typical velocity of DM particles annihilating in the galactic halo at the present time) and reduced or absent at $v \sim 0.2$ (the velocity at decoupling). More precisely, the enhancement of a non-relativistic s-wave DM annihilation [555, 556, 557, 554] can be approximatively characterized in terms of two critical velocities $v_{\min}$ and $v_{\max}$ as follows:

$$\sigma v = \text{constant} \times \begin{cases} 1 & \text{for } v > v_{\max} \\ v_{\max}/v & \text{for } v_{\min} < v < v_{\max} \\ v_{\max}/v_{\min} & \text{for } v < v_{\min} \end{cases} . \tag{4.4}$$

In terms of particle-physics parameters, assuming that the long-range force that gives rise to the Sommerfeld enhancement is a vector with mass $M_V \ll m_\chi$ and gauge coupling g_V to DM, one has $v_{\max} \approx g_V^2/4$. The value of $v_{\min}$ is $v_{\min} \approx M_V/m_\chi$ unless a DM DM bound state with small binding energy E_B is present; in such a case the Sommerfeld effect grows down to a smaller $v_{\min} \approx \sqrt{E_B/m_\chi}$. In the exemplar model of class a1),

the enhancement is automatically present (via the exchange of weak gauge bosons). Extra states are instead required in class b), so that [517] suggested that DM might be charged under an extra U(1), proposing a specific model. More proposals along these or different lines have followed [554, 558]. Alternatively one can invoke either non-thermal DM or very large boost factors [559]. However, the latter can only arise in rather exotic scenarios (e.g. DM mini-spikes around black holes [467]), but not in the framework of DM subhalos with realistic properties [560].

Photon fluxes associated to DM annihilations are produced:

i) directly as a product of the DM annihilations themselves (mainly from the bremsstrahlung of charged particles and the fragmentation of hadrons, e.g. π^0, produced in the annihilations), at energies comparable to the DM mass m_χ, i.e. in the γ-ray energy range of tens of GeV to multi-TeV.

ii) at much lower energies, e.g. radio to visible frequency, by the synchrotron radiation emitted in the galactic magnetic field by the electrons and positrons produced by DM annihilations.

In the next sections we compute the constraints in the plane $(\sigma v) - m_\chi$ coming from photon observations of the Milky Way Galactic Center, the Milky Way Galactic Ridge and the Sagittarius Dwarf spheroidal satellite galaxy.

4.6 γ ray observations

We start by considering the γ-ray fluxes produced by DM annihilations directly. Since DM is neutral, a tree-level annihilation into γ's is of course not possible, thus the flux is the sum of various effects that arise at higher order in $\alpha_{\rm em}$: i) a continuum at lower energies produced by the bremsstrahlung of charged particles and the fragmentation of hadrons produced in the annihilations; ii) a line at $E \approx m_\chi$ produced by one-loop effects; iii) possibly a continuum at E just below m_χ produced by three-body annihilations [561]. Infrared divergences in the total annihilation rate cancel among i) and one loop corrections without photons in the final state, and these contributions are separately gauge invariant in the energy ranges where they are separately relevant. The details of contributions ii) and iii) are model dependent, so that we only consider the contribution i).

The differential flux of photons from a given angular direction $d\Omega$ is

$$\frac{d\Phi_\gamma}{d\Omega\, dE} = \frac{1}{2}\frac{r_\odot}{4\pi}\frac{\rho_\odot^2}{m_\chi^2} J \sum_f \langle\sigma v\rangle_f \frac{dN_\gamma^f}{dE}, \qquad J = \int_{\rm line-of-sight} \frac{ds}{r_\odot}\left(\frac{\rho(r)}{\rho_\odot}\right)^2 \tag{4.5}$$

where $r_\odot \approx 8.5$ kpc is the distance of the Sun from the galactic center, $\rho_\odot = 0.3$ GeV/cm^3 is the DM density at the location of the solar system and f runs over all the γ-ray produc-

MW halo model	r_s in kpc	ρ_s in GeV/cm^3	$\bar{J}\ (10^{-5})$
NFW [486]	20	0.26	$15 \cdot 10^3$
Einasto [489]	20	0.06	$7.6 \cdot 10^3$
Isothermal [548]	5	1.16	13

Table 4.1: Parameters of the density profiles for the Milky Way discussed in the text and corresponding value of $\bar{J}$ for $\Delta\Omega = 10^{-5}$. In all cases we imposed the normalization $\rho(r_\odot) = 0.3\ \mathrm{GeV/\,cm^3}$.

ing channels with annihilation cross section $\langle\sigma v\rangle_f$ and individual spectrum dN_γ^f/dE. The adimensional quantity J encodes the astrophysical uncertainty. When observing a region with total angular size $\Delta\Omega$ the factor $J\ d\Omega$ gets replaced by $\bar{J} \cdot \Delta\Omega = \int_{\Delta\Omega} J\ d\Omega$.

In order to compute the flux, one thus has to specify the DM density profile as a function of the galactocentric coordinate, $\rho(r)$. We consider the standard NFW profile

$$\rho_{\rm NFW}(r) = \frac{\rho_s}{\frac{r}{r_s}\left(1+\frac{r}{r_s}\right)^2}\,. \tag{4.6}$$

It is however unclear whether this analytic formula, obtained by fitting DM halos in N-body simulations, actually captures the behaviour of the density profile down to the innermost regions. In fact, although there is general agreement on the shape of profiles at large scales, profiles steeper than NFW, with $\rho(r) \propto r^{-1.2}$ at radii much smaller than the virial radius, have been found to provide a better fit to simulated halos [562]. This claim has been subsequently challenged, e.g. by Ref. [489], where it was found that the so-called *Einasto* profile

$$\rho_{\rm Einasto}(r) = \rho_s \cdot \exp\left[-\frac{2}{\alpha}\left(\left(\frac{r}{r_s}\right)^\alpha - 1\right)\right], \qquad \alpha = 0.17 \tag{4.7}$$

should be preferred, since the profiles of simulated halos appeared to become shallower and shallower towards the Galactic center, without converging to a definite power-law.

Finally, a truncated isothermal profile

$$\rho_{\rm iso}(r) = \frac{\rho_s}{1+\left(\frac{r}{r_s}\right)^2} \tag{4.8}$$

is sometimes adopted as a benchmark, since it is representative of 'shallow' DM profiles [548].

In Table 4.1, we show the parameters of the aforementioned density profiles (plotted in fig.4.7a) for the case of the Milky Way and the value of the quantity J averaged over a solid angle $\Delta\Omega = 10^{-5}$ sr, corresponding to the angular resolution of gamma-ray experiments such as HESS and Fermi LAT. Note that, for the Einasto profile, we choose a value of

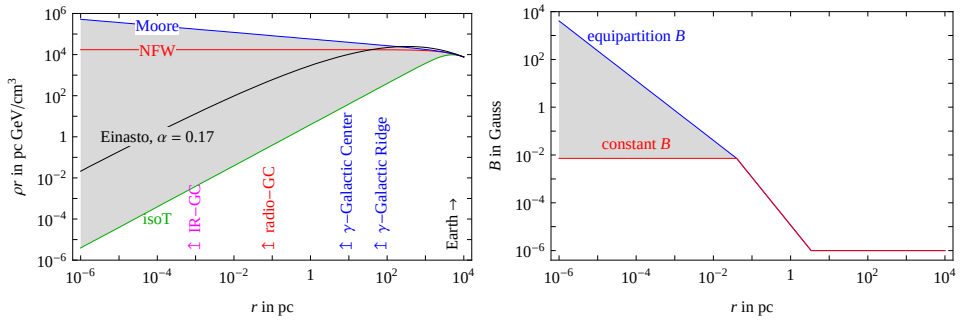

`Figure 4.7:` Shape of DM density (left) and magnetic field (right) profiles discussed in the text, as a function of the galactocentric coordinate r.

$r_s = 20$ kpc representative of the results of Ref. [489] for different simulations; the value of $\bar{J}\left(\Delta\Omega = 10^{-5}\right)$ is only a factor ~ 2 smaller than the one for NFW.

We stress that aside from these uncertainties, the DM distribution is further complicated by a number of physical processes that are not accounted for in most numerical simulations, such as the presence of a supermassive black hole that dominates the gravitational potential within 1 pc from the Galactic center, and a stellar cusp that inevitably interacts with the DM fluid, a circumstance that makes it difficult to accurately estimate the DM profile in the central region (see e.g. Ref. [464] and references therein). We do not include these model-dependent processes in the following. More generally, the extrapolation of the numerical Dark Matter profiles in the regions very close to the Galactic Center ($\lesssim 10$ pc) is of course to be taken with care, as simulations cannot resolve small radii. As we will see, however, some of the constraints come from regions as large as $\mathcal{O}(100)$ pc (the size of the Galactic Ridge region, for instance, or of the Sagittarius Dwarf galaxy) where the impact of these uncertainties is much less important. Keeping in mind these remarks and possible caveats, in the following we will discuss the astrophysical constraints for different choices of the DM profile.

4.6.1 γ-ray observations of the Galactic Center

HESS observations in the direction of the Galactic Center have revealed a source of Very High Energy γ-ray emission (HESS J1745-290) lying within $7'' \pm 14''_{\rm stat} \pm 28''_{\rm syst}$ from the supermassive black hole Sgr A*, and compatible with a point source of size less then $1.2'$ [282]. The corresponding energy spectrum, shown in figure 4.8a, is well fitted by a power law $d\Phi_\gamma/dE \propto E^{-2.25\pm0.04}$, over two decades in energy, and it has been confirmed by the MAGIC collaboration [563]. The EGRET experiment had actually previously reported the detection of a point source (3EG J1746-2851) within 0.2 degrees from Sgr A* [564]. How-

ever, a re-analysis based on photons with energies above 1 GeV has shown that the source is slightly offset with respect to the galactic center [565].

The possibility to interpret both sets of γ observations (separately or at the same time) in terms of DM annihilations has been discussed e.g. in Refs. [287, 286, 566, 283, 567, 383, 306], and Ref. [499] discussed the prospects for the detection of DM with Fermi LAT. Here, we take a conservative approach and consider the observed gamma-ray emission as an upper limit to the DM annihilation flux, in order to test the compatibility with a DM interpretation of the PAMELA data. We compute the constraints in the σv versus mass plane, by requiring that DM annihilation flux does not exceed (at 3σ) the observed emission *at any data point*.

As an example of our confrontation with data, the left panel of fig.4.8 shows the gamma-ray flux from the Galactic center (assuming a NFW profile) produced by the annihilations of 10 TeV DM particles into W^+W^-, the aforementioned sample model a1), with an annihilation cross section $\sigma v = 10^{-23}$ cm^3/sec. This mimics the Minimal Dark Matter theory [557]. As one can see, the DM γ flux does not exceed any of the HESS data points, and correspondingly this point in parameter space will lie in the allowed region of fig.4.10 (see below). The left panel of fig.4.8 also shows the superposition of the DM signal with a sample power-law background: while in this case one would conclude that the model is excluded because the summed flux exceeds the HESS observations by more than 3σ at several data points, this conclusion would not be solid. Indeed, choosing a different background (e.g. lower in normalization) within its large uncertainties can re-allow the model. Adopting the criterion of comparing each single data point with the DM-only flux allows us to have more conservative and robust results. Moreover, we recall that the signal from DM annihilations that we consider here does not include all the model dependent contributions (see the discussion at the beginning of sec. 4.6). In specific theories a full computation of the gamma-ray spectrum is possible; for instance for the case of Minimal Dark Matter it has been obtained in Ref. [557]. These contributions can change somewhat the shape of the DM signal and bring it closer to the shape of the observed spectrum, even in absence of a power-law background. For this additional reason, it is apparent that it would be wrong to exclude a model such as the one illustrated in the left panel of fig.4.8.

The HESS collaboration has also recently discovered a diffuse gamma-ray emission, correlated spatially with the Galactic Ridge (GR), a complex of giant molecular clouds in the central 200 pc of the Milky Way [568]. Once point sources, including HESS J1745-290, are subtracted, the reconstructed gamma-ray spectrum for the region with galactic longitude $-0.8^\circ < \ell < 0.8^\circ$ and latitude $|b| < 0.3^\circ$ is well described by a power law with photon index $\Gamma = 2.29 \pm 0.07_{\rm stat} \pm 0.20_{\rm syst}$. In this region, the predicted DM signal is smaller than in a small cone pointing towards the Galactic center, but the astrophysical background is also significantly reduced, and the constraints are less sensitive to the slope of the DM density profile. Fig.4.8b shows the HESS data and the signal in our sample model

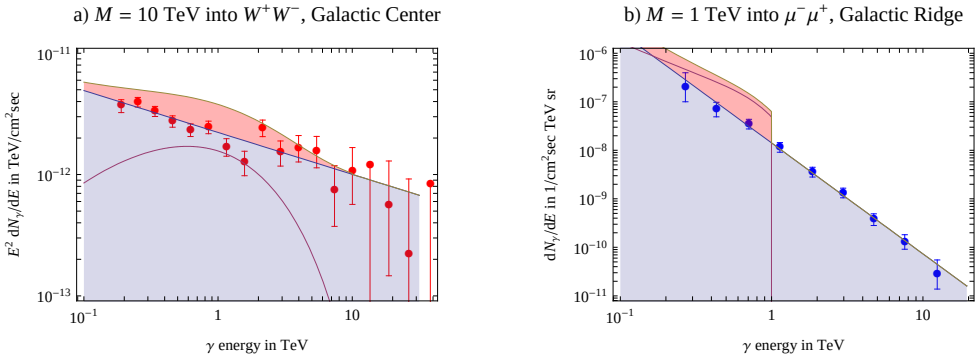

Figure 4.8: HESS observations of the Galactic Center (left) and Galactic Ridge (right) compared with the annihilation signals from our two sample models a1) (left) and b) (right), assuming a NFW profile and an annihilation cross section of $(\sigma v) = 10^{-23}$ cm^3/sec, and with the sum of the annihilation signal and a possible astrophysical background flux.

b), i.e. a candidate with $m_\chi = 1$ TeV annihilating to $\mu^+\mu^-$, assuming a NFW profile. The cross section has been taken here to be $\sigma v = 10^{23}$ cm^3/sec as in the left panel. The same discussion as above applies: what is seen here is that the DM γ signal (marginally) exceeds the data points and therefore the model will lie slightly within the border of the excluded region.

In figures 4.9 and 4.10 we show the results of the analysis of the data described above. The continuous blue lines shows our conservative bounds on the annihilation cross section σv from HESS observations of the Galactic Center and the dot-dashed blue lines show the comparable bounds from Galactic Ridge observations. Figs.4.9 refer to DM annihilation into leptons, while fig.s4.10 show the more 'traditional' DM annihilation modes into W^+W^-, $b\bar{b}$ and $t\bar{t}$. Barring the possibility of boost factors or Sommerfeld enhancements different for γ and $e^\pm$ observations, we see in fig.s4.9 that the green regions that can fit the PAMELA anomaly (and the red regions that can also fit the ATIC anomaly) are excluded for masses $m_\chi \gtrsim 300\,\text{GeV}$, by two orders of magnitude if DM follows the NFW density profile, by an order unity factor if DM follows the Einasto profile and are allowed if DM follows the isothermal profile (somewhat disfavored, however, by N-body simulations).
In fig.s 4.10 a similar situation holds. The green PAMELA bands are here truncated because low DM masses do not allow a good fit to the anti-proton data; the truncation is conservatively put at 1 TeV, but masses up to multi-TeV still do not give a good fit, as discussed in the Sec.4.5 (see [517] for the full analysis).

Sgr dSph halo	Parameters	Core/Scale radius	$\bar{J}\,(2\cdot 10^{-5})$	$\bar{\mathcal{J}}\,(2\cdot 10^{-5})$
Small core [569]	$v_a = 13.4$ km/s	$r_c = 1.5$ pc	$31\cdot 10^3$	$74\ 10^{24}\,\mathrm{GeV}^2/\mathrm{cm}^5$
NFW [486]	$\rho_s = 5.2\mathrm{GeVcm}^3$	$r_s = 0.62$ kpc	$1\cdot 10^3$	$2.46\ 10^{24}\,\mathrm{GeV}^2/\mathrm{cm}^5$
Large core [570]	$v_a = 22.9$ km/s	$r_c = 0.23$ kpc	$0.14\cdot 10^3$	$0.32\ 10^{24}\,\mathrm{GeV}^2/\mathrm{cm}^5$

`Table 4.2:` Parameters of the density profiles for the Sagittarius Dwarf galaxy discussed in the text and the corresponding value of $\bar{J}(\Delta\Omega)$ (normalized by convention in terms of the solar quantities $r_\odot$ and $\rho_\odot$, as in eq. (4.5)) for $\Delta\Omega = 2\cdot 10^{-5}$. For reference, the value of the rescaled $\bar{\mathcal{J}}(\Delta\Omega) = r_\odot\rho_\odot^2\,\bar{J}(\Delta\Omega)$ is also given.

4.6.2 Sagittarius dwarf spheroidal galaxy

Dwarf spheroidal galaxies are among the most DM-dominated structures, so that they allow to search for γ ray signals of DM annihilations with minimal astrophysical backgrounds. In particular, HESS has observed the Sagittarius Dwarf galaxy [569], a satellite of the Milky Way which is located at a distance of $d = 24\,\mathrm{kpc}$ from the Sun. The satellite is thought to be in the process of being disrupted by multiple passages through the Milky Way disk, and the fact that it still exists is taken as an indication of the existence of a substantial amount of Dark Matter in it.

The DM density profile in Dwarf Galaxies is uncertain as much as the one in the Milky Way, with which it might have some correlations. For Sgr dSph we consider the possibilities of a cusped NFW profile [569, 570] with density given by eq. (4.6) and of the class of cored profiles

$$\rho_{\mathrm{core}}(r) = \frac{v_a^2}{4\pi G_N}\frac{3r_c^2 + r^2}{(r_c^2 + r^2)^2}. \tag{4.9}$$

The normalization factors and the characteristic radii are reported in Table 4.2, where also the corresponding values of $\bar{J}$, defined according to eq. (4.5), are given. The area of observation corresponds to an aperture angle of 0.14° i.e. to a size of $\Delta\Omega = 2\cdot 10^{-5}$ [569].

HESS has observed Sagittarius Dwarf for $T_{\mathrm{obs}} = 11\,\mathrm{h}$ finding no γ-ray excess: the integrated photon flux is $N_\gamma \lesssim 85$ at about 3σ. Hence an upper bound can be imposed on the annihilation cross section

$$\sigma v < \frac{8\pi}{T_{\mathrm{obs}}}\frac{m_\chi^2 N_\gamma r_\odot \rho_\odot^2 \bar{J}\Delta\Omega}{\int dE\ A_{\mathrm{eff}}(E)\, dN_\gamma/dE} \tag{4.10}$$

where the effective area of HESS $A_{\mathrm{eff}}(E) \sim 10^5\,\mathrm{m}^2$ in the range $E \gtrsim 70$ GeV is taken from [571].

The resulting bounds on σv are shown as dashed blue lines in figures4.9 and 4.10. The top rows of the figures assume a NFW DM density profile in Sgr dSph: the bounds are overall comparable or slightly less powerful than the bounds from the Galactic Center and

Ridge. In all the lower rows we use for Sgr dSph a 'large core' profile, which gives the minimum γ flux among the profiles considered in the literature. The bound becomes the most constraining one when the Milky Way profile is taken to be isothermal. We have not explored whether even smoother profiles of Sgr dSph can be designed (compatibly with observations) that can lift such bound. It is interesting to note that the typical velocity dispersion of DM in Dwarf Spheroidal galaxies is about 10 km/s [570], smaller than in our galaxy: thereby their constraint becomes stronger and dominant for models where light particles give a Sommerfeld enhancement down to a small $v_{\rm min}$ [554].

Notice that the regions suggested by PAMELA for light DM mass are not probed by HESS observations due to its high energy threshold. DM that annihilates into leptons tends to give most of the signal at γ energies just below the DM mass: the forthcoming Fermi/GLAST γ observations are not expected to be very significant for our purposes, as they will extend the HESS observations down to lower energies but will overlap with the HESS observation at the $\gtrsim 100\,{\rm GeV}$ gamma energies suggested by the PAMELA/ATIC excesses. We now turn to radio-wave observations.

4.7 Radio observations of the Galactic Center

The $e^{\pm}$ produced by DM annihilations within the galactic magnetic field radiate synchrotron radiation. The Galactic Center is presumably the best region to search for this effect, because of the large local value of the DM density and magnetic fields [572, 306, 566, 573, 381, 382, 383]. We first detail the necessary astrophysical and particle physics ingredients, and then move to the comparison with observations.

The GC region contains a black hole with mass $M_{\rm BH} \approx 4.3 \times 10^6 M_\odot$ (see e.g. the recent Ref. [574] and references therein). This implies two length-scale: the Schwarzschild radius $R_{\rm BH} = 2G_N M_{\rm BH} \approx 4 \times 10^{-7}\,{\rm pc}$ and the radius of the accretion region, $R_{\rm acc} \equiv 0.04\,{\rm pc}$, defined to be the region where the velocity flow due to the gravity of the black hole, $v = -\sqrt{R_{\rm BH}/r}$ is larger than the random galactic motion, $v \sim 10^{-3}$.

Assuming a constant accretion of the BH mass, $\dot{M}_{\rm BH} \approx 5 \cdot 10^{-12}\ M_\odot/{\rm sec}$, the matter density is given by $\rho(r) = \dot{M}_{\rm BH}/4\pi r^2 v(r) \propto r^{-3/2}$. Assuming equipartition of the matter kinetic energy with the magnetic pressure, $\rho v^2/2 = B^2/2$, the magnetic field is $B(r < R_{\rm acc}) = \sqrt{\rho v^2} = 7.2\,{\rm mG} \cdot (R_{\rm acc}/r)^{5/4}$. Outside the accretion region, assuming that the magnetic flux is conserved, $B(r > R_{\rm acc})$ scales as $1/r^2$, down to the typical constant galactic value $B \sim \mu{\rm G}$ reached at $r \sim 100 R_{\rm acc}$. This defines the 'equipartition' magnetic field, plotted in fig.4.7b. Another possibility is that B stays constant inside the accretion region: this defines the 'constant' magnetic field, again plotted in fig.4.7b. As we will see, bounds from observations at lowest frequencies are robust, and mildly vary even when the magnetic field is varied within these extremal possibilities.

Next, we need to compute the number density $n_e(r,p,t)$ of the $e^{\pm}$ generated by DM annihilations. We assume stationary conditions, spherical symmetry, and, in view of the large magnetic fields, we neglect diffusion and assume that synchrotron radiation dominates energy losses. Writing the injection term (numerical coefficients are given in particle-physics natural units in the following) $Q = \sigma v(\rho^2/2m_\chi^2)(dN_{e^\pm}/dE)$ as $Q = 4\pi p^2 q$ and the number density as $n_e = 4\pi p^2 f$, $f(r,p)$ obeys the transport equation

$$v\frac{\partial f}{\partial r} + \frac{1}{p^2}\frac{\partial}{\partial p}\left[\dot{p}_{\rm syn} p^2 f\right] + \dot{p}_{\rm adv}\frac{\partial f}{\partial p} = q \tag{4.11}$$

with energy losses

$$\dot{p}_{\rm adv} = -\frac{p}{3r^2}\frac{\partial(r^2 v)}{\partial r}, \qquad \dot{p}_{\rm syn} = \frac{e^4 B^2 E p}{9\pi m_e^4}. \tag{4.12}$$

We assume $p \gg m_e$, such that $E \simeq p$ and $\dot{E}_{\rm syn} \simeq \dot{p}_{\rm syn}$. If one can neglect advection (because $\dot{p}_{\rm adv} \ll \dot{p}_{\rm syn}$: this happens at $r > R_{\rm acc}$ and at large p), the above equation is solved as

$$n_e(r,E) \simeq \frac{1}{\dot{E}_{\rm syn}}\int_E^\infty dE'\; Q(E',r) = \sigma v \frac{\rho^2}{2m_\chi^2}\frac{N_e(E)}{\dot{E}_{\rm syn}} \tag{4.13}$$

where $N_e(E)$ is the number of e^+ or e^- generated with energy larger than E in one DM annihilation.

Finally, we can now compute the synchrotron power $W_{\rm syn}$ generated by the n_e electrons and positrons in the turbulent magnetic field B

$$\frac{dW_{\rm syn}}{d\nu} = \frac{\sqrt{3}}{6\pi}\frac{e^3 B}{m_e}F(\frac{\nu}{\nu_{\rm syn}}), \qquad F(x) = x\int_x^\infty K_{5/3}(\xi)d\xi \approx \frac{8\pi}{9\sqrt{3}}\delta(x-1/3) \tag{4.14}$$

where

$$\nu_{\rm syn} = \frac{3eBp^2}{4\pi m_e^3} = 4.2\,{\rm MHz}\frac{B}{\rm G}\left(\frac{p}{m_e}\right)^2. \tag{4.15}$$

Reducing the magnetic field B, the spectrum of synchrotron radiation moves to lower energies, but the total energy into synchrotron radiation remains constant, until B becomes so small that other energy-loss mechanisms start to dominate.

Inserting eq. (4.13) in (4.14) we find

$$\nu\frac{dW_{\rm syn}}{d\nu} = \frac{\sigma v}{2m_\chi^2}\int_{\rm cone} dV\; \rho^2\; p\; N_e(p) \tag{4.16}$$

where the integral extends over the observed volume and p is obtained from eq.s (4.14) and (4.15) as $p = \sqrt{4\pi m_e^3 \nu/B} = 0.43\,{\rm GeV}(\nu/{\rm GHz})^{1/2}(B/{\rm mG})^{-1/2}$. A lower B leads to a higher synchrotron flux at the low frequency we consider.

We move now to the comparison with observations. Since the observed GC microwave spectrum is harder than what DM decays can produce, the dominant bound is obtained considering the observation available at the lowest observed frequency, $\nu = 0.408\,{\rm GHz}$,

performed by [575] in a region with full width half maximum of $4''$. The observation found an upper limit to the measured flux $S = (\nu\, dW_{\rm syn}/d\nu)/(4\pi r_\odot^2) < 2\ 10^{-16}\,{\rm erg/cm^2 sec}$, that constraints from above the flux in eq.4.16. The resulting bounds are plotted in fig.s4.9 and4.10 as red lines. What is seen is that this constraint excludes a large portion of the parameter space for NFW and Einasto DM profiles. The constraint extends to low DM masses (where the γ-ray bounds from HESS are not effective). The variation of the magnetic field between 'equipartition' and 'constant' in the inner region at $r < R_{\rm acc}$ negligibly affects the bound, because the radio emission is predominantly produced by the outer region. We have also verified that for the relatively shallow profiles under consideration, the synchrotron self-absorption is negligible.

The subdominant bound (purple lines) comes from the VLT observation at the larger infrared/visible frequency, $\nu = 0.5\ 10^5\,{\rm GHz}$: $S < 3\ 10^{-12}\,{\rm erg/cm^2 sec}$ from a region with angular size $0.04''$ i.e. $r < 0.0016\,{\rm pc}$. It somewhat depends on the magnetic field profile, and it becomes numerically significant only for spiked DM density profiles [383]. Similarly, observations at higher frequencies give possibly strong but not robust bounds [383], that also strongly depend on the possibility of having an intense 'equipartition' magnetic field close to the Milky Way black hole.

Finally, we need to consider the possible effect of advection, that we neglected so far. We numerically studied it, and, as it depends on the density profile, magnetic field, DM mass and annihilation mode we try to qualitatively summarize some general lessons rather than presenting a large number of specific plots. At VLT-like (and higher) frequencies, $\nu \sim 10^{14}\,{\rm Hz}$, synchrotron radiation is dominantly generated by $e^\pm$ with energy above 1 GeV. The density of such higher energy $e^\pm$ is negligibly affected by advection. Presumably, advection can be neglected also for the observation by [575] at the lower frequency $\nu = 0.408$ GHz, because the angular aperture of $4''$ corresponds to a region with size $R_{\rm obs} = 0.14$ pc, which is larger than the (presumed) accretion radius $R_{\rm acc} \approx 0.04$ pc, inside which advection is a significant effect[1]. Advection can be neglected because the total luminosity is dominated by radii comparable to $R_{\rm obs}$, unless one considers DM density profiles that grow at $r \to 0$ more strongly than the NFW profile, leading to very strong constraints possibly affected by advection (and by the reduction of the Sommerfeld enhancement, as the DM velocity grows, becoming relativistic around the Schwarzschild radius). The Davies bounds can possibly be weakened if the accretion region is larger.

[1] Advection typically reduces the $e^\pm$ density just below $R_{\rm acc}$ and $e^\pm$ accumulate in the inner region.

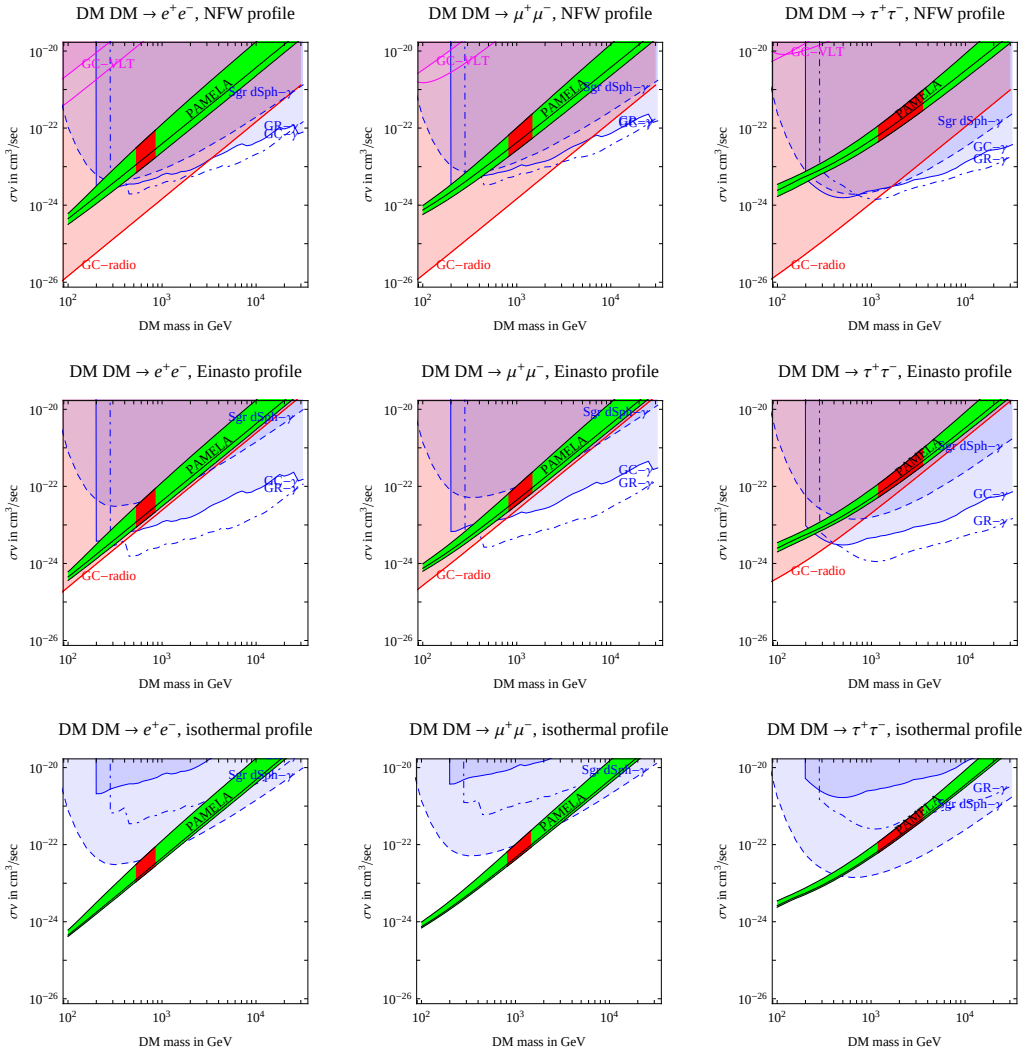

Figure 4.9: We compare the region favored by PAMELA (green bands) and ATIC (red regions within the bands) with the bounds from HESS observations of the Galatic Center [282] (blue continuous line), Galactic Ridge [568] (blue dot-dashed), and SgrDwarf [569] (blue dashed) and of observations of the Galactic Center at radio-frequencies $\nu = 408\,\mathrm{GHz}$ by Davies et al. [575] (red lines) and at $\nu \sim 10^{14}\,\mathrm{Hz}$ by VLT [576] (upper purple lines, when present, for equipartition and constant magnetic field). We considered DM annihilations into e^+e^- (left column), $\mu^+\mu^-$ (middle), $\tau^+\tau^-$ (right), unity boost and Sommerfeld factors and the NFW (upper row), Einasto (middle), isothermal (lower) MW DM density profiles and the NFW (upper), large core (middle and lower) Sgr dSph DM density profiles.

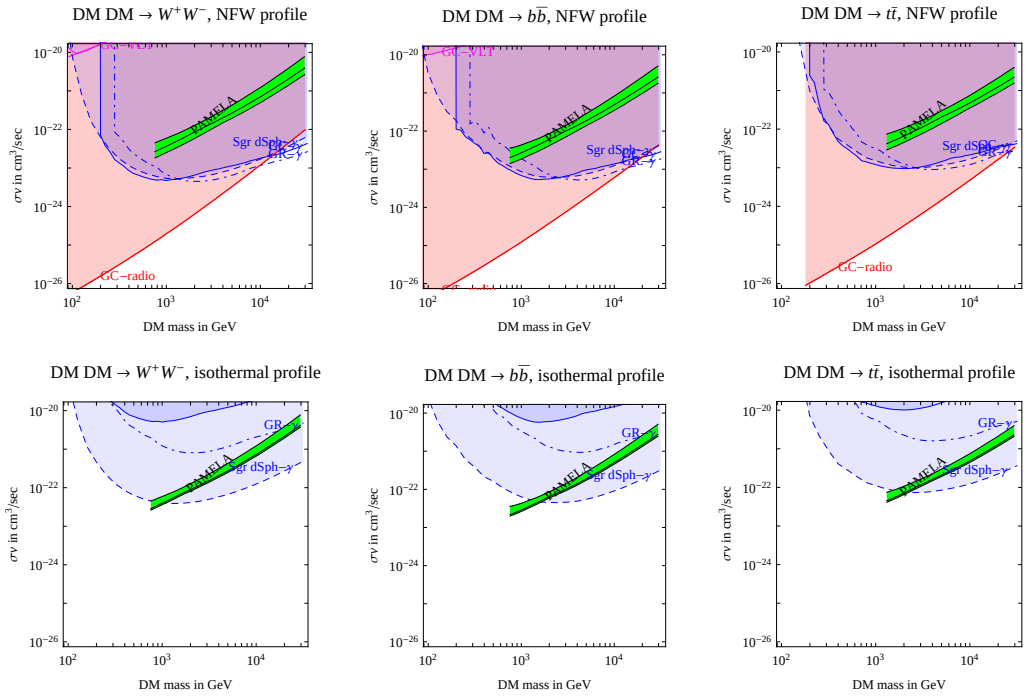

Figure 4.10: As in the previous Fig.4.9, but for the cases of DM annihilations into W^+W^- (left), $b\bar{b}$ (middle), $t\bar{t}$ (right) and for a NFW (upper row) and isothermal/large core (lower row) DM density profile.

4.8 Summary

In this chapter we explored the compatibility of the interpretation in terms of DM annihilations of the excesses in the CR $e^{\pm}$ spectra claimed by PAMELA and ATIC with observations of photons at gamma and radio frequencies, inevitably produced by brehmstrahlung (in DM annihilations) and synchrotron radiation (of $e^{\pm}$ in galactic magnetic fields) respectively.

Figures 4.9 and 4.10 summarize the results. The green (red) bands show the region allowed by PAMELA (PAMELA and ATIC combined). The regions shaded in blue (red) are excluded by our fit of gamma (radio) observations. One sees that the two data-sets are incompatible if the DM density profile is Einasto, NFW or steeper: the gamma and radio observations are violated by one or two orders of magnitude. As we conservatively fitted the various data-sets, our results are robust.

Plots are made assuming unit boost factors and Sommerfeld enhancement, and our results remain unchanged (up to a rescaling) if these factors are constant. In line of principle, it is possible that the $e^{\pm}$ excess (if dominantly due to DM annihilations in the solar neigh-

borhood) is significantly more enhanced than DM annihilations around the Galactic Center. However, numerical simulations suggest that boost factors much larger than unity are unlikely [560], and we have verified that a realistic subhalo population among those discussed in Ref. [578] actually produces $\mathcal{O}(1)$ boost factors for ~ 100 GeV positrons and gamma-rays in a 10^{-5} cone towards the galactic center. It should however be mentioned that a boost factor of a few units is possible for positrons, and the first effect of adding substructures to the the smooth DM component of the Milky Way actually is to *reduce* the flux from the Galactic center by a factor $(1-f)^2$, where f is the fraction of the mass of the smooth halo that goes into clumps, which is expected to be $\mathcal{O}(0.1)$. In absence of a precise prescription, we limit ourselves to caution the reader that this introduces an $\mathcal{O}(1$–$10)$ uncertainty on the exclusion plots discussed above. Similarly, the variation in the Sommerfeld enhancement due to the different DM velocity dispersion at the Galactic center can only lead to $\mathcal{O}(1)$ uncertainties on the constraints, since the annihilation signal does not arise from regions near the Galactic Black Hole horizon where DM has a larger velocity dispersion.

In order to perform a model-independent analysis, we considered DM annihilations into pairs of SM particles. Recently, it was proposed that DM might instead annihilate into some new *light* particle with mass $m \lesssim m_p$ that can only decay into SM leptons ℓ or pions in view of kinematical constraints [554]. We analyze this possibility in the next sections.

The DM annihilation interpretation of the PAMELA/ATIC excesses is compatible with gamma and radio observations if the DM density profile is significantly less steep than the Einasto and NFW profiles. We also notice that this would mean that $e^{\pm}$ observed by PAMELA and ATIC dominantly come from regions of the galaxy that are close to us (as the isothermal profile predicts less concentration of DM at the galactic center) and thereby suffer little energy losses. This implies in particular that the direct annihilation channel DM DM $\to e^+e^-$ is disfavored: in this case the spectrum would remain close to a peak at $E = m_\chi$, which seems to be disfavored by the PAMELA+ATIC $e^{\pm}$ spectra (that show a broader shape). In other words, a combined fit of PAMELA, ATIC and photon data from a e^+e^- primary channel does not yield a good fit for smooth DM density profiles. Other channels that produce broader spectra (such as $\mu^+\mu^-$) do a better job.

These results are compatible with other recent analyses [577], including those [383] performed assuming the very steep DM density profiles of Ref. [464].

4.9 Dark Matter annihilating into New Light Particles

In the previous sections we have shown that in models where the DM annihilate directly into a pair of SM particles, the associated photon emission lead to rather severe constraints.

It remains to consider another possibility, where DM annihilates into a new type of light (sub-GeV) particles ϕ that in turn dominantly decay into light leptons (see [554] for

Arkani-Hamed al. type					Nomura-Thaler type		
	m_ϕ[GeV]	type	e^+e^-	$\mu^+\mu^-$		m_s[GeV]	m_a[GeV]
AH1	0.1	scalar	100%	-	$N1$	5	0.5
AH2	0.1	vector	100%	-	$N2$	20	0.36
AH3	0.25	vector	67%	33%	$N3$	20	0.5
AH4	0.25	scalar	-	100%	$N4$	20	0.8
					$N5$	50	0.5

Table 4.3: Benchmark scenarios that we consider here. The DM mass is taken to be 1 TeV, but is easily generalized to other masses (see text).

a general account of this idea). The advantage of this type of models is that the decay into hadronic modes (for which very stringent bounds exist – see, e.g., [517]) is kinematically forbidden and that Sommerfeld enhancements in the limit of the small galactic DM velocities expected today allow for the very large annihilation cross sections that are needed to explain the PAMELA/ATIC results, but which at first seem to be at odds with the cross sections required to get the right thermal relic density for the DM. Another interesting feature of the Arkani-Hamed et al. model [554] is that it encompasses ideas that have been proposed to explain the WMAP haze [579, 580] and the INTEGRAL excess [581].

As pointed out in [554, 582], one may basically distinguish between scalar and vector ϕ and whether or not $m_\phi < 2m_\mu$ (in which case it dominantly decays into e^+e^-). For $m_\phi \gtrsim m_\pi$, even decays into pions should be taken into account (which we neglect here). As for lower bounds on the mass of the new particle, $m_\phi \gtrsim 10\,\mathrm{MeV}$ is roughly needed not to be in conflict with Big Bang Nucleosynthesis, and one has to require $m_\phi \gtrsim 100\,\mathrm{MeV}$ in order to get Sommerfeld enhancements of the order $10^3 - 10^4$ that are needed to explain the PAMELA/ATIC result with these types of DM models. Based on this discussion, we work in the following with the four benchmark settings A1–A4 summarized in Tab. 4.3.

While [554] describes a rather general set-up, [583] introduces a concrete realization of this idea; the proposed model has the appealing feature of containing a "standard" Peccei-Quinn axion and can be embedded in a fully realistic supersymmetric scenario. Here, DM annihilates into a scalar s and a pseudoscalar a, $\chi\chi \to sa$. With a mass scale of $360\,\mathrm{MeV} \lesssim m_a \lesssim 800\,\mathrm{MeV}$, the latter mostly decays into muons, which subsequently decay into electrons or positrons. The benchmark models for this setup N1–N5 are given in Tab. 4.3.

For the first a particle created in the $\chi\chi$ annihilation, we analytically compute the photon multiplicity $(dN/dE_\gamma)^{(a)}$ from $a \to \mu^+\mu^-\gamma$ in the rest frame of a. We then make a

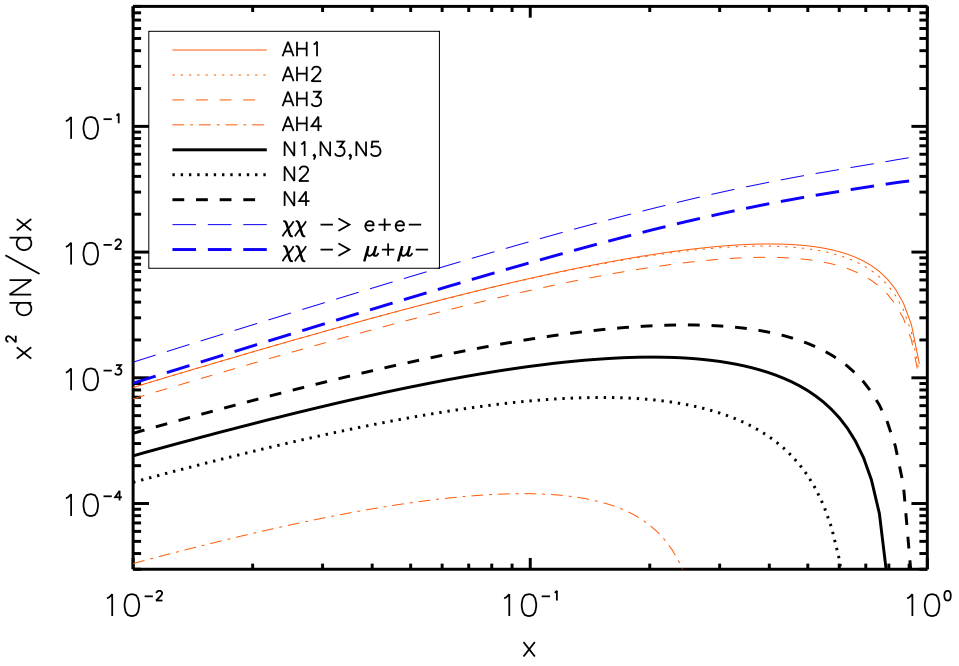

Figure 4.11: The various possible photon spectra that can arise from DM annihilating to new light particles which in turn decay into charged leptons. For the models $N1$ – $N5$, we neglect here the decay of s to tau-leptons or bottom quarks – see Fig. 4.12 for an example of how this changes the spectra. For comparison, we also indicate the spectrum from DM directly annihilating to charged leptons.

Lorentz boost back to the DM frame, i.e. the Galactic rest frame, to get

$$\left(\frac{dN}{dE_\gamma}\right)^{(\mathrm{DM})} = \frac{1}{2\beta\gamma}\int_{E/(\gamma(1+\beta))}^{E/(\gamma(1-\beta))}\frac{dE'}{E'}\left(\frac{dN}{dE'_\gamma}\right)^{(a)}\,, \tag{4.17}$$

with $\gamma = (m_\chi/m_a)\left[1-(m_s^2-m_a^2)/(4m_\chi^2)\right]$ since the annihilation takes place essentially at rest (typical galactic velocities are 10^{-3}). Axions resulting from $s \to aa$ we treat in a similar way, boosting them first to the s-frame and from this to the DM frame. Since s may have a mass up to 50 GeV, the gamma-ray spectrum may even receive important contributions from its decay into bottom quarks or tau leptons, a possibility which we will shortly return to. (Bremsstrahlung from electrons in the muon decay will give γs of lower energies and will thus not be important for our constraints.)

Summing up all these contributions, we arrive at the total photon spectrum in the DM frame that we show in Fig. 4.11 for the models N1–N5 in Tab. 4.3. We also include the corresponding spectra obtained in the Arkani-Hamed et al. set-up (models A1–A4) and,

for comparison, the case of 1 TeV DM particles directly annihilating into e^+e^- or $\mu^+\mu^-$. Please note that, from Eq. (4.17), the quantity dN/dx for the models listed in Tab. 4.3 is independent of m_χ as long as $m_\chi \gg m_a, m_s$; the direct annihilation of DM into leptons, on the other hand, *does* contain a logarithmic dependence on m_χ. In fact, if the DM particles χ annihilate directly into a pair of charged leptons, the photon distribution from the process $\chi\chi \to \ell^+\ell^-\gamma$, for $m_\chi \gg m_\ell$, is to a good approximation of the Weizsäcker-Williams form (see, e.g., [584]):

$$\frac{d(\sigma v)}{dx} = (\sigma v)_{\ell\ell}\frac{\alpha_{\rm em}}{\pi}\frac{((1-x)^2+1)}{x}\ln\left[\frac{4m_\chi^2(1-x)}{m_\ell^2}\right], \tag{4.18}$$

where $x = E_\gamma/m_\chi$ and $(\sigma v)_{\ell\ell}$ is the annihilation rate for the lowest order process $\chi\chi \to \ell^+\ell^-$ (Note that the above approximation also breaks down when there is a symmetry that suppresses the annihilation into two-body, but not into three-body final states [585]). Let us mention that Eq. (4.18) provides indeed a rather good approximation to our analytic results for photons radiated from e^+e^- pairs. However, it overestimates the photon yield from muons (especially when the mass of the decaying particle is close to m_μ like, e.g., in model AH4).

4.10 Constraints from photon observations

Once a DM profile $\rho(r)$ is assumed, we estimate the corresponding gamma-ray flux from a solid angle $\Delta\Omega$ towards the galactic center using Eq.4.5.

Following Sec.4.6.1, we compare the resulting flux to the gamma-ray data from the galactic center taken by the H.E.S.S. telescope. In Fig. 4.12, we show the results for model N3 and indicate separately the case where $s \to aa$ 100% of the time and the example cases with 5% going to $\bar{b}b$ or $\tau^+\tau^-$. It is straightforward to get the spectra for the other models in Tab. 4.3 by comparing with Fig. 4.11. Here, a NFW profile has been adopted, with the same parameters as in Sec.4.6.1. Note that the gamma-ray spectra in this case are consistent with the HESS data, unlike the case of the annihilation modes discussed in [384], for the same density profile. We note here that if one assumes a profile $\rho(r) \propto r^{-1.2}$, as needed to explain the WMAP 'Haze' (see Ref. [579, 580]) the constraints become much more stringent. However, at the same they become much more sensitive to the dependence of σv on the velocity dispersion of DM, which inevitably increases in the vicinity of the supermassive black hole at the Galactic center. As we shall see, however, it is possible to derive even tighter constraints without making assumptions on the small-v behaviour of σv.

Before that, we consider the constraints derived from gamma-rays observations of dwarf galaxies. Assuming an NFW profile in the Sagittarius dwarf galaxy, we obtain the limit $\sigma v < 7.4 \times 10^{-22}$ cm^3 s^{-1} for model N3 (we compare with the observations in[569] as done in Sec.4.6.2). For an isothermal profile in the Sagittarius dwarf, the limit is instead

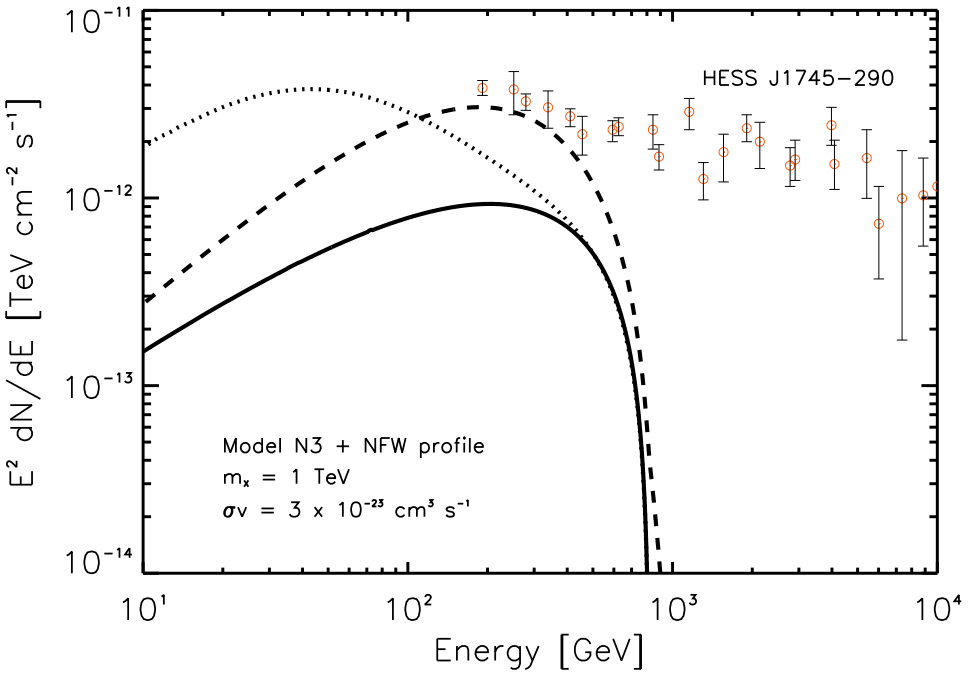

Figure 4.12: The total gamma-ray spectrum dN/dE_γ, for an NFW halo, from a 1 TeV DM particle annihilating into a pseudoscalar a (decaying to muons) and a scalar s which decays to aa (solid line) or only in 95% of the cases into aa and in 5% into $b\bar{b}$ (dotted line) or $\tau^+\tau^+$ (dashed line). The masses for a and s are those of model $N3$ of Tab. 4.3, so the solid line corresponds to the $N3$-line shown in Fig. 4.11.

$\sigma v < 2.2 \times 10^{-23}$ cm^3 s^{-1}. For the other models in Tab. 4.3, the limits are higher/lower by a factor of a few as indicted by the spectra in Fig. 4.11. For other dwarf galaxies, the limits are similar. For example, for the Willman 1 dwarf, using a conservative estimate of the line of sight integral from Ref. [586], the limits on the gamma flux from Magic [587] translate to $\sigma v < 1.3 \times 10^{-21}$ cm^3 s^{-1}. However, the uncertainties from dynamical constraints [586] are large and better data may be able to give better constraints in the future. Remembering that we typically need a boost of order 10^3 to explain the PAMELA data (see the PAMELA band in Fig. 4.13), we note that the limits derived here are very close to the needed σv. Given the uncertainties of the dark matter profile in the dwarf galaxies, we cannot exclude these models though, but note that for some models, like the AH1–AH3, the more optimistic scenarios for the halo profile of e.g. the Sagittarius dwarf are excluded.

Now we move to the constraints from radio observations of the Galactic center, following the same procedure as in Sec.4.7.

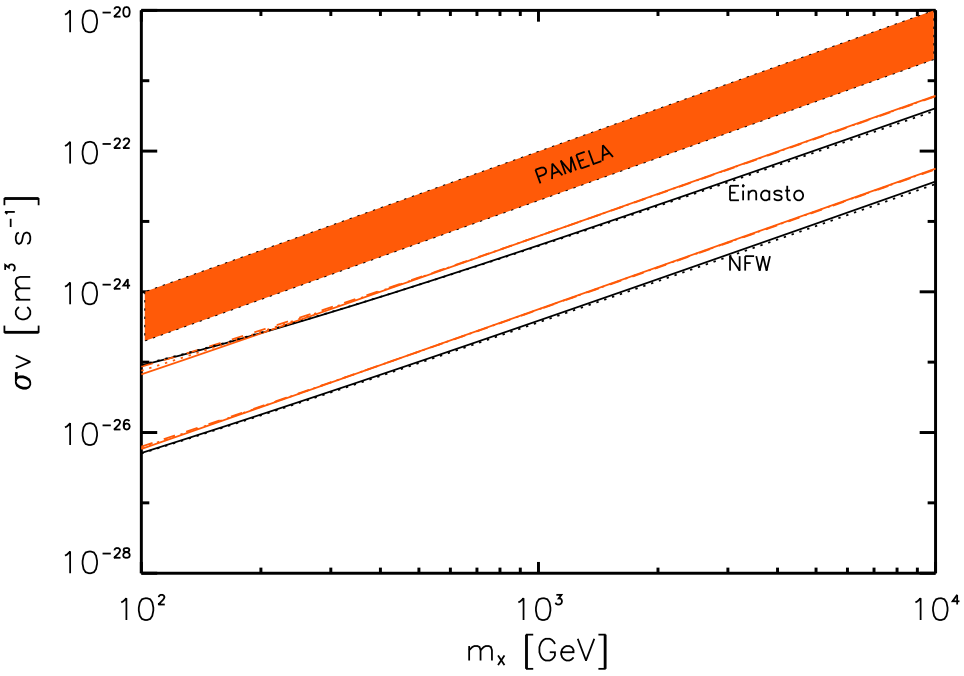

Figure 4.13: Exclusion plot in the σv vs. mass plane. The two sets of curves give the maximum annihilation cross section compatible with radio observations of Sgr A* for Einasto and NFW profiles. The color code of the curves is the same as in Fig. 4.11. The shaded region, corresponding to the range of annihilation cross sections that provide a good fit to the PAMELA and ATIC data, appears to be in conflict with observations, unless the DM profile is more shallow than Einasto.

We show the results in Fig. 4.13 in the σv vs. mass plane. Let us stress that the σv plotted in Fig. 4.13 is the *effective* annihilation cross section, including both Sommerfeld enhancements and boosts due to substructures. The only way to avoid our constraints would thus be to boost the local anti-matter fluxes by more than one order of magnitude without affecting the gamma-ray or radio fluxes. Although this theoretical possibility cannot be ruled out (e.g. Refs.[588]), it appears to be unlikely for a realistic distribution of substructures in the Milky Way halo (see the discussion in Ref. [384]).

The two sets of curves give the maximum annihilation cross section compatible with radio observations of Sgr A* for two different DM profiles: Einasto and NFW. The shaded region, corresponding to the range of annihilation cross sections that provide a good fit to the PAMELA and ATIC data, appears to be in conflict with observations, unless the DM profile is more shallow than expected in current models of structure formation. Profiles steeper than NFW – like the $\rho(r) \propto r^{-1.2}$ needed to explain the WMAP 'Haze' [579,

580] – are ruled out by a rather larger margin. This confirms the dramatic importance of the multi-wavelength approach, especially for DM models tailored to explain anomalies in astrophysical observations.

Chapter 5

Dark Matter and stars

We study the impact of the capture and annihilation of WIMPs on the evolution of Pop III stars.

This chapter is based on [589].

5.1 Overview

Despite their weak interactions, WIMPs can lead to macroscopic effects in astrophysical objects, provided that they have a sizeable scattering cross section off baryons, as we have already discussed in Chapter . In this case, in fact, DM particles traveling through stars can be captured, and sink at the center of the stars. Direct searches and astrophysical arguments, however, severely constrain the strength of DM-baryons interactions (see e.g. Ref. [171] and references therein). Since the capture rate is proportional to the product of the scattering cross section times the local DM density, large effects are thus expected in regions where the DM density is extremely high (this was already noticed in the context of the so called 'cosmions' [208, 209, 210, 211]). Recent progress in our understanding of the formation and structure of DM halos has prompted a renewed interest in the consequences of DM capture in stars, in particular in the case of White Dwarfs [218], compact objects [220] and main sequence stars [217, 216] at the Galactic center, where the DM density could be extremely high [464].

Alternatively, one may focus on the first stars, which are thought to form from gas collapsing at the center of $10^6 - 10^8 M_\odot$ DM halos at redshift $z \lesssim 10 - 30$. The consequences of DM annihilations in Pop III stars were first investigated by Spolyar, Freese and Gondolo [590], who have shown that the energy released by WIMP annihilations in these mini-halos, during the formation of a proto-star, may exceed any cooling mechanism, thus leading to a new phase of stellar evolution (see also Ref. [591, 592, 593]). The formation of proto-stars with masses between $6M_\odot$ and $600M_\odot$ in DM halos of $10^6 M_\odot$ at

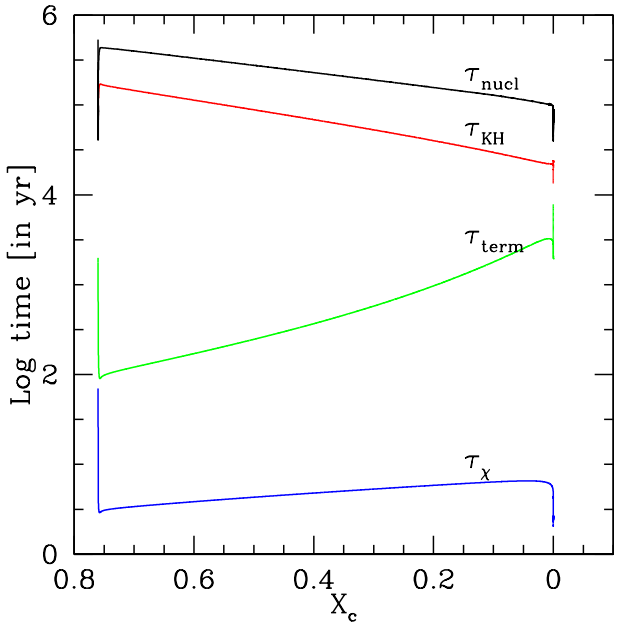

Figure 5.1: Timescales during star evolution. The plot is for a 20 $M_\odot$ star and a DM density $\rho_\chi = 10^9$ GeV cm^{-3}.

z=20, can actually be delayed by $\sim 10^3 - 10^4$ yrs [592]. It was subsequently shown in Refs. [594, 595], that the annihilation of DM particles captured at the center of the star, due to scattering off the stellar nuclei, can lead to an energy injection that overwhelms nuclear reactions. Under these circumstances, the core H-burning phase of Pop III stars, in DM halos of density of 10^{11} GeV cm^{-3}, is substantially prolonged, especially for small mass stars ($M_* < 40 M_\odot$) [592].

In this Chapter, we perform a detailed study of the impact of DM capture and annihilation on the evolution of Pop. III stars implementing in the Geneva stellar evolution code [596] a WIMP luminosity term. With respect to previous analyses, this already allows us to properly take into account the stellar structure.

5.2 WIMPs capture and annihilations

The capture rate is computed following Ref. [597], as

$$C = 4\pi \int_0^{R_*} dr r^2 \frac{dC(r)}{dV} \tag{5.1}$$

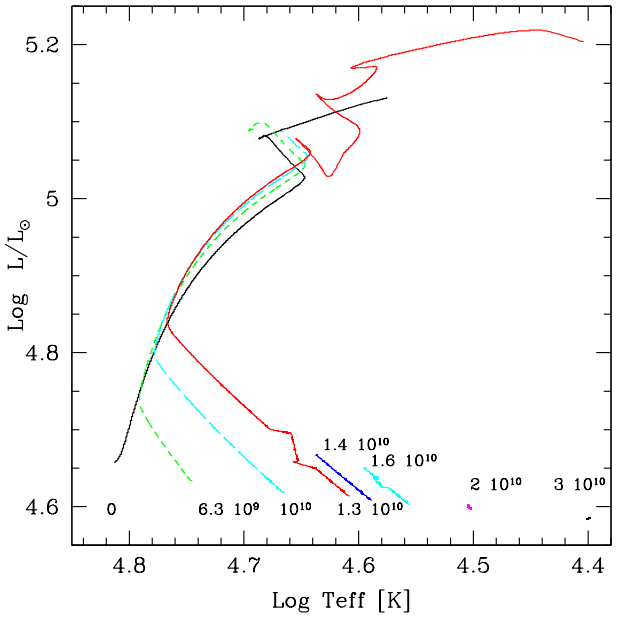

Figure 5.2: Evolutionary tracks of a Pop III 20 $M_\odot$ star for different WIMP densities (labels in units of GeV cm^{-3}). We have adopted a WIMP model with $m_\chi = 100$ GeV and $\sigma_p^{SD} = 10^{-38}$ cm^2.

with

$$\frac{dC(r)}{dV} = \left(\frac{6}{\pi}\right)^{1/2} \sigma_{\chi,N} \frac{\rho_i(r)}{M_i} \frac{\rho_\chi}{m_\chi} \frac{v^2(r)}{\bar{v}^2} \frac{\bar{v}}{2\eta A^2} \tag{5.2}$$
$$\times \left\{ \left(A_+ A_- - \frac{1}{2} \right) [\chi(-\eta, \eta) - \chi(A_-, A_+)] + \frac{1}{2} A_+ e^{-A_-^2} - \frac{1}{2} A_- e^{-A_+^2} - \frac{1}{2} \eta e^{-\eta^2} \right\}$$

$$A^2 = \frac{3v^2(r)\mu}{2\bar{v}^2\mu_-^2}, \qquad A_\pm = A \pm \eta, \qquad \eta^2 = \frac{3v_*^2}{2\bar{v}^2}$$

$$\chi(a,b) = \frac{\sqrt{\pi}}{2}[\mathrm{Erf}(b) - \mathrm{Erf}(a)] = \int_a^b dy e^{-y^2}$$

$$\mu_- = (\mu_i - 1)/2, \qquad \mu_i = m_\chi / M_i$$

where $\rho_i(r)$ is the mass density profile of a given chemical element in the interior of the star and M_i refers to its atomic mass, while ρ_χ, and $\bar{v}$ are respectively the WIMP density and velocity dispersion at the star position. The velocity of the star with respect to an observer, labeled as v_*, is assumed to be equal to $\bar{v}$, giving therefore $\eta = \sqrt{3/2}$. The radial escape velocity profile depends on $M(r)$, i.e. the mass enclosed within a radius r, $v^2(r) = 2\int_r^\infty GM(r')/r'^2 dr'$.

The WIMP scattering cross section off nuclei, $\sigma_{\chi,N}$ is constrained by direct detection experiments and for a WIMP mass of 100 GeV the current upper limits are $\sigma_{SI} =$

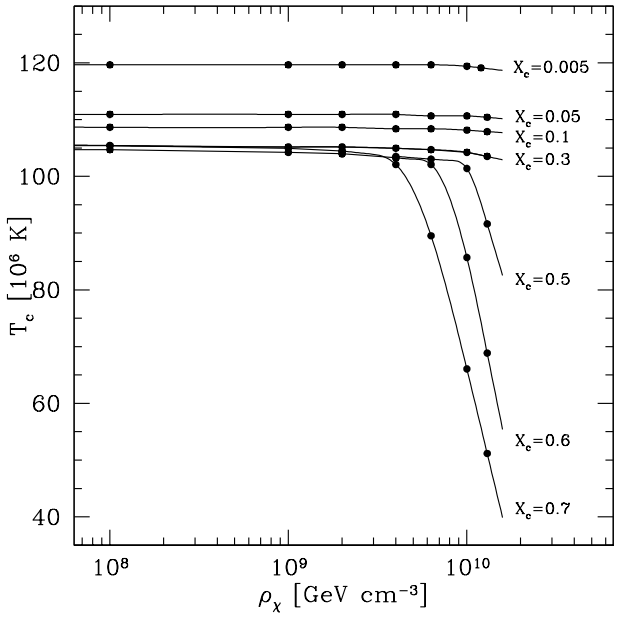

Figure 5.3: Temperature of the core as a function of the DM density for the 20 $M_\odot$ model, at different stages of the core H-burning phase. X_c denotes the mass fraction of hydrogen at the center of the star($X_c = 0.76$ at the beginning of the core H-burning phase). WIMP parameters as in Fig. 1.

10^{-43} cm^2 [256, 598] and $\sigma_{SD} = 10^{-38}$ cm^2 [599] respectively for spin-independent and spin-dependent WIMP interactions off a proton. We will adopt these reference values throughout this chapter, but the capture rate can be easily rescaled for other scattering cross sections by using Eq. 5.3. The spin-independent interactions with nucleons inside nuclei add up coherently giving an enhancement factor A^4 with respect to the interaction with a single nucleon: $\sigma^{SI}_{\chi,N} = A^4\sigma_{\chi,p}$, where A is the mass number. There is no such enhancement for the spin-dependent interactions. We consider the contribution to the capture rate from WIMP-hydrogen spin dependent interactions and WIMP-helium ^{4}He spin-independent interactions, neglecting the presence of other elements because of their very low abundance. The contribution of Helium, for the WIMPs parameters above, is found to be negligible with respect to that from hydrogen.

Once captured, WIMPs get redistributed in the interior of the star reaching, in a characteristic time τ_{th}, a thermal distribution [600]:

$$n_\chi(r) = n_0 e^{\frac{-r^2}{r_\chi^2}} \text{ with } r_\chi = \sqrt{\frac{3kT_c}{2\pi G\rho_c m_\chi}} \tag{5.3}$$

with T_c and ρ_c referring to the core temperature and density. The distribution results quite

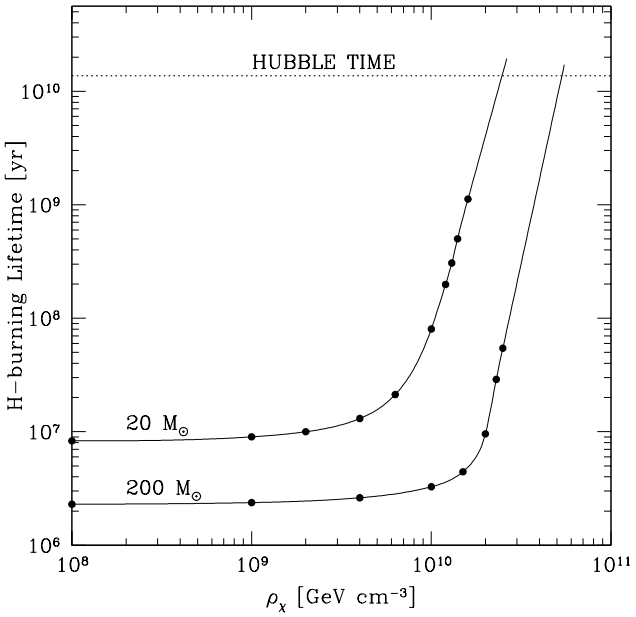

Figure 5.4: Variation of the core H-burning lifetime as a function of the WIMP densities for the Pop III 20 and 200 $M_\odot$ models. WIMP parameters as in Fig.5.2

concentrated toward the center of the star: e.g. for a $20M_\odot$ star immersed in a WIMP density of $\rho_\chi = 10^9$ GeV cm^{-3} at the beginning of the core H-burning phase we obtain $r_\chi = 2 \times 10^9$cm, a value much lower than the radius of the star, $R_* = 10^{11}$cm. This consideration underlines the importance of an accurate spatial resolution in the core to properly treat the luminosity produce from WIMPs annihilations. We have also checked that regardless the extremely high concentrations of WIMPs obtained at the center of the stars, the gravity due to WIMPs is completely negligible.

The number of scattering events needed for DM particles to thermalize with the nuclei in the star is of order $\approx m_\chi/M_H$, thus an upper limit on the thermalization time can be obtained as $\tau_{th} = (m_\chi/M_H)/(\sigma_{SD}\bar{n}_H\bar{v})$ where $\bar{n_H}$ is the average density on the star.

The WIMPs emissivity is $\epsilon_\chi(r) = 4\pi(\sigma v)m_\chi c^2 n_\chi^2(r)$ and the total WIMPs luminosity, L_χ, is simply the integral over the volume of the star. For the annihilation cross section times relative velocity (σv), we assume the value 3×10^{-26} cm^2, as appropriate for a thermal WIMP, but note that the total WIMP luminosity at equilibrium does not depend on this quantity. After a time $\tau_\chi = \sqrt{C(\sigma v)\pi^{-3/2}r_\chi^{-3}}$ an equilibrium between capture and annihilation is established, and this incidentally allows to determine the normalization constant n_0 above.

We have checked that the two transients τ_χ and τ_{th} remain much smaller, during the

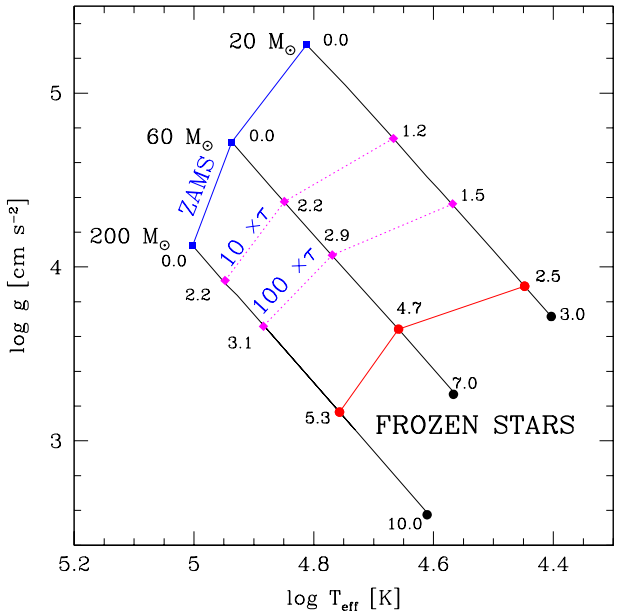

Figure 5.5: ZAMS positions of 20, 60 and 200 $M_\odot$ Pop. III stars in the g vs. T_{eff} plane for different DM densities (labels in units of GeV cm^{-3}). Big red circles correspond to the critical WIMP density (see text). The lines labeled as 10 τ and 100 τ correspond to models with lifetime prolonged by 10 and 100 times with respect to the case without WIMPs. WIMP parameters as in Fig.5.2

evolution of the star, than the Kelvin-Helmotz timescale, τ_{KH} and the timescale needed for the nuclear reactions to burn a small hydrogen fraction, e.g. $\Delta X_c = 0.002$, of the convective core, τ_{nucl}:

$$\tau_{KH} = \frac{GM_*^2}{R_* L_*} \qquad \tau_{nucl} = \frac{q_c \Delta X_c M_* 0.007 c^2}{L_*}$$

where the * labels quantities relative to the the star and q_c is the core convective mass fraction. We show an example in Fig.5.1. This argument justifies the assumption of equilibrium between capture and annihilation and the use of the radial distribution in Eq. 5.3. We assume here an average WIMP velocity $\bar{v} = 10$ Km s^{-1}, the virial velocity in an halo of $10^5 - 10^6 M_\odot$ at z=20 (see [594] and references therein). As for the DM density, semi-analytic computations of the adiabatic contraction of DM halos [590], in agreement with the results extrapolated from simulations of first star formation [602, 603], suggest DM densities of order 10^{12} GeV cm^{-3} or even higher.

5.3 PopIII evolution with Dark Matter

We have implemented the effects of WIMPs annihilation in the Geneva stellar evolution code (see Ref. [596] for details), and followed the evolution of a $20M_{\odot}$ and $200M_{\odot}$ stars for different DM densities. We show in Fig.5.2 the evolutionary tracks for the $20M_{\odot}$ model, and show for comparison (black line) the case of a standard Pop III star without WIMPs. For DM densities smaller than 10^9 GeV cm^{-3} the evolutionary tracks closely follow that of a normal star and they are not shown for simplicity. The position of the star at the beginning of the core H-burning phase (zero-age main sequence, or ZAMS) is obtained when, after a short transient, the luminosity produced at the center of the star equals the total luminosity and the star settles down in a stationary regime. For increasing DM densities the WIMPs luminosity produced at the center overwhelms the luminosity from nuclear reactions and makes the star inflate, producing therefore a substantial decrease of the effective temperature and a moderate decrease of the star luminosity at the ZAMS position, with respect to the standard scenario. For $\rho_\chi = 10^{10}$ GeV cm^{-3}, the energy produced by WIMPs present in the star at a given time, estimated as $E_\chi \simeq L_\chi \tau_{KH}$, is, at the ZAMS, ~ 0.8 times the gravitational potential energy of the star, and the star therefore starts to contract. In this phase, the core temperature, and consequently also the nuclear reactions, increase. When the latter become comparable with the WIMPs luminosity, the standard situation is recovered and the evolutionary track joins the classical tracks of a star without WIMPs. An important difference from standard evolution is that in the first phase, the nuclear reactions are slowed down and therefore the core H-burning lifetime is prolonged. For Dark Matter densities $\rho_\chi \leq 1.6\ 10^{10}$ GeV cm^{-3}, the picture is qualitatively the same, and for these models we only show in Fig. 5.2the first phases of the evolution. In Fig. 5.3, we show the core temperature as a function of the DM density, at different stages of the core H-burning phase. At high DM densities hydrogen burns at much lower core temperatures than in the usual scenario, till a certain mass fraction is reached, e.g. $X_c = 0.3$ for $\rho_\chi = 10^{10}$ GeV cm^{-3}, and the standard evolutionary track is joined. For increasing DM densities the nuclear reaction rate is more and more delayed till the contraction of the star is inhibited, due to the high DM energy accumulated, and the evolution is frozen. In Fig.5.2 for $\rho_\chi = 2 \cdot 10^{10}$ GeV cm^{-3} and $\rho_\chi = 3 \cdot 10^{10}$ GeV cm^{-3} the stars seems to remain indefinitely at the ZAMS position. In Fig. 5.4 we show the core H-burning lifetime as a function of the DM density. In the case of a $20M_{\odot}$ model, for $\rho \leq 10^9$ GeV cm^{-3} the core H-burning phase is prolonged by less then 10 % but the delay increases rapidly for higher DM densities. Extrapolating the curve we determine a critical density, $\rho_c = 2.5 \cdot 10^{10}$ GeV cm^{-3}, beyond which the core H-burning lifetime is longer then the age of the Universe. All the calculations have been repeated for the $200M_{\odot}$ model and we find that both the $20M_{\odot}$ and $200M_{\odot}$ stars evolutions are stopped for DM densities higher than $5.3 \cdot 10^{10} (\frac{\sigma_p^{SD}}{10^{-38}\ \mathrm{cm}^2})^{-1}$ GeV cm^{-3}. We have also verified that the results weakly depend on the WIMP mass, e.g. the core H-lifetime

is modified by a factor 0.2% and 5% respectively for $m_\chi = 10$ GeV and $m_\chi = 100$ GeV, if $\rho_\chi = 10^{10}$ GeV cm^{-3}.

It is remarkable that under these circumstances, frozen Pop III stars can survive until the present epoch, and can be searched for as an anomalous stellar population. In Fig.5.5 we show the effective temperature and gravity acceleration at the surface of these frozen Pop III stars, kept in the H-burning phase, for different DM densities. Frozen stars would thus appear much bigger and with much lower surface temperatures with respect to normal stars with the same mass and metallicity. Our results are qualitatively consistent with the preliminary estimates in [594, 595] and the analysis in [592]. However, for a given DM density, we obtain a somewhat longer core H-burning lifetime with respect to [592], possibly due to their use of an approximated expression for the capture rate. We have also followed, for selected models, the evolution during the core He-burning phase. During this evolutionary stage, the Dark Matter luminosity is lower than the nuclear reaction luminosity, therefore the impact of DM annihilations is found to be rather weak. For the $20 M_\odot$ model and for $\rho_\chi = 1.6 \cdot 10^{10}$ GeV cm^{-3} the He-lifetime is prolonged by a factor 1.2, rather than a factor 37 found for the H-burning phase for the same DM density.

5.4 Conclusions

In conclusion, we have adapted a stellar evolution code to the study the evolution of Pop. III stars in presence of WIMPs. The two key ingredients in our analysis are the ambient DM density and the scattering section off nucleon, that we have taken at the experimental limit. We have shown that provided the DM density remains above a critical value, the annihilation of WIMPs *captured* by Pop. III stars can dramatically alter the evolution of these objects, and prolong their lifetime beyond the age of the Universe. These results are in good agreement with those at the same time obtained by Yoon, Iocco and Akiyama [604].

In order to estimate the DM density at the star position, we consider the results of cosmological simulations that follow the gravitational collapse of baryons in DM mini-halos. Unfortunately, these simulations resolve the DM profile only down to ~ 1 pc, therefore to obtain the DM density at the center of the halo, where the star is formed, it is necessary to extrapolate these density profiles to low radii. In the inner regions of the halos the DM profile is expected to steepen, because of adiabatic contraction in the baryon-dominated core and indication of this process is indeed found in the simulations. The extrapolation method gives very high DM densities at the center of the halos, consistent with the results inferred from semi-analytic models of adiabatically contracted NFW profiles (the DM density obtained depends on the simulation considered, we note that in [593] they find $\rho_\chi \sim 10^{11}$ GeV cm^{-3} or higher). Remarkably, these DM densities are above the critical value necessary to indefinitely prolong the first stars lifetime.

In principle, it is not guaranteed that the DM distribution in the halo remains unchanged during its evolution and that the Dark Star remains at the central point. This may however occur if the Dark Matter mini-halos hosting the star does not experience mergers, a scenario similar to that proposed for DM mini-spikes around IMBHs (see Chapter 3). In this case, the 'frozen' stars could still exist today. We have determined its properties, and determined the observational characteristics that may allow to discriminate these objects from ordinary stars.

Frozen stars could be detected by future observations, for example with the James Webb Space Telescopes. Alternatively, if the properties of first stars will point to a standard evolution, the properties of the Dark Matter could be constrained.

Chapter 6

Conclusions

In this thesis we have faced the Dark matter problem and in particular we have considered astrophysical observations as a possible tool to study the nature of Dark Matter.

In the first chapter we have studied the constraints on Dark Matter properties and on the parameter space of Dark Matter models coming from particle physics, astrophysics and cosmological measurements. We have than moved to indirect Dark Matter searches through gamma-rays.

We have focused on DM mini-spikes, large DM over-densities which can be formed around IMBHs. This scenario offers particulary promising prospect for detection and peculiar signatures. We have studied the properties of a population of IMBHs in the Andromeda galaxy. We have shown that mini-spikes would be distributed in a few degrees region around the Andromeda center, each of them presenting the same gamma-ray spectrum, with an identical cut-off at the WIMP mass. This characteristic pattern would allow a more clear identification of the sources with respect to the case of IMBHs in the Milky Way.

We have shown that the detection of several IMBHs in Andromeda is within the reach of current Air Cherenkov Telescopes, the exact number depending on the mass and annihilation cross section of the MSSM neutralino, the Dark Matter candidate that we have considered. For a large range of neutralino masses, a significant number of mini-spikes can be detected with FERMI, allowing therefore a straightforward probe of this scenario.

Dark Matter annihilations in cosmological mini-spikes could contribute significantly to the Cosmic Gamma-ray Background measured by EGRET at gamma-ray energies of $(1-10)$ GeV. We have indeed shown that, for a WIMP mass of the order of 100 GeV and a "thermal" annihilation cross section, $(\sigma v) = 3\ 10^{-26}\ \mathrm{cm^3 s^{-1}}$, the predicted gamma-ray flux from DM annihilations is comparable to the EGRET CGB data. These estimates are however largely affected by particle physics and astrophysical uncertainties, the latter referring to

the DM mini-spikes profile and IMBHs number density and distribution. On the other hand, unresolved blazars certainly contribute to the CGB flux, with a fraction which is currently unknown but that should be modeled with good accuracy from the FERMI catalog of detected blazars. Anyway, the more recent analysis show that the most favored blazar models can explain roughly 20-50 % of the CGB intensity at 10 GeV. Generally, standard astrophysical sources are a background for Dark Matter searches in the CGB and in absence of spectacular spectral features it will be difficult to distinguish their contribution to the mean CGB intensity from those of DM annihilations. However, more information can be extracted from anisotropy data.

We have computed the angular power spectrum of the CGB in the mini-spikes model (at energy of detection $E_0 = 10$ GeV) and we have show it is quite different from that for blazars, providing therefore a tool to discriminate between the two scenarios. Moreover, the power spectrum of standard power-law gamma-ray emitters is energy independent and therefore it could be calibrated at low energies, where Dark Matter annihilations are negligible. We have considered blazars and Dark Matter annihilations as the main components of the CGB and we have varied their relative contribution. Taking unresolved blazars as a known background, we have shown that there are promising prospects for detecting DM annihilations in the CGB anisotropy with FERMI.

We have then studied the robustness of our results with respect to changes of the particle physics setup and energy of detection. We have found that the results are significantly affected by these parameters, although the prospects for detection remains good, provided that DM annihilations substantially contribute to the mean CGB intensity (generally at least 30%). In principle, this means that information on particle physics parameters could be extracted from CGB anisotropy data. However, a dedicated analysis is needed for a quantitative assessment. Finally, we have compared our results with the predictions for a scenario with Dark Matter subhalos dominating the Dark Matter signal. The prospects for distinguish the two models with FERMI depend on the contribution of DM annihilations to the total CGB intensity.

Our analysis show that FERMI have the potentiality to detect mini-spikes in the Milky Way and in the Andromeda galaxy and a confirmation should be provided by the CGB anisotropy data.

We have then studied the multi-wavelength constraints to the DM interpretation of the positron excess recently reported by PAMELA and ATIC experiments. DM models surviving bounds from, e.g, antiproton production generally fall into two classes, where either DM annihilates directly with a large branching fraction into light leptons, or the annihilation gives low-mass (pseudo)scalars or vectors which then decay into muon or electron pairs. If the ATIC peak is ignored, annihilations into SM gauge bosons or quarks are viable for DM

mass above 10 TeV. For all these kind of models, we have computed the photon flux and the synchrotron emission associated with Dark Matter annihilations and $e^{\pm}$ propagation in the galactic magnetic field.

We have show that the predicted synchrotron radiation in the central part of the Galaxy violates radio observations, unless the Dark Matter density profile is significantly less steep than the benchmark NFW and Einasto profiles. For the same choice of DM profiles, HESS observations of the galactic center and dwarf Spheroidals rule out models with DM annihilations into SM particles. These conclusions could be circumvented if there are physical processes that enhance the local anti-matter fluxes more than one order of magnitude, while not affecting the gamma-ray and radio fluxes. In principle, the presence of subhalos would indeed produce different boost factors at the galactic center and at the Sun position. However, it has to be noticed that according to recent simulations such large boost factors as needed by $e^{\pm}$ data are unlikely.

In models with Dark Matter annihilations into new light states, the γ-ray flux is reduced by more than a factor $\ln(m_\chi/m_\ell)/\ln(m/m_\ell) \sim 2$, with m_χ, m_ℓ and m respectively the mass of DM, the final lepton and the new light state. We find indeed that the gamma-ray constraints are alleviated and the models that fit the $e^{\pm}$ data are in conflict with observations for DM profiles steeper than NFW. However, already for an Einasto profile, these models are ruled out by the radio constraints. Some of the models predicting extra light states can simultaneously explain the positron excess and the WMAP Haze, the latter observation requiring a Dark matter profile $\rho(r) \propto r^{-1.2}$, at least down to radii $r \sim 500$ pc. In this case however the models violates gamma-ray bound at the galactic center, unless the DM profile rapidly flattens at $r \lesssim 500$ pc.

In conclusion, current bound from photon observations disfavor Dark Matter annihilations as origin of the positron excess. However, given the large uncertainties on the Dark Matter density profile and clumpiness, this interpretation of the current cosmic-ray data can not be excluded. Future observations should clarify the situation and eventually they will allow to determine the properties of Dark Matter. In particular, new PAMELA results will tell us if the positron fraction continues to increase for energies above 100 GeV, favoring in this case high Dark Matter masses. It is crucial in this sense a better insight on the $e^+ + e^-$ peak detected by ATIC-2. FERMI measurements of the cosmic-ray electron spectrum will be able to confirm or reject this excess and more precise measurements should be obtained from ATIC-4. Upcoming cosmic-ray data could confirm the existence of a primary source in the positron flux and tell us its origin.

We have then studied the effects of WIMPs annihilations in the first stars. Potentially, these objects are interesting targets for Dark Matter studies since very high DM densities could be reached in their surroundings as a consequence of their formation mechanism. We

have shown that for these high DM concentrations and for DM scattering cross section off baryons compatible with current bounds, the evolution of these stars is dramatically altered. In particular, nuclear reactions are inhibited and the star is sustained uniquely by DM annihilations. Therefore, first stars could have experienced an exotic evolution, maybe successively interrupted by astrophysical feedback or because of exhaustion of the DM fuel. However, some of these stars could have survived till present epoch. In this case, we have shown that their peculiar properties may allow to distinguish them from ordinary stars.

FERMI is currently operating and further astrophysical data are expected from other experiments. At the same time, direct detection experiments are continuously improving their sensitivity and LHC is expected to start at the beginning of 2010. Hopefully, the interplay of all these observations will help us to understand the nature of Dark Matter.

Bibliography

[1] E.W. Kolb and M.S. Turner, The Early Universe, Addison-Wesley, Redwood City, 1990.

[2] S. Dodelson, Modern Cosmology, Academic Press, London, San Diego, California, 2003.

[3] W.L. Freedman *et al.*, Astrophys.J. **553** (2001) 47.

[4] G. Jungman, M. Kamionkowski, K. Griest, Phys. Rept. **267** (1996) 195 [arXiv:hep-ph/9506380].

[5] L. Bergstrom, Rep. Progr Phys. 63 (2000) 793, [arXiv:hep-ph/0002126].

[6] G. Bertone, D. Hooper, J. Silk, Phys. Rept. **405** (2005) 279 [arXiv:hep-ph/0404175].

[7] D. Hooper and S. Profumo, [arXiv:hep-ph/0701197].

[8] F. Zwicky, 1933, Helv. Phys. Acta 6, 110.

[9] W. H. Tucker, H. Tananbaum and R. A. Remillard, ApJ (1995) 444.

[10] Review of Particle Physics. By Particle Data Group (C. Amsler et al.). 2008. Phys. Lett. B 667 (2008) 1.

[11] M.Taoso, G.Bertone and A.Masiero, JCAP 0803 (2008) 022, arXiv:0711.4996 [astro-ph].

[12] D. Scott and G.F. Smoot, by Particle Data Group 2006 [arXiv:astro-ph/0601307].

[13] Dunkley et al. arXiv: 0803.0586 [astro-ph].

[14] http://lambda.gsfc.nasa.gov

[15] B.D. Fields and S. Sarkar, by Particle Data Book 2006 [arXiv:astro-ph/0601514].

[16] J.R. Ellis, J.S. Hagelin, D.V. Nanopoulos, K.A. Olive and M. Srednicki, Nucl.Phys.B **238** (1984) 453.

[17] H. Goldberg, Phys. Rev. Lett. **50** (1983) 1419.

[18] T. Appelquist, H.C. Cheng and B.A. Dobrescu, Phys. Rev. D **64** (2001) 035002.

[19] H.C. Cheng and I. Low, Journal of High Energy Physics **0309** (2003) 051.

[20] P. Binetruy, G. Girardi and P. Salati, Nucl. Phys. B **237** (1984) 285.

[21] K. Griest and D. Seckel, Phys. Rev. D **43** (1991) 3191.

[22] P. Gondolo, J. Edsjö, P. Ullio, L. Bergstrom, M. Schelke and E.A. Baltz, JCAP 0407 (2004) 008 [arXiv:astro-ph/0406204].

[23] G. Belanger, F. Boudjema, A. Pukhov, and A. Semenov, Comput. Phys. Commun. 176, (2007) 367, [arXiv:hep-ph/0607059].

[24] J. Edsjö, M. Schelke, P. Ullio and P. Gondolo, New Astron. Rev. **49** (2005) 159-162.

[25] G. Servant, T.M.P. Tait, Nucl. Phys. B 650 (2003) 391-419, [arXiv:hep-ph/0206071].

[26] F. Burnell and a G.D. Kribs, Phys. Rev D **73** (2006) 015001.

[27] K. Kong and a K.T. Matchev, JHEP **0601** (2006) 038

[28] P. Salati, Phys. Lett. B **571** (2003) 121, [arXiv:astro-ph/0207396].

[29] R. Catena, N. Fornengo, A. Masiero, M. Pietroni and F. Rosati, Phys. Rev. D **70** (2004) 063519.

[30] M. Kawasaki, K. Kohri and N. Sugiyama, Phys. Rev. Lett. **82** (1999) 4168.

[31] K. Abazajian and S.M. Koushiappas, Phys. Rev. D **74** (2006) 023527, [arXiv:astro-ph/0605271].

[32] T. Asaka, A. Kusenko and M. Shaposhnikov, Phys. Lett. B **638** (2006) 401, [arXiv:hep-ph/0602150].

[33] J. Ellis, J.L. Lopez, and D.V. Nanopoulos, Phys. Lett. B **247** (1990) 257.

[34] J.L. Feng, A. Rajaraman, F. Takayama, Phys. Rev. Lett. 91 (2003) 011302, [arXiv:hep-ph/0302215].

[35] J. Ellis, K.A. Olive, Y. Santoso and V. Spanos, Phys. Lett. B 588 (2004) 7, [arXiv:hep-ph/0302262].

[36] J.L. Feng, A. Rajaraman and F. Takayama, Phys. Rev. D **68** (2003) 085018 [arXiv:hep-ph/0307375].

[37] J.L. Feng, A. Rajaraman and F. Takayama, Phys. Rev. D **68** (2003) 063504 [arXiv:hep-ph/0306024].

[38] M. Boltz, A. Brandenburg and W. Buchmüller, Nucl. Phys. B **606** (2001) 518.

[39] K. Griest, M. Kamionkowski and M.S. Turner, Phys. Rev. Lett. **64** (1990) 615.

[40] L. Hui, Phys. Rev. Lett. 86 (2001) 3467.

[41] E.W. Kolb, D.J. Chung and A. Riotto, Proceedings of 2nd International Conference on Dark Matter in Astro and Particle Physics (DARK98), Heidelberg,Germany,1998 [arXiv:hep-ph/9810361].

[42] D.J.H. Chung, E.W. Kolb and A. Riotto, Phys. Rev. D **60** (1999) 063504.

[43] E.W. Kolb, A. Riotto, and I.I. Tkachev, Phys. Lett. B **423** (1998) 348.

[44] G.F. Giudice, M. Peloso, A. Riotto, and I.I. Tkachev, Journal of High Energy Physics **08** (1999) 014.

[45] J.D. Barrow, E.J. Copeland, E.W. Kolb, and A.R. Liddle, Phys. Rev. D **43** (1991) 977.

[46] D.J.H. Chung, P. Crotty, E.W. Kolb and A. Riotto, Phys. Rev. D **64** (2001) 043503.

[47] E.W. Kolb, A.A. Starobinsky and I.I. Tkachev, (2007) [arXiv:hep-th/0702143].

[48] K.Benakli, J. Ellis, and D.V. Nanopoulos, Phys. Rev. D **59** (1999) 047301, [arXiv:hep-ph/9803333].

[49] T. Han, T. Yanagida and R.J. Zhang, Phys. Rev D **58** (1998) 095011.

[50] S. Sarkar and R. Toldra, Nucl. Phys.B **621** (2002) 495

[51] H. Ziaeepour, Astropart. Phys. **16** (2001) 101

[52] D. V. Semikoz, 30th International Cosmic Ray Conference (ICRC 2007), Mexico, arXiv:0706.2960 [astro-ph].

[53] HiRes Collaboration (R. Abbasi *et* al.) 2007 [arXiv:astro-ph/0703099].

[54] P. Sikivie, AIP Conf.Proc. **805** (2006) 23-29, [arXiv:hep-ph/0509198].

[55] G.G. Raffelt (2006), J.Phys.A 40 (2007) 6607, [arXiv:hep-ph/0611118].

[56] H. Pagels and J. R. Primack, Phys. Rev. Lett. 48 (1982) 223.

[57] J. R. Ellis, D. V. Nanopoulos, and S. Sarkar, Nucl. Phys. B 259 (1985) 175.

[58] V. S. Berezinsky, Phys. Lett. B 261 (1991) 71.

[59] T. Moroi, H. Murayama and M. Yamaguchi, Phys. Lett. B 303, 289 (1993).

[60] J. R. Ellis, D. V. Nanopoulos, K. A. Olive, and S. J. Rey, Astropart. Phys. 4 (1996) 371 [arXiv:hep-ph/9505438].

[61] M. Bolz, W. Buchmuller, and M. Plumacher, Phys. Lett. B 443 (1998) 209 [arXiv:hep-ph/9809381].

[62] F.D. Steffen, JCAP 0609:001, 2006 [arXiv:hep-ph/0605306].

[63] W. Buchmuller, AIP Conf.Proc. 903 (2007) 56, [arXiv:hep-ph/0611368].

[64] J. Pradler and F.D. Steffen, Phys. Lett. B 648:224-235, 2007[arXiv:hep-ph/0612291].

[65] G.F. Giudice, A. Riotto and I.I. Tkachev, Journal of High Energy Physics **9911** (1999) 036.

[66] H. P. Nilles, M. Peloso, and L. Sorbo, Phys. Rev. Lett. 87 (2001) 051302 [hep-ph/0102264].

[67] B. Brahmachari and R.N. Mohapatra, Phys. Lett. B **437** (1998) 100.

[68] Z.G. Berezhiani and R.N. Mohapatra, Phys. Rev. D **52** (1995) 6607.

[69] P. Langacker, Phys.Rev.D **58** (1998) 093017, [arXiv:hep-ph/9805281].

[70] N. Arkani-Hamed, S. Dimopoulos, G.R. Dvali and J. March-Russell, Phys. Rev. D **65** (2002) 024032, [arXiv:hep- ph/9811448].

[71] T. Asaka, S. Blanchet, and M. Shaposhnikov, Phys. Lett. B **631** (2005) 151 [arXiv:hep-ph/0503065].

[72] C. Athanassopoulos *et* al. Phys. Rev. Lett. **81** (1998) 1774.

[73] A. Kusenko and G. Segre, Phys. Lett. B **396** (1997) 197.

[74] A. A. Aguilar-Arevalo *et* al, Phys. Rev. Lett. 98 (2007) 231801, arXiv:0704.1500 [hep-ex].

[75] M. Maltoni and T.Schwetz, Phys.Rev. D 76 (2007) 093005 arXiv:0705.0107 [hep-ph].

[76] K. Abazajian, Phys. Rev. D **73** (2006) 063506.

[77] X.D. Shi and G.M. Fuller, Phys. Rev. Lett. **82** (1999) 2832.

[78] K. Abazajian G.M. Fuller and M. Patel, Phys.Rev.D **64** (2001) 023501.

[79] J. Silk, Astrophys. J. **151** (1968) 459.

[80] J.R. Bond and A.S. Szalay, Astrophys. J. **276** (1983) 443.

[81] J.R. Primack, SLAC Beam Line 31N3 50 (2001) [arXiv:astro-ph/0112336].

[82] Ø. Elgarøy and O. Lahav, Journal of Cosmology and Astro-particle Physics **0304** (2003) 004.

[83] D.N. Spergel *et* al. ApJS **148** (2003) 175.

[84] S. Hannestad, Journal of Cosmology and Astro-Particle Physics **0305** (2003) 004.

[85] E. Pierpaoli, Mon. Not. Roy. Astron. Soc. **342** (2003) L63.

[86] U. Seljak, A. Slosar and P. McDonald, JCAP **0610** 014,2006 [arXiv:astro-ph/0604335]

[87] G.L. Fogli, E. Lisi, A. Melchiorri, A. Palazzo, P. Serra, J. Silk and A. Slosar, Phys. Rev. D 75 (2007) 053001, [arXiv:hep-ph/0608060].

[88] S. Hannestad and G. Raffelt, JCAP **0404** (2004) 008 [hep-ph/0312154].

[89] S. Hannestad, A. Mirizzi and G. Raffelt, JCAP 0507 (2005) 002 [hep-ph/0504059].

[90] S. Dodelson, A. Melchiorri, A. Slosar, Phys. Rev. Lett. 97 (2006) 04301, [arXiv:astro-ph/0511500].

[91] S.Hofmann, D.J. Schwarz and H. Stöcker, Phys. Rev. D **64** (2001) 083507.

[92] A.M. Green, S. Hofmann and D.J. Schwarz, Mon. Not. Roy. Astron. Soc. 353 (2004) L23, [arXiv:astro-ph/0309621].

[93] J.R. Primack, [arXiv:astro-ph/0112255].

[94] B. Moore *et* al. Astrophys. Journal **524** (1999) L19.

[95] A.A. Klypin, A.V. Kravtsov, O. Valenzuela and F. Prada, ApJ 522 (1999) 82.

[96] R.A. Flores and J.R. Primack, Astrophys.J. **427** (1994) L1.

[97] S.S. McGaugh and W.J.G. de Blok, 1998, Astrophys.J. **499**, 41.

[98] G. Gentile, A. Burkert, P. Salucci, U. Klein and F. Walter, Astrophys. J 634 (2005) 145, [arXiv:astro-ph/0510607].

[99] G. Gentile, P. Salucci, U. Klein, D. Vergani and P. Kalberla, MNRAS 351 (2004) 903, [arXiv:astro-ph/0403154].

[100] J.S. Bullock *et* al. ApJ **555** (2001) 240.

[101] M. Vitvitska, A.A. Klypin, A.V. Kravtsov, R.H. Wechsler, J.R. Primack, J.S. Bullock, Astrophys. J. **581** (2002) 799, [arXiv:astro-ph/0105349].

[102] J.S. Bullock, A.V. Kravtsov and D.H. Weinberg, APJ **539** (2000) 517.

[103] O.Y.Gnedin [arXiv:astro-ph/0611270].

[104] B.Moore, J. Diemand, P. Madau, M. Zemp and J. Stadel, MNRAS, 368, 563 (2006) [arXiv:astro-ph/0510370].

[105] J.D. Simon and M. Geha, 2007 e-Print: arXiv:0706.0516 [astro-ph].

[106] L. Mayer, F. Governato, M. Colpi, B. Moore, T. Quinn, J. Wadsley J. Stadel and G. Lake, ApJ 547 L123 (2001).

[107] A.V. Kravtsov, O.Y. Gnedin and A.A. Klypin, ApJ 609 482 (2004).

[108] E. Hayashi, J.F. Navarro and V. Springel, Mon. Not. Roy. Astron. Soc. 377 (2007) 50, [arXiv:astro-ph/0612327].

[109] S. Hofmann, D.J. Schwarz and H. Stocker, Phys. Rev. D 64 (2001) 083507.

[110] A. El-Zant, I. Sclosman and Y. Hoffman, ApJ 560 (2001) 636.

[111] M.D. Weinberg and N. Katz, ApJ 580 (2002) 627.

[112] D.N. Spergel and P.J. Steinhardt, Phys. Rev. Lett. **84** (2000) 3760.

[113] M. Kaplinghat, L. Knox and M.S. Turner, Phys. Rev. Lett. 85 (2000) 3335.

[114] P. Bode, J.P. Ostriker and N. Turok, ApJ **556** (2001) 93.

[115] J. Sommer-Larsen, A. Dolgov, ApJ 551 (2001) 608, [arXiv:astro-ph/9912166].

[116] M. Viel, J. Lesgourgues, M.G. Haehnelt, S. Matarrese and A. Riotto, Phys. Rev. D **71** (2005) 063534, [arXiv:astro-ph/0605706].

[117] E.A. Baltz, H. Murayama, JHEP **0305** (2003) 067, [arXiv:astro-ph/0108172].

[118] S. Dodelson and L.M. Widrow, Phys. Rev. Lett. **72** (1994) 17.

[119] S. Colombi, S. Dodelson, L. M. Widrow, Astrophys.J. **458** (1996) 1, [arXiv:astro-ph/9505029].

[120] K.Abazajian, Phys. Rev. D **73** (2006) 063513.

[121] M. Viel, J. Lesgourgues, M.G. Haehnelt, S. Matarrese and A. Riotto, Phys. Rev. D **97** (2006) 071301, [arXiv:astro-ph/0605706].

[122] U. Seljak, A. Makarov, P. McDonald and H. Trac, Phys. Rev. Lett. **97** (2006) 191303, [arXiv:astro-ph/0602430].

[123] M. Viel, G.D. Becker, J.S. Bolton, M.G. Haehnelt, M. Rauch and W.L.W. Sargent, 2007, arXiv:0709.0131 [astro-ph].

[124] A.Boyarsky, J. Lesgourgues, O. Ruchayskiy and M. Viel, 2008 arXiv:0812.0010 [astro-ph].

[125] R. Barkana, Z. Haiman and J.P. Ostriker, ApJ **558** (2001) 483, [arXiv:astro-ph/0103050].

[126] N. Yoshida, A. Sokasian, L. Hernquist and V. Springel, ApJ **591** (2003) L1.

[127] K. Jedamzik, M. Lemoine and G. Moultaka, JCAP 0607 (2006) 010, [arXiv:astro-ph/0508141].

[128] P.L. Biermann and A. Kusenko, Phys. Rev. Lett. **96** 091301, 2006 [astro-ph/0601004].

[129] J. Stasielak, P. L. Biermann, and A. Kusenko, Astrophys. J. 654 (2007) 290-303, [arXiv:astro-ph/0606435].

[130] E. Ripamonti, M. Mapelli and A. Ferrara, Mon. Not. Roy. Astron. Soc. 375 (2007) 1399-1408, [arXiv:astro-ph/0606483].

[131] S. Dimopoulos, G.F. Giudice and A. Pomarol, Phys. Lett. B 389 (1996) 37.

[132] A. De Rujula, S. L. Glashow and U. Sarid, Nucl. Phys. B 333 (1990) 173.

[133] S. Dimopoulos, D. Eichler, R. Esmailzadeh and G. D. Starkman, Phys. Rev D 41 (1990) 2388.

[134] L. Chuzhoy and E.W. Kolb, 2008 arXiv:0809.0436 [astro-ph].

[135] A. Kudo and M. Yamaguchi, Phys. Lett. B 516 (2001) 151-155.

[136] D. E. Groom *et* al, Particle Data Group, E.P.J.C. 15 (2001) 1.

[137] T. Hammick *et* al, Phys. Rev. D 41 (1990) 2074.

[138] M. L. Perl *et* al, Int. J. Mod. Phys. A16:2137-2164, 2001 [arXiv:hep-ex/0102033].

[139] S. W. Barwick *et* al, Phys. Rev. Lett. 64 (1990) 2859.

[140] D. P. Snowden-Ifft *et* al APJ 364 (1990) L25.

[141] A. Gould *et* al, Phys. Lett. B 238, 337 (1990).

[142] R. S. Chivukula et al., Phys. Rev. Lett. 65, 957 (1990).

[143] B. Holdom, Phys. Lett. B 166, 196 (1986).

[144] B. Holdom, Phys. Lett. B 259, 329 (1991).

[145] S. A. Abel, J. Jaeckel, V. V. Khoze and A. Ringwald, [arXiv:hep-ph/0608248].

[146] E. Masso and J. Redondo, Phys. Rev. Lett. 97, 151802 (2006) [arXiv:hep-ph/0606163].

[147] S. A. Abel and B. W. Schofield, Nucl. Phys. B 685, 150 (2004) [arXiv:hep-th/0311051].

[148] B. Batell and T. Gherghetta, Phys. Rev. D 73 (2006) 045016, [arXiv:hep-ph/0512356].

[149] S. Davison, S. Hannestad and G. Raffelt, JHEP 0005 (2000) 003, [arXiv:hep-ph/0001179].

[150] S. Dubovsky, D. Gorbunov, G. Rubtsov, JETP Lett. 79 (2004) 1 [hep-ph/0311189].

[151] S.N. Gninenko, N.V. Krasnikov, A. Rubbia, Phys. Rev. D 75 (2007) 075014, [arXiv:hep-ph/0612203].

[152] E. Zavattini et al. [PVLAS Collaboration], Phys. Rev. Lett. 96 (2006) 110406 [hep-ex/0507107].

[153] [PVLAS Collaboration] E. Zavattini *et* al. (2007) arXiv:0706.3419 [hep-ex].

[154] H. Gies, Holger and J. Jaeckel and A. Ringwald, Phys. Rev. Lett. 97 (2006) 140402, [arXiv:hep-ph/0607118].

[155] A. Melchiorri, A. D. Polosa and A. Strumia, [arXiv:hep-ph/0703144].

[156] U. Sarid and S. D. Thomas, Phys. Rev. Lett. 85, 1178 (2000) [arXiv:hep-ph/9909349].

[157] G. Farrar, Phys. Lett. B 265 (1991) 395;

[158] S. Rabi and K. Tobe, Nucl. Phys. B 539 (1999) 3.

[159] Z. Chacko, B. Dutta R. N. Mohapatra and S. Nandi, Phys. Rev. D 56 (1997) 5466.

[160] Z.G. Berezhiani and R.N. Mohapatra, Phys. Rev. D 52 (1995) 6611.

[161] J. Kang, M.A. Luty and S. Nasri, [arXiv:hep-ph/0611322].

[162] G. Starkman, A. Gould, R. Esmailzadeh and S. Dimopoulos, Phys. Rev. D 41, 3594 (1990).

[163] P. Natarajan, A. Loeb, J.P. Kneib and I. Smail, Astrophys. J. 580 L17 (2002) [arXiv:astro-ph/0207045].

[164] R.H. Cyburt, B.D. Fields, V. Pavlidou and B. Wandelt, Phys. Rev. D 65 (2002) 123503.

[165] X.L. Chen, S. Hannestad and R.J. Scherrer, Phys. Rev. D 65 (2002) 123515, [arXiv:astro-ph/0202496].

[166] D. Javorsek II, E. Fishbach and V. Teplitz, ApJ 568 (2001) 1-8.

[167] B. Wandelt, R. Davé, G.R. Farrar, P.C. McGuire, D.N. Spergel and P.J. Steinhardt, [arXiv:astro-ph/0006344].

[168] P.C. McGuire and P.J. Steinhardt, [astro-ph/0105567].

[169] A.L. Erickcek, P.J. Steinhardt, D. McCammon and P.C. McGuire, Phys. Rev. D 76 (2007) 042007, arXiv:0704.0794 [astro-ph].

[170] I.F.M. Albuquerque and L. Baudis, Phys. Rev. Lett. 90 (2003) 221301, [arXiv:astro-ph/0301188].

[171] G.D. Mack, J.F. Beacom and G. Bertone, Phys. Rev. D 76 (2007) 043523, arXiv:0705.4298 [astro-ph].

[172] R.N. Mohapatra and S. Nussinov, Phys. Rev. D 57 (1998) 3.

[173] A. Zhitnitsky, Phys. Rev. D 74 (2006) 043515, [astro-ph/0603064].

[174] K. A. Olive, G. Steigman and T.P. Walker, Phys. Reports 333:389-407 (2000), [arXiv:astro-ph/9905320].

[175] R. H. Cyburt, and B. D. Fields, K. A. Olive and E. Skillman, Astropart. Phys. 23 (2005) 313-323, [arXiv:astro-ph/0408033].

[176] M. Maggiore, Phys. Rept. 331:283-367, 2000 [arXiv:gr-qc/9909001].

[177] J. A. Grifols, R. N. Mohapatra and A. Riotto, Phys. Lett. B 400 (1997) 124 [arXiv:hep-ph/9612253].

[178] E.W. Kolb, M.S. Turner and T.P. Walker, Phys. Rev. D 34 (1986) 2197.

[179] P.D. Serpico and G.G. Raffelt Phys. Rev. D 70 (2004) 043526, [arXiv.astro-ph/0403417].

[180] K. Jedamzik Phys. Rev. D 70, (2004) 063524, [arXiv:astro-ph/0402344].

[181] M. Kawasaki, K. Kohri and T. Moroi, Phys. Rev.D 71, (2005) 083502, [arXiv:astro-ph/0408426].

[182] F.D. Steffen, JCAP 0609:001, 2006 [arXiv:hep-ph/0605306].

[183] R.H. Cyburt, J.R. Ellis, B.D. Fields and K.A. Olive, Phys. Rev. D 67 (2003) 103521, [arXiv:astro-ph/0211258].

[184] K. Jedamzik, Phys. Rev. D 74, (2006) 103509, [arXiv:hep-ph/0604251].

[185] T. Gherghetta *et* al, Nuclear Physics B 559 (1999) 27-47.

[186] M. Ibe, R. Kitano, H. Murayama and T. Yanagida, Phys. Rev. D 70 (2004) 075012.

[187] M. Pospelov, Phys. Rev. Lett. 98 (2007) 231301, [arXiv:hep-ph/0605215].

[188] K. Kohri and F. Takayama, Phys. Rev. D 76 (2007) 063507, [arXiv:hep-ph/0605243].

[189] M. Kawasaki, K. Kohri and T. Moroi, Phys. Lett. B 649:436-439, 2007 [arXiv:hep-ph/0703122].

[190] R.H. Cyburt, J. Ellis, B.D. Fields K.A. Olive and V.C. Spanos, JCAP 0611 (2006) 014.

[191] K. Jedamzik, 2007 e-Print: arXiv:0710.5153 [astro-ph].

[192] J.L. Feng, S. Su and F. Takayama, Phys. Rev. D 70 (2004) 063514.

[193] W. Buchmuller, L. Covi, J. Kersten and K. Schmidt-Hoberg, JCAP 0611 (2006) 007, [arXiv:hep-ph/0609142].

[194] D.G. Cerdeno, K.Y. Choi, K. Jedamzik, L. Roszkowski and R. Ruiz de Austri, JCAP 0606:005, 2006 [arXiv:hep-ph/0509275].

[195] T. Kanzaki, M. Kawasaki, K. Kohri and T. Moroi, Phys. Rev. D 75 (2007) 025011, [arXiv:hep-ph/0609246].

[196] J.L. Diaz-Cruz, J. Ellis, K.A. Olive and Y. Santoso, JHEP 0705 (2007) 003, [arXiv:hep-ph/0701229].

[197] K. Hamaguchi, T. Hatsuda, M. Kamimura, Y. Kino and T.T. Yanagida, Phys. Lett. B 650:268-274, 2007 [arXiv:hep-ph/0702274].

[198] G. G. Raffelt, Ann. Rev. Nucl. Part. Sci. 49 (1999) 163-216, [arXiv:hep-ph/9903472].

[199] G. G. Raffelt, Stars as Laboratories for Fundamental Physics. Chicago: University of Chicago Press (1996).

[200] Georg G. Raffelt [arXiv:hep-ph/0611350].

[201] P. Fayet, D. Hooper and G. Sigl, Phys. Rev. Lett. 96 (2006) 211302, [arXiv:hep-ph/0602169].

[202] J. Hidaka and G. M. Fuller, Phys. Rev. D 74 (2006) 125015,2006 [arXiv:astro-ph/0609425].

[203] E.D. Carlson, P. Salati, Phys. Lett B 218:79 (1989).

[204] G. Raffelt, G. Starkman, Phys. Rev. D 40:942 (1989).

[205] G. Steigman, G. L. Sarazin, H. Quintana and J Faulkner, ApJ83, 1050 (1978).

[206] D. N. Spergel and W. Press, ApJ 294, 663 (1985).

[207] J. Faulkner and R. L. Gilliland, ApJ 299, 994 (1985).

[208] A. Renzini, Astr. Ap. 171, 21.

[209] A. Bouquet and P. Salati, ApJ 346, 284 (1989).

[210] D. Dearborn, G. Raffelt, P. Salati, J. Silk and A. Bouquet, ApJ 354, 568 (1990).

[211] P. Salati, G. Raffelt and D. Dearborn, ApJ 357, 566 (1990).

[212] A. Bottino, G. Fiorentini, N. Fornengo, B. Ricci, S. Scopel and F.L. Villante, Phys. Rev. D 66 (2002) 053005, [arXiv:hep-ph/0206211].

[213] I. P. Lopes, G. Bertone and J. Silk, Mon. Not. Roy. Astron. Soc. **337** (2002) 1179 [arXiv:astro-ph/0205066].

[214] P. Salati and J. Silk, ApJ 338 (1989) 24.

[215] P. Scott, J. Edsjo and M. Fairbairn, Nov 2007, arXiv:0711.0991 [astro-ph].

[216] M. Fairbairn (CERN), P. Scott and J. Edsjo, Phys.Rev.D 77 (2008) 047301, arXiv:0710.3396 [astro-ph].

[217] P.Scott, M. Fairbairn and J. Edsjo 2008 arXiv:0809.1871 [astro-ph].

[218] I.V. Moskalenko and L.L. Wai, Astrophys. J. 659:L29-L32, 2007 [arXiv:astro-ph/0702654].

[219] I.V. Moskalenko and L.L. Wai, AIP Conf. Proc. 921:508-509, 2007 e-Print: arXiv:0704.1324 [astro-ph].

[220] G. Bertone and M. Fairbairn, Phys. Rev. D **77** (2008) 043515, arXiv:0709.1485 [astro-ph].

[221] X.L. Chen and M. Kamionkowski, Phys. Rev. D 70 (2004) 043502, [arXiv:astro-ph/0310473].

[222] A. Kusenko and M. Shaposhnikov, Phys. Lett B 418 (1998) 46.

[223] G. R. Farrar, Phys. Rev. Lett. 53 (1984) 1029.

[224] M. C. Bento, O. Bertolami, R. Rosenfeld and L. Teodoro, Phys. Rev. D 62 (2000) 041302, [arXiv:astro-ph/0003350].

[225] N. Yoshida, V. Springel, S.D.M. White and G. Tormen, ApJ 544 (2000) L87D.

[226] R. Dave, D. N. Spergel, P. J. Steinhardt and B. D. Wandelt, ApJ 547 (2001) 574.

[227] P. Colin, V. Avila-Reese, O. Valenzuela and C. Firmani, ApJ 581 (2002) 777.

[228] K. Ahn and P.R. Shapiro, J. Korean Astronomical Soc. 36 (2002) 89, [arXiv:astro-ph/0212575].

[229] K. Ahn and P.R. Shapiro, Mon. Not. Roy. Astron. Soc. 363:1092-1124, 2005. [arXiv:astro-ph/0412169].

[230] O.Y. Gnedin and J.P. Ostriker, ApJ 561 (2001) 61.

[231] S.R. Furlanetto and A. Loeb, ApJ 565 (2002) 854.

[232] P. Natarajan, A. Loeb, J-P. Kneib and I. Smail, ApJ 580 (2002) L17, [arXiv:astro-ph/0207045].

[233] J.S. Arabadjis, M.W. Bautz and G.P. Garmire, ApJ 572 (2002) 66.

[234] J. F. Hennawi and J. P. Ostriker, ApJ 572 (2002) 41.

[235] J. Miralda-Escude, ApJ 564 (2002) 60.

[236] M. Markevitch, A. H. Gonzales, D. Clowe, A. Vikhlinin, W. Forman, C. Jones, S. Murray and W. Tucker, ApJ 606 (2004) 819, [arXiv:astro-ph/0309303].

[237] S. W. Randall, M. Markevitch, D. Clowe, A. H. Gonzalez and M. Bradac, e-Print: arXiv:0704.0261 [astro-ph].

[238] C. Firmani, E. D'Onghia, V. Avila-Reese, G. Chincarini and X. Hernández, 2001, MNRAS 315, L29.

[239] F.J. Sánchex-Salcedo, Astrophys.J.631 (2005) 244, [arXiv:astro-ph/0506345].

[240] J. F. Beacom, N.F. Bell and G.D. Mack, [arXiv:astro-ph/0608090].

[241] C. Munoz, Int. J. Mod. Phys. A **19** (2004) 3093 [arXiv:hep-ph/0309346].

[242] A. Kurylov and M. Kamionkowski, Phys. Rev. D 69, 063503 (2004).

[243] V.A. Bednyakov and F. Simkovic, Phys. Part. Nucl. 37:S106-S128, 2006 [arXiv:hep-ph/0608097].

[244] D. S. Akerib *et* al, Phys. Rev. D 73 (2006) 011102.

[245] J. Ellis, R.A. Flores and J.D. Lewin, Phys. Lett. B 212 (1988) 375;

[246] G.D. Starkman and D.N. Spergel, Phys. Rev. Lett. 74 (1995) 2623.

[247] A. K. Drukier, K. Freese and D. N. Spergel, Phys. Rev. D 37 (1988) 3388.

[248] R. Bernabei *et* al, AIP Conf. Proc. 878 (2006) 91-98.

[249] A. Benoit *et* al, Phys. Lett. B 545 (2002) 43 [arXiv:astro-ph/0206271].

[250] D. S. Akerib *et* al, Phys. Rev. D 68 (2003) 082002 [arXiv:hep-ex/0306001].

[251] P. Belli, R. Bernabei, A. Bottino, N. Fornengo, D. Prosperi and S. Scopel, Phys. Rev. D 61 (2000) 023512.

[252] R. Bernabei *et* al, Phys. Lett. B 480 (2000) 23.

[253] P. Belli, R. Cerulli, N. Fornengo and S. Scopel, Phys. Rev D 66 (2002) 043503 [arXiv:hep-ph/0203242].

[254] C. J. Copi, L. M. Krauss, Phys. Rev D 67 (2003) 103507 [arXiv:astro-ph/0208010].

[255] D. S. Akerib *et* al, Phys. Rev. Lett. 96 (2006) 011302.

[256] J. Angle *et al.* [XENON Collaboration], Phys. Rev. Lett. **100** (2008) 021303 [arXiv:0706.0039 [astro-ph]].

[257] P. Gondolo and G. Gelmini, Phys. Rev. D 71 (2005) 123520,[arXiv:hep-ph/0504010].

[258] V. Sanglard *et* al, Phys.Rev.D 71:122002, 2005 [arXiv:astro-ph/0503265].

[259] G. Angloher *et* al, Astropart. Phys. 23 (2005) 325-339.

[260] G.J. Alner *et* al, [arXiv:astro-ph/0701858].

[261] P. Benetti *et* al, [arXiv:astro-ph/0701286].

[262] H. Baer, C. Balazs, A. Belyaev and J. O'Farrill , 2003 [arXiv:hep-ph/0305191]

[263] R. Ruiz de Austri, R. Trotta and L.Roszkowski, JHEP 0605:002, 2006 [arXiv:hep-ph/0602028].

[264] E. A. Baltz and P. Gondolo, JHEP 0410:052,2004.

[265] E. A. Baltz and P. Gondolo, Physical Review D 67 (2003) 063503.

[266] C. Savage, P. Gondolo and K. Freese, Phys. Rev. D 70:123513, 2004 [arXiv:astro-ph/0408346].

[267] G. J. Alner et al. [UKDMC], Phys. Lett. B 616 (2005), 17.

[268] M. Barnabe-Heider et al., Phys. Lett. B624 (2005), 186-194.

[269] V. Kudryavtsev, IDM2004.

[270] V. Sanglard et al., Phys. Lett. B 616 (2005), 25-30.

[271] S. Desai et al., Phys. Rev. D 70 (2004), 083523.

[272] H.S. Lee *e*t al, 2007 [arXiv:0704.0423].

[273] W. J. Bolte *e*t al, J. Phys. Conf. Ser. 39 (2006) 126-128.

[274] A. Bottino, F. Donato, N. Fornengo and S. Scopel, Phys. Rev. D 78 (2008) 083520, arXiv:0806.4099 [hep-ph].

[275] C. Savage, G. Gelmini, P. Gondolo and K. Freese, 2008 arXiv:0808.3607 [astro-ph].

[276] J.M. Russell, C. McCabe and M. McCullough, 2008 arXiv:0812.1931 [astro-ph].

[277] J. Ellis, K. A. Olive, Y. Santoso and V. C. Spanos, Phys. Rev. D 71 (1005) 095007.

[278] A. Bottino, F. Donato, N. Fornengo and S. Scopel, Phys. Rev. D 72 (2005) 083521 [arXiv:hep-ph/0508270].

[279] H-S Lee, K.T. Matchev, S. Nasri, Phys. Rev. D 76 (2007) 041302, [hep-ph/0702223].

[280] C. Arina and N. Fornengo, JHEP 0711 (2007) 029, arXiv:0709.4477 [heo-ph].

[281] G. Bertone, Astrophys. Space Sci. 309:505-515, 2007 [arXiv:astro-ph/0608706].

[282] F. Aharonian *et al.* [The HESS collaboration], Astron. Astrophys. 425 (2004) L13 [astro-ph/0408145]. F. Aharonian *et al.* [H.E.S.S. Collaboration], Phys. Rev. Lett. **97** (2006) 221102 [Erratum-ibid. **97** (2006) 249901] [arXiv:astro-ph/0610509].

[283] G. Zaharijas and D. Hooper, Phys. Rev. D **73** (2006) 103501 [arXiv:astro-ph/0603540].

[284] V. Berezinsky, A. Bottino, and G. Mignola, Phys. Lett. B 325, 136 (1994), hep-ph/9402215.

[285] L. Bergstrom, P. Ullio, and J. H. Buckley, Astropart. Phys. 9, 137 (1998), astro-ph/9712318.

[286] S. Profumo, Phys. Rev. D **72** (2005) 103521 [arXiv:astro-ph/0508628].

[287] A. Cesarini, F. Fucito, A. Lionetto, A. Morselli and P. Ullio, Astropart. Phys. **21** (2004) 267 [arXiv:astro-ph/0305075].

[288] A. Bouquet, P. Salati and J. Silk, Phys. Rev. D **40** (1989) 3168.

[289] J. Silk and A. Stebbins, Astrophys. J. **411** (1993) 439.

[290] L. Bergstrom, J. Edsjo and P. Ullio, Phys. Rev. D **58**, 083507 (1998) [arXiv:astro-ph/9804050].

[291] C. Calcaneo-Roldan and B. Moore, Phys. Rev. D **62**, 123005 (2000) [arXiv:astro-ph/0010056].

[292] R. Aloisio, P. Blasi and A.V. Olinto, Astrophys. J. **601** (2004) 47 [arXiv:astro-ph/0206036].

[293] S.M. Koushiappas, A.R. Zentner and T.P. Walker, Phys. Rev. D **69** (2004) 043501 [arXiv:astro-ph/0309464].

[294] J. Diemand, B. Moore and J. Stadel, Nature **433** (2005) 389 [arXiv:astro-ph/0501589].

[295] E.A. Baltz, C. Briot, P. Salati, R. Taillet and J. Silk, Phys. Rev. D 61 (2000) 023514 [astro-ph/9909112].

[296] N.W. Evans, F. Ferrer and S. Sarkar, Phys. Rev. D 69 (2004) 123501, [arXiv:astro-ph/0311145].

[297] C. Tyler, Phys. Rev. D 66 (2002) 023509 [arXiv:astro-ph/0203242]

[298] L. Pieri and E. Branchini, Phys. Rev. D **69**, 043512 (2004) [arXiv:astro-ph/0307209].

[299] C.J. Hogan, Phys. Rev. D 64, 063515 (2001).

[300] L. Bergstrom, J. Edsjo and C. Gunnarsson, Phys. Rev D, 63 083515 (2001).

[301] L. Pieri and E. Branchini, J. Cosmol. Astropart. Phys. JCAP05 (2005) 007.

[302] R. Mohayaee and S.F. Shandarin, Mont. Not. Roy. Astron. Soc. 366, 1217 (2006).

[303] A. Natarajan, Phys. Rev. D 75:123514, 2007 [arXiv:astro-ph/0703704].

[304] G. Bertone and D. Merritt, Phys. Rev. D **72** (2005) 103502 [arXiv:astro-ph/0501555].

[305] G. Bertone and D. Merritt, Mod. Phys. Lett. A20, 1021 (2005), [arXiv:astro-ph/0504422].

[306] G. Bertone, G. Sigl, and J. Silk, Mon. Not. Roy. Astron. Soc. 337, 98 (2002), [arXiv:astro-ph/0203488].

[307] D. Merrit, M. Milosavljevic, L. Verde, R. Jimenez, Phys. Rev. Lett. 88 (2002) 191301 [arXiv:astro-ph/0201376].

[308] P. Ullio, H. Zhao, M. Kamionkowski, Phys. Rev. D 64 (2001) 043504 [arXiv:astro-ph/0101481].

[309] D. Merrit, S. Harfst and G. Bertone, Phys. Rev. D 75 (2007) 043517 [arXiv:astro-ph/0610425].

[310] G. Bertone, A.R. Zentner and J. Silk, Phys. Rev. D 72 (2005) 103517 [arXiv:astro-ph/0509565].

[311] M. Fornasa, M. Taoso and G. Bertone, Phys. Rev. D 76 (2007) 043517, [arXiv:astro-ph/0703757].

[312] http://icrhp9.icrr.u-tokyo.ac.jp/.

[313] http://mpi-hd.mpg.de/hfm/HESS/HESS.html.

[314] http://hegra1.mppmu.mpg.de/MAGICweb/.

[315] http://veritas.sao.arizona.edu/index.html.

[316] http://www-glast.stanford.edu.

[317] J.G. Skibo, W.N. Johnson, J.D. Kurfess, R.L. Kinzer, G. Jung, J.E. Grove, W.R. Purcell, M.P. Ulmer, N. Gehrels and J. Tueller, [arXiv:astro-ph/9704207].

[318] G. Weidenspointner *et* al. Feb 2007, [arXiv:astro-ph/0702621].

[319] G. Weidenspointner *et* al, A&A, 450, 1013 (2006).

[320] A.W. Strong, H. Bloemen, R. Diehl, W. Hermsen and V. Schoenfelder, Astrophys. Lett. Commun. 39 (1999) 209, [arXiv:astro-ph/9811211].

[321] A. N. Cillis, R. C. Hartman, Astrophys. J. 621 (2005) 291.

[322] N. Fornengo, L. Pieri and S. Scopel, Phys. Rev. D 70 (2004) 103529 [arXiv:hep-ph/0407342].

[323] D. Hooper and B.L. Dingus, Phys. Rev. D 70 (2004) 113007 [arXiv:astro-ph/0210617].

[324] S.D. Hunter *et* al, Astrophys. J. 481 (1997) 205.

[325] A.W. Strong, I.V. Moskalenko and O. Reimer, Astrophys. J 613 (2004) 956.

[326] D. Elsässer and K. Mannheim, Astropart. Phys. 22 (2004) 65, [arXiv:astro-ph/0405235].

[327] W. de Boer, M. Herold, C. Sander and V. Zhukov, Eur. Phys. J. C 33 (2004) S981, [arXiv:hep-ph/0312037].

[328] W. de Boer, C. Sander, V. Zhukov, A. V. Gladyshev and D. I. Kazakov, Phys. Lett. B 636 (2006) 13, [arXiv:hep-ph/0511154].

[329] G. Bertone, Astrophys. Space Sci. **309** (2007) 505 [arXiv:astro-ph/0608706].

[330] L. Bergstrom, J. Edsjo and P. Ullio, Phys. Rev. Lett. 87 (2001) 251301 [arXiv:astro-ph/0105048].

[331] J. E. Taylor and J. Silk, Mon. Not. Roy. Astron. Soc. 339 (2003) 505 [arXiv:astro-ph/0207299].

[332] P. Ullio, L. Bergstrom, J. Edsjo and C. Lacey, Phys. Rev. D 66 (2002) 123502 [arXiv:astro-ph/0207125].

[333] S. Ando, Phys. Rev. Lett. 94 (2005) 171303 [arXiv:astro-ph/0503006].

[334] S. Horiuchi and S. Ando, Phys. Rev. D 74, 103504 (2006) [arXiv:astro-ph/0607042].

[335] E. J. Ahn, G. Bertone and D. Merritt, Phys. Rev. D 76:023517, 2007 [arXiv:astro-ph/0703236].

[336] S. Ando and E. Komatsu, Phys. Rev. D 73 (2006) 023521, [arXiv:astro-ph/0512217].

[337] S. Ando, E. Komatsu, T. Narumoto and T. Totani, Phys. Rev. D 75:063519, 2007 [arXiv:astro-ph/0612467].

[338] M.Taoso, S.Ando, G.Bertone and S.Profumo, 2008 arXiv:0811.4493 [astro-ph].

[339] B. Kozlowsky and A. Loeb, Astrophys. J. 316 (1987) 801.

[340] Sturrock, P.A., 1971, ApJ, 164, 529.

[341] M. Cassé, B. Cordier, J. Paul and S. Schanne, Astrophys. J 602, L17 (2004), [arXiv:astro-ph/0309824].

[342] G. Bertone, A. Kusenko, S. Palomares-Ruiz, S. Pascoli and D. Semikoz, Phys. Lett. B 636 (2006) 20, [arXiv:astro-ph/0405005].

[343] N. Guessoum, Pierre Jean, N. Prantzos, [arXiv:astro-ph/0607296].

[344] M. Pospelov and A. Ritz, [arXiv:hep-ph/0703128].

[345] D.P. Finkbeiner and N. Weiner, Phys. Rev. D **76**, 083519 (2007) [arXiv:astro-ph/0702587].

[346] C. Boehm, T.A. Ensslin and J. Silk, J.Phys.G 30:279-286, 2004 [arXiv:astro-ph/0208458].

[347] D. Hooper and L.T. Wang, Phys. Rev. D 70, 063506 (2004) [arXiv:hep-ph/0402220].

[348] C. Picciotto and M. Pospelov, Phys. Lett. B 605, 15 (2005) [arXiv:hep-ph/0402178].

[349] F. Ferrer and T. Vachaspati, Phys. Rev. Lett. 95, 261302 (2005) [arXiv:astro-ph/0505063].

[350] M. Kawasaki and T. Yanagida, Phys. Lett. B 624, 162 (2005) [arXiv:hep-ph/0505167].

[351] S. Kasuya and F. Takahashi, Phys. Rev. D 72, 085015 (2005) [arXiv:astro-ph/0508391].

[352] J.F. Beacom, N.F. Bell and G. Bertone, Phys. Rev. Lett. 94, 171301 (2005) [arXiv:astro-ph/0409403].

[353] J.F. Beacom and H. Yuksel, Phys. Rev. Lett. 97, 071102 (2006) [arXiv:astro-ph/0512411].

[354] P. Sizun, M. Casse and S. Schanne, Phys. Rev. D 74 (2006) 063514, [arXiv:astro-ph/0607374].

[355] C. Boehm and P. Uwer, [arXiv:hep-ph/0606058].

[356] G. Weidenspointner *et* al, Nature 451 (2008) 159-162.

[357] S. Rudaz and F.W. Stecker, Astrophys.J.368:406,1991.

[358] F. Boudjema, A. Semenov and D. Temes, Phys. Rev. D 72 (2005) 055024, [arXiv:hep-ph/0507127].

[359] L. Bergstrom, T. Bringmann, M. Eriksson and M. Gustafsson, JCAP 0504 (2005) 004, [arXiv:hep-ph/0412001].

[360] C. Boehm, J. Orloff and P. Salati, Phys. Lett. B 641 (2006) 247. [arXiv:astro-ph/0607437].

[361] M. Gustafsson, L. Bergstrom., J. Edsj*ö* and E. Lundstr*ö*m, 2007 [arXiv:astro-ph/0703512].

[362] G. Bertone, arXiv:0710.5603 [astro-ph].

[363] F. Halzen and D. Hooper, Phys. Rev. D 73 (2006) 123507, [arXiv:hep-ph/0510048].

[364] J. Lundberg and J. Edsjo, Phys. Rev. D 69 (2004) 123505, [arXiv:hep-ph/0401113].

[365] A. Achterberg *et* al, Astropart. Phys. 26 (2006) 129.

[366] L. Bergstrom, J. Edsjo and P. Gondolo, Phys. Rev. D 58 (1998) 103519 [arXiv:hep-ph/9806293].

[367] M. Ackermann *et* al, Astropart. Phys. 24 (2006) 459.

[368] D. Hooper and G.D. Kribs, Phys. Rev. D 67 (2003) 055003.

[369] G. Bertone, E. Nezri, J. Orloff and J. Silk, Phys. Rev. D 70 (2004) 063503 [arXiv:astro-ph/0403322].

[370] G. Bertone, Phys. Rev. D 73 (2006) 103519 [arXiv:astro-ph/0603148].

[371] A. Achterberg *et* al, Phys. Rev. D 76:027101, 2007 arXiv:0705.1781 [astro-ph].

[372] E. Aslanides *et* al, [arXiv:astro-ph/9907432].

[373] J. Carr *et* al, Nucl. Instrum. Meth. A 567:428-432, 2006

[374] P.K.F. Grieder *et* al, Nucl. Phys. Proc. Suppl. 97 (2001) 105-108.

[375] P. Sapienza *et* al, 2006 [arXiv:astro-ph/0611105].

[376] J. Carr *et* al, ICRC0865; http://www.km3net.org.

[377] A.W. Strong, I.V. Moskalenko, V.S. Ptuskin, Ann. Rev. Nucl. Part. Sci. 57:285-327, 2007 [arXiv:astro-ph/0701517].

[378] W. de Boer, C. Sander, A. V. Gladyshev and D. I. Kazakov, Astron. & Astrophysics 444 (2005) 51, [arXiv:astro-ph/0508617].

[379] L. Bergstrom, J. Edsjo, M. Gustafsson and P. Salati, JCAP 0605 (2006) 006, [arXiv:astro-ph/0602632].

[380] W. de Boer, I. Gebauer, C. Sander, M. Weber and V. Zhukov, AIP Conf. Proc. 903 (2007) 607-612, [arXiv:astro-ph/0612462].

[381] R. Aloisio, P. Blasi and A.V. Olinto, JCAP 0405:007, 2004 [arXiv:astro-ph/0402588].

[382] L. Bergstrom, M. Fairbairn and L. Pieri, Phys. Rev. D 74:123515, 2006 [arXiv:astro-ph/0607327].

[383] M.Regis and P.Ullio, Phys. Rev.D 78 (2008) 043505, arXiv:0802.0234 [hep-ph].

[384] G.Bertone, M.Cirelli, A.Strumia and M.Taoso, 2008 arXiv:0811.3744 [astro-ph].

[385] S. Colafrancesco, S. Profumo and P. Ullio, Astron. Astrophys. 455:21, 2006 [arXiv:astro-ph/0507575].

[386] S. Colafrancesco, P. de Bernardis, S. Masi, G. Polenta and P. Ullio, 2007 [arXiv:astro-ph/0702568].

[387] S.Profumo Phys. Rev. D 77 (2008)103510, arXiv:0801.0740 [astro-ph].

[388] T.E. Jeltema, J. Kehayias and S. Profumo, 2008 arXiv:0812.0597 [astro-ph].

[389] E.A. Baltz and L. Wai (SLAC), Phys. Rev. D 70 (2004) 023512, [arXiv:astro-ph/0403528].

[390] S. Colafrancesco, S. Profumo and P. Ullio, Phys. Rev. D 75 (2007) 023513 [arXiv:astro-ph/0607073].

[391] T.E. Jeltema and S. Profumo, 2008 arXiv:0805.1054 [astro-ph].

[392] A. Boyarsky, A. Neronov, O. Ruchayskiy, and M. Shaposhnikov, Mon. Not. Roy. Astron. Soc. 370 (2006) 213-218, [arXiv:astro-ph/0512509].

[393] A. Boyarsky, A. Neronov, O. Ruchayskiy and M. Shaposhnikov, Phys. Rev. D 74 (2006) 103506, [arXiv:astro-ph/0603368].

[394] K. Abazajian, Phys. Rev. D 74 (2006) 023527, [arXiv:astro-ph/0605271].

[395] C. R. Watson, J. F. Beacom, H. Yuksel and T. P. Walker, Phys. Rev. D 74 (2006) 033009, [arXiv:astro-ph/0605424].

[396] A. Palazzo, D. Cumberbatch, A. Slosar and J. Silk, Phys. Rev. D 76 (2007) 103511, arXiv:0707.1495 [astro-ph].

[397] K. Petraki and A. Kusenko, arXiv:0711.4646 [hep-ph].

[398] K.Y. Choi and L. Roszkowski, AIP Conf.Proc. 805 (2006) 30, [arXiv:hep-ph/0511003].

[399] J.A.R. Cembranos, Jonathan L. Feng, A. Rajaraman, F. Takayama, [arXiv:hep-ph/0701011].

[400] K. Hamaguchi, Y. Kuno, T. Nakaya and M.N. Nojiri, Phys. Rev. D 70 (2004) 115007.

[401] A. De Roeck, J. R. Ellis, F. Gianotti, F. Moortgat, K.A. Olive and L. Pape, Eur. Phys. J. C 49 (2007) 1041, [arXiv:hep-ph/0508198].

[402] W. Buchmuller, K. Hamaguchi, M. Ratz and T. Yanagida, Phys. Lett B 588 (2004) 90.

[403] J.R. Ellis, A.R. Raklev and O.K. Oye, JHEP 0610 (2006) 061, [arXiv:hep-ph/0607261].

[404] K. Hamaguchi, M.M. Nojiri and A. de Roeck, JHEP 0703:046, 2007 [arXiv:hep-ph/0612060].

[405] J.L. Feng and B.T. Smith, Phys. Rev. D 71 (2005) 015004, Erratum-ibid. D71 (2005) 0109904, [arXiv:hep-ph/0409278].

[406] H.U. Martyn, Eur.Phys.J.C 48 (2006) 15 [arXiv:hep-ph/0605257].

[407] L. Covi and S. Kraml, [arXiv:hep-ph/0703130].

[408] W. Buchmuller, L. Covi, K. Hamaguchi, A. Ibarra, T. Yanagida, [arXiv:hep-ph/0702184].

[409] M. Hirsch, W. Porod and D. Restrepo, JHEP 0503 (2005) 062, [arXiv:hep-ph/0503059].

[410] S. Lola, P. Osland and A.R. Raklev, 2007 arXiv:0707.2510 [hep-ph].

[411] A. Ibarra and D. Tran, arXiv:0709.4593 [astro-ph].

[412] G. Bertone, W. Buchmuller, L. Covi and A. Ibarra, arXiv:0709.2299 [astro-ph].

[413] L. Covi, L. Roszkowski and M. Small, J. High Energy Phys. 0207 (2002) 023 [arXiv:hep-ph/0206119].

[414] F.D. Steffen, [arXiv:hep-ph/0507003].

[415] L. Covi, L. Roszkowski, R. Ruiz de Austri and M. Small, J. High Energy Phys. 0406 (2004) 003 [arXiv:hep-ph/0402240].

[416] A. Brandenburg, L. Covi, K. Hamaguchi, L. Roszkowski and F.D. Steffen, Phys. Lett B 617 (2005) 99.

[417] R. Battesti *e*t al, 2007 arXiv:0705.0615 [hep-ex].

[418] S. J. Asztalos *e*t al, Phys. Rev. D 69, 011101 (2004) [astro-ph/0310042].

[419] Andriamonje [CAST Collaboration], J. Cosmol. Astropart. Phys. 010 (2007), [hep-ex/0702006].

[420] E. Masso and J. Redondo, JCAP 0509 (2005) 015 [arXiv:hep-ph/0504202].

[421] R. N. Mohapatra and S. Nasri, Phys.Rev.Lett. 98 (2007) 050402, [arXiv:hep-ph/0610068].

[422] J. Jackel, E. Masso, J. Redondo, A. Ringwald and F. Takahashi, Phys.Rev.D 75 (2007) 013004, [arXiv:hep-ph/0610203].

[423] K. Ehret *e*t al, [arXiv:hep-ex/0702023].

[424] A. Mirizzi, G.G. Raffelt and P.D. Serpico, Phys.Rev.D 76 (2007) 023001, arXiv:0704.3044 [astro-ph].

[425] D.Hooper and P.D. Serpico, arXiv:0706.3203 [hep-ph].

[426] A. De Angelis, M. Roncadelli and O. Mansutti, Phys. Rev. D 76 (2007) 121301, [arXiv:0707.4312].

[427] A. De Angelis, O. Mansutti and M. Roncadelli, arXiv:0707.2695 [astro-ph].

[428] J. S. Hagelin, G. L. Kane and S. Raby, Nucl. Phys. B 241 (1984) 638 (1984).

[429] L. E. Ibanez, Phys. Lett. B 137 (1984) 160.

[430] J.R. Ellis, K.A. Olive, Y. Santoso and V.C.Spanos, Phys. Lett. B 565 (2003) 176, [arXiv:hep-ph/0303043].

[431] J. Ellis, S. Heinemeyer, K. Olive, A.M. Weber and G.Weiglein, JHEP 0708 (2007) 083, arXiv:0706.0652 [hep-ph].

[432] H. Baer and C. Balazs, JCAP 0305 (2003) 006 [arXiv:hep-ph/0303114].

[433] R. Arnowitt, B. Dutta and B. Hu, [arXiv:hep-ph/0310103].

[434] A.B. Lahanas and D.V. Nanopoulos, Phys.Lett.B 568 (2003) 55-62, [arXiv:hep-ph/0303130].

[435] J.R. Ellis, K.A. Olive, Y. Santoso and V.C. Spanos, Phys.Rev.D 70 (2004) 055005, [arXiv:hep-ph/0405110].

[436] J. R. Ellis, K. A. Olive and P. Sandick, Phys. Lett. B 642 (2006) 389 [arXiv:hep-ph/0607002];

[437] I. Gogoladze and C. Macesanu, Phys. Rev. D 74 (2006) 093012, [arXiv:hep-ph/0605207].

[438] T.Flacke, D. Hooper and J. March-Russell, Phys.Rev.D 73 (2006) 095002, Erratum-ibid.D74:019902,2006, [arXiv:hep-ph/0509352].

[439] C. Csaki, J. Hubisz, G. D. Kribs, P. Meade and J. Terning, Phys. Rev. D 68 (2003) 035009, [arXiv:hep-ph/0303236].

[440] D.R. Tovey, Eur. Phys. J. direct C 4, N4 (2002).

[441] H. Baer, C. Balazs, A. Belyaev and T. Krupovnickas, JHEP 0306 (2003) 054, [arXiv:hep-ph/0304303].

[442] By ATLAS Collaboration, U. De Sanctis *et* al. Nuovo Cim. 121 B (2006) 761-770.

[443] CMP TP, Report CERN/LHCC/94-38 (1994).

[444] B.K. Gjelsten, D.J. Miller and P.Osland, JHEP 0412 (2004) 003, [arXiv:hep-ph/0410303].

[445] B. K. Gjelsten, D. J. Miller and P. Osland, JHEP 0506, 015 (2005) [arXiv:hep-ph/0501033].

[446] C. G. Lester, M. A. Parker and M. J. White, JHEP 0601 (2006) 080, [arXiv:hep-ph/0508143].

[447] S.P. Das, A. Datta, M. Guchait, M. Maity and S. Mukherjee, 2007 arXiv:0708.2048 [hep-ph].

[448] H. Baer, V. Barger, G. Shaughnessy, H. Summy and L.T. Wang , Phys. Rev. D 75, 095010 (2007).

[449] E.A. Baltz, M. Battaglia, M.E. Peskin and T. Wizansky, Phys. Rev. D 74 (2006) 103521, [arXiv:hep-ph/0602187].

[450] G. Weiglein *et* al. Phys. Rept. 426 (2006) 47-358, [hep-ph/0410364].

[451] C. Macesanu, C.D. McMullen and S. Nandi, Phys. Rev. D 66 (2002) 015009, [arXiv:hep-ph/0201300].

[452] H.C. Cheng, K.T. Matchev and M. Schmaltz, Phys. Rev. D 66 (2002) 056006, [arXiv:hep-ph/0205314].

[453] N. Arkani-Hamed, G.L. Kane, J. Thaler and L.T. Wang, JHEP 0608 (2006) 070, [arXiv:hep-ph/0512190].

[454] P. Binetruy, G. L. Kane, B. D. Nelson, L. T. Wang and T. T. Wang, Phys. Rev. D 70, 095006 (2004) [arXiv:hep-ph/0312248].

[455] M. Battaglia, A. Datta, A. De Roeck, K. Kong and K.T. Matchev, JHEP 0507 (2005) 033, [arXiv:hep-ph/0507284].

[456] A. Datta, K. Kong and K.T. Matchev, Phys. Rev. D 72 (2005) 096006 [Erratum ibid D 72 (2005) 119901], [arXiv:hep-ph/0509246].

[457] J.M. Smillie and B.R. Webber, JHEP 0510 (2005) 069, [arXiv:hep-ph/0507170].

[458] A. Alves, O. Eboli and T. Plehn, Phys. Rev. D 74 (2006) 095010, [arXiv:hep-ph/0605067].

[459] A. Datta, P. Dey, S.K. Gupta, B. Mukhopadhyaya and A. Nyffeler, Aug 2007 arXiv:0708.1912 [hep-ph].

[460] S.Matsumoto, J.Sato, M.Senami and M. Yamanaka, Phys. Lett. B 647 (2007) 466, [hep-ph/0607331].

[461] P. Gondolo, J. Silk, Phys. Rev. Lett. **83** (1999) 1719 [arXiv:astro-ph/9906391].

[462] P. Gondolo, Phys. Lett. B **494**, 181 (2000) [arXiv:hep-ph/0002226].

[463] H. S. Zhao and J. Silk, Phys. Rev. Lett. **95**, 011301 (2005) [arXiv:astro-ph/0501625].

[464] G. Bertone and D. Merritt, Phys. Rev. D **72** (2005) 103502 [arXiv:astro-ph/0501555].

[465] F. Aharonian, *et* al. [HESS collaboration], Phys. Rev. D 78 (2008) 072008, [arXiv:0806.2981].

[466] G. Bertone, Phys. Rev. D 73 (2006) 103519, [arXiv:astro-ph/0603148].

[467] P.Brun, G.Bertone, J.Lavalle and P.Salati, Phys. Rev. D 76 (2007) 083506, [arXiv:0704.2543].

[468] C. L. Fryer and V. Kalogera, Astrophyis. J. (2001), 554 [arXiv:astro-ph/9911312].

[469] L. Ferrarese and H. Ford, Space Science Reviews (2005), 116.

[470] M. C. Miller, E. J. M. Colbert, Int. J. Mod. Phys. D **13** (2004) 1 [arXiv:astro-ph/0308402].

[471] D. A. Swartz, K. K. Ghosh, A. F. Tennant and K.-W. Wu , arXiv:astro-ph/0405498.

[472] X. Fan *et al.* [SDSS Collaboration], Astron. J. **122** (2001) 2833 [arXiv:astro-ph/0108063].

[473] A. J. Barth, P. Martini, c. H. Nelson and L.C. Ho, Astrophys. Lett. **594** (2003) L95.

[474] C. J. Willott, R. J. McLure and M. J. Jarvis, Astrophys. J. **587** (2003) L15 [arXiv:astro-ph/0303062].

[475] Z. Haiman, and A. Loeb, Astrophys. J. **552** (2001) 459.

[476] R. Islam, J. Taylor and J. Silk, Mon. Not. Roy. Astron. Soc. **340** (2003) 6471 [arXiv:astro-ph/0208189].

[477] S. M. Koushiappas, J. S. Bullock and A. Dekel, Mon. Not. Roy. Astron. Soc. **354** (2004) 292 [arXiv:astro-ph/0311487].

[478] M. Volonteri, F. Haardt, and P. Madau, Astrophys. J. **582** (2003) 559 [arXiv:astro-ph/0207276].

[479] K. S. Thorne and V. B. Braginsky, Astrophys. J. Lett. **204** (1976) L1.

[480] É É Flanagan and S. A. Hughes, Phys. Rev. D **57** (1998) 4566.

[481] É É Flanagan and S. A. Hughes, Phys. Rev. D **57** (1998) 4535.

[482] R. Islam, J. Taylor and J. Silk, Mon. Not. Roy. Astron. Soc. **354** (2004) 629 [arXiv:astro-ph/0309559].

[483] T. Matsubayashi, H. Shinkai and T. Ebisuzaki, Astrophys. J.**614** (2004), 864.

[484] S.M.Koushiappas and A.R.Zentner, Astrophys. J. 639 (2006) 7, [arXiv:astro-ph/0503511].

[485] http://lisa.nasa.gov/.

[486] J. F. Navarro, C. S. Frenk and S. D. White, Astrophys. J. 462 (1996) 563 [astro-ph/9508025].

[487] G. D. Quinlan, L. Hernquist, S. Sigurdsson, Astrophys. J. **440** (1995) 554.

[488] D. Merritt, Proceedings of Carnegie Observatories Centennial Symposium *Coevolution of Black Holes and Galaxies* [arXiv:astro-ph/0301257].

[489] A. W. Graham, D. Merritt, B. Moore, J. Diemand and B. Terzic, Astron. J. 132 (2006) 2685 [arXiv:astro-ph/0509417]. J. F. Navarro et al., arXiv:0810.1522.

[490] J. J. Geehan, M. A. Fardal, A. Babul, P. Guhathakurta, Mon. Not. Roy. Astron. Soc. **366** (2006) 996 [arXiv:astro-ph/0501240].

[491] J. F. Navarro, E. Hayashi, C. Power, A. R. Jenkins, C. S. Frenk, S. D. M. White, V. Springel, J. Stadel and T. R. Quinn, Mon. Not. R. Astron. **349** (2004) 1039 [arXiv:astro-ph/0311231].

[492] http://projects.hepforge.org/pythia6/.

[493] S. Kretzer, Phys. Rev. D **62** (2000) 054001 [arXiv:hep-ph/0003177] and www.pv.infn.it/%7Eradici/FFdatabase.

[494] L. Bergström, T. Bringmann, M. Eriksson, M. Gustafsson, Phys. Rev. Lett. **94** (2005) 131301 [arXiv:astro-ph/0410359].

[495] T. Gaisser, M. Honda, P. Lipari and T. Stanev, in Proc. of the 27th ICRC, (2001).

[496] L. Bergström, D. Hooper, Phys. Rev D **73** (2006) 063510 [arXiv:hep-ph/0512317].

[497] http://wwwmagic.mppmu.mpg.de/physics/results/index.html.

[498] http://www.mpi-hd.mpg.de/hfm/CTA/CTA_home.html.

[499] E. A. Baltz *et al.*, JCAP 0807, 013 (2008) [arXiv:0806.2911].

[500] A. N. Cillis, R. C. Hartman, Astrophys. J. **621** (2005) 291.

[501] http://heasarc.gsfc.nasa.gov/FTP/compton/data/egret/diffuse_maps.

[502] http://www-glast.slac.stanford.edu/software/IS/glast_lat_performance.htm

[503] G. Bertone, T. Bringmann, R. Rando, G. Busetto and A. Morselli, arXiv:astro-ph/0612387.

[504] E. A. Baltz, J. E. Taylor and L. L. Wai, arXiv:astro-ph/0610731.

[505] P. Sreekumar et al. (EGRET), Astrophys. J. 494, 523 (1998), astro-ph/9709257.

[506] T. Narumoto and T. Totani, Astrophys. J. 643, 81 (2006), astro-ph/0602178.

[507] H. Liang, V. Dogiel, and M. Birkinshaw, Mon. Not. Roy. Astron. Soc. 337, 567 (2002), astro-ph/0208509.

[508] Y. Rephaeli, J. Nevalainen, T. Ohashi, and A. M. Bykov (2008), 0801.0982.

[509] V. Pavlidou and B. D. Fields, Astrophys. J. 575, L5 (2002), astro-ph/0207253.

[510] T. Oda, T. Totani, and M. Nagashima, Astrophys. J. 633, L65 (2005), astro-ph/0504096.

[511] A. Cuoco, J. Brandbyge, S. Hannestad, T. Haugboelle, and G. Miele, Phys. Rev. D77, 123518 (2008), 0710.4136.

[512] J. M. Siegal-Gaskins, JCAP 0810, 040 (2008), 0807.1328.

[513] D. Hooper and P. D. Serpico, JCAP 0706, 013 (2007), astro-ph/0702328.

[514] S. K. Lee, S. Ando, and M. Kamionkowski (2008), 0810.1284.

[515] T. Sjostrand, Comput. Phys. Commun. 82, 74 (1994).

[516] T. Sjostrand (1995), hep-ph/9508391.

[517] M. Cirelli, M. Kadastik, M. Raidal and A. Strumia, 2008, arXiv:0809.2409.

[518] R. K. Sheth and G. Tormen, Mon. Not. Roy. Astron. Soc. 308, 119 (1999), astro-ph/9901122.

[519] G. L. Bryan and M. L. Norman, Astrophys. J. 495, 80 (1998), astro-ph/9710107.

[520] D. J. Eisenstein and W. Hu, Astrophys. J. 511, 5 (1997), astro-ph/9710252.

[521] A. W. Strong, I. V. Moskalenko, and O. Reimer, Astro- phys. J. 613, 962 (2004), astro-ph/0406254.

[522] S. Ando, E. Komatsu, T. Narumoto, and T. Totani, Mon. Not. Roy. Astron. Soc. 376, 1635 (2007), astro- ph/0610155.

[523] H. J. Mo and S. D. M. White, Mon. Not. Roy. Astron. Soc. 282, 347 (1996), astro-ph/9512127.

[524] S. Profumo, Phys. Rev. D78, 023507 (2008), 0806.2150.

[525] http://cossc.nasa.gov/docs/cgro/cgro/egret.htm.

[526] W. B. Atwood (GLAST), Nucl. Instrum. Meth. A342, 302 (1994).

[527] P. F. Michelson (GLAST-LAT), AIP Conf. Proc. 921, 8 (2007).

[528] L. Bergstrom, G. Bertone, T. Bringmann, J. Edsjo and M. Taoso, 2008, arXiv:0812.3895 [astro-ph].

[529] S. W. Barwick *et* al, Astrophys. J. Lett. 482 L191 (1997), [arXiv:astro-ph/9703192].

[530] A. Coutu *et* al, Astropart. Phys. 11 (1999) 429, [astro-ph/9902162].

[531] AMS-01 Collaboration: M. Aguilar et al. Phys. Lett. B 646 145-154 2007, [arXiv:astro-ph/0703154].

[532] PAMELA collaboration [arXiv:0810.4995].

[533] PAMELA collaboration [arXiv:0810.4994].

[534] ATIC collaboration, Nature 456 (2008) 362.

[535] See T. Delahaye, F. Donato, N. Fornengo, J. Lavalle, R. Lineros, P. Salati and R. Taillet, [arXiv:0809.5268].

[536] F. Donato, D. Maurin, P. Brun, T. Delahaye and P. Salati, [arXiv:0810.5292].

[537] A. M. Atoian, F. A. Aharonian and H. J. Volk, Phys. Rev. D 52 (1995) 3265. I. Büsching et al. [arXiv:0804.0220]. T. Kobayashi, Y. Komori, K. Yoshida and J. Nishimura, Astrophys. J. 601 (2004) 340 [arXiv:astro-ph/0308470]. See also the recent study in: D. Hooper, P. Blasi and P. D. Serpico, arXiv:0810.1527.

[538] H. Yuksel, M. D. Kistler and T. Stanev, arXiv:0810.2784. See also P. D. Serpico, arXiv:0810.4846 for an agnostic analysis.

[539] I.V. Moskalenko and A.W. Strong, Astrophys. J. **493** (1998) 694, [arXiv:astro-ph/9710124].

[540] M. Simon, A. Molnar, and S. Roesler, Astrophys. J. 499, 250 (1998).

[541] F. Donato et al., Astrophys. J. 563, 172 (2001).

[542] V. S. Ptuskin et al., Astrophys. J. 642, 902 (2006).

[543] H.E.S.S. Collaboration, arXiv:0811.3894.

[544] T. Delahaye, R. Lineros, F. Donato, N. Fornengo and P. Salati, Phys. Rev. D 77 (2008) 063527, arXiv:0712.2312 [astro-ph].

[545] F. Donato, N. Fornengo, D. Maurin and P. Salati, Phys. Rev. D 69 (2004) 063501, [arXiv:astro-ph/0306207].

[546] D.Maurin, R. Taillet and C. Combet, 2006, [arXiv:astro-ph/0609522].

[547] J.Diemand, B.Moore and J.Stadel, Mont. Riy. Astron. Soc. 353 (2004) 624, [arXiv:astro-ph/0402267].

[548] J. N. Bahcall and R. M. Soneira, Astrophys. J. Suppl. 44 (1980) 73.

[549] E.Baltz and J.Edsjo, Phys. Rev. D. 59 (1999) 023511, [arXiv:astro-ph/9808243].

[550] T.Bringmann and P.Salati, Phys. Rev. D 75 (2007) 083006, [arXiv:astro-ph/0612514].

[551] M. Cirelli, N. Fornengo and A. Strumia, Nucl. Phys. B753 (2006) 178, [arXiv:hep-ph/0512090].

[552] Talk by J.P. Wefel at ISCRA 2008, Erice, Italy, 2008, http://laspace.lsu.edu/ISCRA/ISCRA2008.

[553] GLAST collaboration, *Measuring 10-1000 GeV Cosmic Ray Electrons with GLAST/LAT', talk at the ICRC07 conference.*

[554] N. Arkani-Hamed, D. P. Finkbeiner, T. Slatyer and N. Weiner, 2008, arXiv:0810.0713.

[555] A. Sommerfeld, Ann. Phys. 11 257 (1931). J. Hisano, S. Matsumoto and M. M. Nojiri, Phys. Rev. Lett. 92 (2004) 031303 [hep-ph/0307216]. J. Hisano, S. Matsumoto, M. M. Nojiri and O. Saito, Phys. Rev. D 71 (2005) 015007 [hep-ph/0407168]. The relevance of non-perturbative electroweak corrections to DM freeze-out was pointed out in J. Hisano, S. Matsumoto, M. Nagai, O. Saito and M. Senami, Phys. Lett. B 646 (2007) 34, [arXivhep-ph/0610249]. See also previous work in K. Belotsky, D. Fargion, M. Khlopov and R. V. Konoplich, Phys. Atom. Nucl. 71 (2008) 147 [arXiv:hep-ph/0411093] and references therein. For a generic unbroken non-Abelian gauge interaction, the group theory needed to compute the Sommerfeld effect was presented in A. Strumia, arXiv:0806.1630.

[556] M. Cirelli, A. Strumia, M. Tamburini, Nucl. Phys. B787 (2007) 152 [arXiv:0706.4071].

[557] M. Cirelli, R. Franceschini and A. Strumia, Nucl. Phys.B 800 (2008) 204, arXiv:0802.3378.

[558] I. Cholis, L. Goodenough, D. Hooper, M. Simet and N. Weiner, arXiv:0809.1683.
Models with enriched dark sectors, often including extra light force mediators: M. Pospelov and A. Ritz, arXiv:0810.1502. A. E. Nelson and C. Spitzer, arXiv:0810.5167. I. Cholis, D. P. Finkbeiner, L. Goodenough and N. Weiner, arXiv:0810.5344. Y. Nomura and J. Thaler, arXiv:0810.5397. D. Feldman, Z. Liu and P. Nath, arXiv:0810.5762. T. Hambye, arXiv:0811.0172. Y. Bai and Z. Han, arXiv:0811.0387. P. J. Fox and E. Poppitz, arXiv:0811.0399. T. Hur, H. S. Lee and C. Luhn, arXiv:0811.0812. E. Ponton and L. Randall, arXiv:0811.1029.
Decaying Dark Matter: P. f. Yin, Q. Yuan, J. Liu, J. Zhang, X. j. Bi and S. h. Zhu, arXiv:0811.0176. C. R. Chen, F. Takahashi and T. T. Yanagida, arXiv:0811.0477. K. Hamaguchi, E. Nakamura, S. Shirai and T. T. Yanagida, arXiv:0811.0737 A. Ibarra and D. Tran, arXiv:- 0811.1555. C. R. Chen, F. Takahashi and T. T. Yanagida, arXiv:0811.3357.
Modified SuperSymmetric DM sectors: K. Ishiwata, S. Matsumoto and T. Moroi, arXiv:-0811.0250. R. Harnik and G. D. Kribs, arXiv:- 0810.5557.

[559] L. Bergstrom, T. Bringmann and J. Edsjo, arXiv:0808.3725.

[560] See, for a recent analysis, J. Lavalle, J. Pochon, P. Salati and R. Taillet, arXiv:astro-ph/0603796 and J. Lavalle, Q. Yuan, D. Maurin and X. J. Bi, arXiv:0709.3634.

[561] L. Bergstrom, Phys. Lett. B 225 (1989) 372. L. Bergstrom, T. Bringmann, M. Eriksson and M. Gustafsson, Phys. Rev. Lett. 95 (2005) 241301 [hep-ph/0507229]. T. Bringmann, L. Bergstrom and J. Edsjo, JHEP 0801 (2008) 049 [arXiv:0710.3169].

[562] J. Diemand, M. Zemp, B. Moore, J. Stadel and M. Carollo, Mon. Not. Roy. Astron. Soc. 364 (2005) 665 [astro-ph/0504215].

[563] J. Albert et al. [MAGIC Collaboration], Astrophys. J. 638 (2006) L101 [astro-ph/0512469].

[564] H.A. Mayer-Haesselwander *et al.*, A&A 335, 161 (1998)

[565] D. Hooper and B. L. Dingus, Phys. Rev. D 70 (2004) 113007 [astro-ph/0210617].

[566] G. Bertone, G. Servant and G. Sigl, Phys. Rev. D 68, 044008 (2003) [hep-ph/0211342].

[567] S. Dodelson, D. Hooper and P. D. Serpico, Phys. Rev. D 77, 063512 (2008) [arXiv:0711.4621].

[568] F. Aharonian et al. [HESS collaboration], Nature 439 (2006) 695 [astro-ph/0603021].

[569] HESS collaboration, arXiv:0711.2369.

[570] N. W. Evans, F. Ferrer and S. Sarkar, Phys. Rev. D 69 (2004) 123501 [astro-ph/0311145].

[571] F. Aharonian et al. [H.E.S.S. Collaboration], Astron. Astrophys. 457 (2006) 899 [arXiv:astroph/ 0607333].

[572] P. Gondolo, Phys. Lett. B 494 (2000) 181 [hep-ph/0002226].

[573] G. Bertone, G. Sigl and J. Silk, Mon. Not. Roy. Astron. Soc. 326 (2001) 799 [astro-ph/0101134].

[574] S. Gillessen, F. Eisenhauer, S. Trippe, T. Alexander, R. Genzel, F. Martins and T. Ott, arXiv:0810.4674.

[575] R.D.Davis, D.Walsh, R.S.Booth, MNRAS 177, 319-333 (1976)

[576] R. Genzel *et al.*, Nature 425 (2003) 934 [astro-ph/0310821].

[577] E. Borriello, A. Cuoco, G. Miele, arXiv:0809.2990. N. F. Bell and T. D. Jacques, arXiv:0811.0821.

[578] L. Pieri, G. Bertone and E. Branchini, Mon. Not. Roy. Astron. Soc. 384 (2008) 1627 [arXiv:0706.2101].

[579] D.P. Finkbeiner, Astrophys. J. **614**, 186 (2004).

[580] D. Hooper, D. P. Finkbeiner and G. Dobler, Phys. Rev. D **76** (2007) 083012 [arXiv:0705.3655 [astro-ph]].

[581] D. P. Finkbeiner and N. Weiner, Phys. Rev. D **76**, 083519 (2007) [arXiv:astro-ph/0702587].

[582] I. Cholis, D. P. Finkbeiner, L. Goodenough and N. Weiner, arXiv:0810.5344.

[583] Y. Nomura and J. Thaler, [arXiv:0810.5397].

[584] A. Birkedal, K. T. Matchev, M. Perelstein and A. Spray, arXiv:hep-ph/0507194,

[585] L. Bergstrom, Phys. Lett. B **225**, 372 (1989).

[586] L.E. Strigari et al., Astrophys. J. **678**, 614 (2008) [arXiv:0709.1510]

[587] E. Aliu et al., [arXiv: 0810.3561].

[588] D. Hooper, A. Stebbins and K. M. Zurek, arXiv:0812.3202, M. Lattanzi and J. I. Silk, arXiv:0812.0360.

[589] M. Taoso, G. Bertone, S. Ekstrom and G. Meynet, Phys. Rev. D 78 (2008) 123510, arXiv:0806.2681 [astro-ph].

[590] D. Spolyar, K. Freese and P. Gondolo, Phys. Rev. Lett. 100 (2008) 051101.

[591] K. Freese, P. Bodenheimer, D. Spolyar and P. Gondolo, 2008 [arXiv:0806.0617].

[592] F. Iocco, A. Bressan, E. Ripamonti, R. Schneider, A. Ferrara and P. Marigo, 2008 [arXiv:0805.4016].

[593] A. Natarajan, J.C. Tan and B.W. O'Shea, 2008, arXiv:0807.3769.

[594] F. Iocco, Astrophys. J. 677 (2008) L1.

[595] K. Freese, D. Spolyar and A. Aguirre, 2008 [arXiv:0802.1724].

[596] S. Ekström, G. Meynet, A. Maeder and F. Barblan, Astronomy and Astrophysics 478 (2008) 467.

[597] A. Gould, ApJ 567 (1987) 532.

[598] Z. Ahmed *et al.* [CDMS Collaboration], Phys.Rev.Lett.102 (2009) 011301, arXiv:0802.3530 [astro-ph];

[599] J. Angle *et al.*, Phys.Rev.Lett.101 (2008) 091301, arXiv:0805.2939 [astro-ph]; E. Behnke *et al.* [COUPP Collaboration], Science **319** (2008) 933 [arXiv:0804.2886 [astro-ph]].

[600] K.Griest and D.Seckel, Nucl. Phys. B 296 (1987) 681.

[601] K. Freese, P. Gondolo, J.A. Sellwood and D. Spolyar, [arXiv:0805.3540].

[602] T. Abel, G.L. Bryan and M.L. Norman, Science 295 (2002) 93.

[603] B.W. O'Shea and M.L. Norman, ApJ 654 (2007) 66.

[604] S. Yoon, F. Iocco and S. Akiyama 2008 [arXiv:0806.2662].